FIRE-RES

Innovative technologies & socio-ecological-economic solutions for fire resilient territories in Europe

D5.4 Modelling of wildfire combustion and convective processes

www.fire-res.eu

fire-res@ctfc.cat

Project Acronym: FIRE-RES

Project name: Innovative technologies and socio-ecological-economic solutions for fire resilient territories in Europe

Call ID: H2020-LC-GD-1-1-2020 (Preventing and fighting extreme wildfires with the integration and demonstration of innovative means)

Work Package: WP5

Task Number: Task 5.3. Modelling and decision support system tools.

Lead beneficiary: VTT Technical Research Centre of Finland Ltd.

Contributing beneficiary: VTT Technical Research Centre of Finland Ltd.

This document was produced under the terms and conditions of Grant Agreement No. 101037419 of the European Commission. It does not necessarily reflect the view of the European Union and in no way anticipates the Commission's future policy in this area.

Publication

Publication date: 30/11/2024

Authors: Terhi Kling, VTT; Timo Korhonen, VTT; Nikhil Verma, VTT; Tuula Hakkarainen, VTT; Tomi Maijala, VTT; Elena Gorshkova, VTT; Timo Niemi, VTT; Sirpa Kallio, VTT

Abstract: Two different computational fluid dynamics (CFD) software, Fire Dynamics Simulator (FDS) and OpenFOAM, were applied to simulate wildfires behaviour. The models were tested in validation cases and sensitivity analysis was used to examine fire behaviour under different conditions. Transition of a wildfire from normal to extreme state was studied by simulations with a simplified forest model, to define precursors that indicate in advance the possibility of a wildfire turning into an extreme wildfire event. Various charts and tables were produced covering the values of chosen precursors to understand the trend for decision making to deal with such fires.

Key words: computational fluid dynamics, wildfire simulation, fire behaviour, extreme wildfire event

Quote as: Kling, T., Korhonen, T., Verma, N., Hakkarainen, T., Maijala, T., Gorshkova, E., Niemi, T., Kallio, S. (2024). Modelling of wildfire combustion and convective processes. Deliverable 5.4. FIRE-RES project. DOI: 10.5281/zenodo.14192901

DOI: 10.5281/zenodo.14245914

Dissemination level

[X] PU- Public: must be available in the website

[ ] CO- Confidential: Only for members of the Consortium and the Commission Services

[ ] CI – Classified: As referred in to Commission Decision 2001/844/EC

Document history

Edition	Date	Status	Author
Version 1	16/10/2024	Draft	Terhi Kling (VTT), Timo Korhonen (VTT), Nikhil Verma (VTT), Tuula Hakkarainen (VTT), Tomi Maijala (VTT), Elena Gorshkova (VTT), Timo Niemi (VTT), Sirpa Kallio (VTT)
Version 2	20/11/2024	Revision	Terhi Kling (VTT), Timo Korhonen (VTT), Nikhil Verma (VTT), Tuula Hakkarainen (VTT), Tomi Maijala (VTT), Elena Gorshkova (VTT), Timo Niemi (VTT), Sirpa Kallio (VTT)
Version 3	25/11/2024	Revision	Jordi Garcia-Gonzalo (CTFC)
Version 4	27/11/2024	Revision	Jordi Corbera (ICGC)
Version 5	29/11/2024	Final version	

Table of contents

1. INTRODUCTION

In the following subsections, we briefly describe the background of the wildfire problem under consideration (subsection 1.1), its main causes, and challenges, as well as the FIRE-RES project (subsection 1.2), which aims to solve these challenges. Finally, we state the main content and objective of deliverable D5.4 (subsection 1.3), and explain how the physical modelling of fire behaviour, described in this deliverable, relates to the project's goals in improving EWE (Extreme Wildfire Event) modelling, simulation, and analysis.

1.1 Background

The International Association for Fire Safety Science (IAFSS) has identified climate change, resilience, and sustainability as one of the Societal Grand Challenges where fire safety science and engineering research can most significantly contribute to the near term (McNamee et al., 2019). Wildland fires and wildland-urban interface is an area of research and actions to respond to this challenge.

The interest of the scientific community in wildfires has increased because, due to many different causes (the effects of global warming, land use changes, the effects of human activities, the expansion of the Wildland-Urban Interface (WUI), etc.), they have become an increasingly serious problem all over the world (Morvan et al., 2022). The number of fires is increasing, as is their scope, rate of spread and intensity. The fires have become so huge that firefighters cannot even go near them, therefore increasing resources alone will not help to fight these fires (Castellnou, 2019).

One of the major challenges in managing such extreme wildfire events (EWEs) is the inability to monitor and predict the fire behaviour (Castellnou et al., 2022a). Vigorous fire behaviour in EWEs is associated with complex interactions between combustion heat transfer and atmospheric flows, which are affected by fuels, meteorology, and topographic conditions. Modelling such phenomena is challenging and just in the early stages (Liu et al., 2021).

Large scale wildland fires present unique challenges for first responders and incident management. A large-scale wildfire may require the mobilization of a large number, hundreds or even thousands, of firefighting and rescue personnel over large areas for long periods of time. More research is needed to optimize incident management in support of enhancing resilience in the face of large events.

Considering increased urbanization broadening the extent of urban areas, the impact of fires in the wildland-urban interface is critical. Understanding the complexity of the wildland-urban interface and how it impacts on the risk of wildfires is critical. There is also spread to locations not typically seen in recent history, including the Nordic countries. It is important to continue efforts to model and understand wildland fire spread to be able to develop modern preventative and mitigation methods. Understanding wildland fire spread will also provide valuable input to pre-planning and hazard risk assessment.

1.2 FIRE-RES project

When extinguishing-focused strategies no longer work in the context of extreme wildfires, new approaches must be developed that consider the root causes and effects of EWEs. The FIRE-RES project combines existing wildfire-related research, technologies, emergency services, policy, and governance areas to innovate processes, methods, and tools to promote a more holistic approach to fire management. To achieve this, FIRE-RES identifies and highlights innovations at the technological, social, health/safety, administrative, ecological, and economic levels. FIRE-RES is an interdisciplinary, multi-stakeholder consortium of researchers, forest fire agencies, technology companies, industry, and civil society from 13 countries, connecting to wider networks in science and disaster reduction management. In the project, the work is done in work packages (WPs), which are divided into tasks and subtasks, but the goals are described in so-called Innovation Actions (IAs), the results of which are applied to the so-called to living laboratories (LLs).

1.3 Goal of this deliverable

WP5 of FIRE-RES aims to provide advanced technological solutions, equipment, and decision support systems (DSS) to stakeholders dealing with EWEs in Europe. Task 5.3 implements modelling and DSS development. Subtask 5.3.1 strives to improve fire modelling to evaluate EWE behaviour more precisely, so that on this basis the prediction of extreme fire behaviour and the assessment of its consequences could be improved. In addition, efforts are made to model and analyse combustion processes to understand why current models do not predict EWE behaviour and to identify the key factors that trigger it. In addition, the exposure of buildings to extreme fire conditions is modelled to assess how their protection could be improved. This deliverable D5.4 collects the work done in Subtask 5.3.1 in relation to IA5.4, i.e., modelling of fire processes leading to EWE are examined to be able to better predict both the occurrence of extreme fire behaviour and its consequences. Simulations are carried out to study the effects of various factors, such as forest materials, humidity, weather, and atmospheric interaction, on fire behaviour, and what kind of thermal effects can be exerted on, e.g., buildings.

2.STATE OF THE ART

In the following subsections, we examine the wildfire problem based on the scientific literature. We start with a description of forest fires and related phenomena (subsection 2.1), after that we talk more about extreme wildfire events (subsection 2.2), and finally we describe different methods used for modelling and simulating forest fires (subsection 2.3).

2.1 Phenomena of wildland fire

2.1.1 Mechanisms of wildfire propagation

The flame front is a buoyancy-controlled plume, whose burning speed is primarily maintained by heat feedback from the flame to the fuel surface. Buoyancy causes the inflow of air around the flame, the rise of flame gases and the formation of convection columns above the fire (Weber, 1991). The heat received by the fuel produces gaseous

volatiles through the pyrolysis reaction. Volatiles are then released from the surface of the fuel to keep the flames burning. The combustion of the flame front is therefore controlled by the energy balance between the net heat feedback and the heat needed to release the volatile substances.

The following sequential processes occur in the propagation of a flame front (Liu et al., 2021): (1) An ignition source causes a pyrolysis reaction that releases gaseous volatiles. When enough volatile substances are formed, they ignite when mixed with the surrounding air. (2) The heat released from the combustion of volatile substances is transferred back to the unburned fuels, which causes the temperature of the fuel to rise. (3) An increase in the temperature of the unburned fuels causes a pyrolysis reaction, which releases more volatile substances and triggers the ignition of the unburned fuels. Fire spreads through such successive ignitions. The progress of the flame front is also affected by the energy balance, i.e., the ratio of the enthalpy of the fuel element in front of the flame and the heat loss to the environment (Weber, 1991).

Wildfires propagate in three typical ways: (1) Ground fire (organic materials under the surface litter on the ground burn), (2) surface fire (litter, wood, grass, and other materials on the surface of the ground burn), (3) crown fire (the tops of trees and bushes are burning). The most common of these is surface fire and it is a well-known fact that surface fire growth is highly dependent on fuel properties, weather conditions, and topography (Liu et al., 2021).

Fuel properties that affect fire growth include, e.g., fuel composition, fuel organic and moisture content, fuel load (mass per unit area), fuel element size, fuel element shape (characterized by surface-to-volume ratio), fuel bed porosity or packing ratio, fuel distribution, and continuity of fuel elements. Of all the fuel properties, the most important is the fuel's moisture content defined as the percentage of water in relation to the dry mass of the fuel (Viegas et al.,1992). Among the weather conditions, the factors most affecting fire growth are air humidity and temperature, wind speed and direction, and the interaction with the atmosphere. The wind accelerates the spread of the fire by tilting the flames forward (fuel preheating) and by feeding them fresh oxygen. In addition, the wind can throw firebrands far ahead of the fire front, causing numerous new ignitions outside the primary fire area. In terms of topographical conditions, uphill is worse than flat terrain, and concave fuel beds like canyons are especially bad (Viegas & Pita, 2004).

The interactions of the above-mentioned factors also have a significant effect on fire behaviour. For example, topography affects the distribution of fuel types, and the moisture content of fuel depends on weather conditions. The interaction between weather and terrain can cause strong surface winds, and in addition, the fire's interaction with the atmosphere can cause strong vertical currents. In addition, various fuel preheating mechanisms, such as heat radiation, conduction, and convection, affect the propagation of the fire. The importance of conduction is minor and can be ignored (Baines, 1990).

2.1.2 Extreme wildfire events (EWEs)

Most of the wildfires are small local fires, but some become large so-called extreme wildfire events (EWEs) that exceed suppression capabilities, cause considerable damage, and often result in the deaths of civilians and firefighters. Examples of such fires are, e.g., the following (Tedim et al., 2018; Castellnou et al., 2022b): China 1987; Portugal 2003 and 2005; Greece, Italy, and USA 2007; Australia 2009; USA 2013; Canada and Chile 2016; Portugal and USA 2017; Greece and USA 2018. For example, the Pedrógão Grande fire in Portugal in 2017 resulted in 65 deaths and over 200 injuries, and 45,328 hectares burned. Fireline intensities (FLIs) of 20,000–60,000 kW/m and rates of spread (ROS) of 65 m/min were observed (Comissão Técnica Independente, 2017; Viegas et al., 2017).

The FIRE-RES project has defined EWEs (Castellnou et al., 2022a) as "wildfires with large-scale complex interactions between fire and atmosphere generating pyroconvective behaviour, coupling processes, that result in fast, intense, uncertain, and fast-paced changing fire behaviour exceeding the technical limits of control (fireline intensity 10.000 kW/m; rate of spread >50 m/min; spotting distance >1 km) and exhibiting prolific to massive spotting and extreme growth rate". According to the expert assessments made in the project, such extreme fire behaviour clearly exceeds the expected fire behaviour estimated by current models and the decision-making ability of the emergency system, which causes an increased threat to the crew, the civilian population and property, as well as to natural values. The technical definition presented above is based on the following table (*Figure 1*) proposed by Tedim et al. (2018).

Fire Category		Real Time Measurable Behavior Parameters			Real Time Observable Manifestations of EFB				Type of Fire and Capacity of Control [a]
		FLI [kW m^{-1}]	ROS [m/min]	FL [m]	PyroCb	Downdrafts	Spotting Activity	Spotting Distance [m]	
Normal Fires	1	<500	<5 [b] <11 [c]	<1.5	Absent	Absent	Absent	0	Surface fire Fairly easy
	2	500–2000	<31 [b] <58 [c]	<2.5	Absent	Absent	Low	<100	Surface fire Moderately difficult
	3	2000–4000	<20 [d] <58 [c]	2.5–3.5	Absent	Absent	High	>100	Surface fire, torching possible Very difficult
	4	4000–10,000	<50 [c] <300 [d]	3.5–10	Unlikely	In some localized cases	Prolific	500–5000	Surface fire, crowning likely depending on vegetation type and stand structure Extremely difficult
Extreme Wildfire Events	5	10,000–30,000	<150 [c] <250 [d]	10–30	Possible	Present	Prolific	>1000	Crown fire, either wind- or plume-driven Spotting plays a relevant role in fire growth Possible fire breaching across an extended obstacle to local spread Chaotic and unpredictable fire spread Virtually impossible
	6	30,000–100,000	<300	50–100	Probable	Present	Massive Spotting	>3000	Plume-driven, highly turbulent fire Chaotic and unpredictable fire spread Spotting, including long distance, plays a relevant role in fire growth Possible fire breaching across an extended obstacle to local spread impossible
	7	>100,000 (possible)	>300 (possible)	>100 (possible)	Present	Present	Massive Spotting	>5000	Plume-driven, highly turbulent fire Area-wide ignition and firestorm development non-organized flame fronts because of extreme turbulence/vorticity and massive spotting impossible

Note: [a] Forest and shrubland; [b] grassland; [c] forest; [d] shrubland and grassland; [e] FLI classes 1–4 follow the classification by Alexander and Lanoville [125].

Figure 1. Wildfire events classification based on (Tedim et al., 2018), where FLI=fireline intensity, ROS=rate of spread, FL=flame length, EFB=Extreme-fire behaviour index, PyroCb= pyrocumulonimbus.

2.2 Modelling and simulation of wildfires

2.2.1 Progress in wildfire modelling

Simulating the behaviour of wildfires is challenging because they combine several non-linear physical mechanisms (pyrolysis, combustion, thermal radiation, convection, turbulence) on different scales. Small-scale experiments carried out in the laboratory do not fully reproduce the phenomena observed on a large scale, and field experiments are limited for safety reasons. The complexity of the problem is also due to many mechanisms that control the behaviour of fires in nature, such as the decomposition process of vegetation in the fire, heat transfer modes between the flame, hot gases and vegetation, interaction with the atmospheric boundary layer, turbulent combustion in the flame, etc. Due to all these reasons, the simulation of wildfires has long been limited to empirical models that are based on fire tests performed in the laboratory. Although the applications of this approach have worked quite well in homogeneous environments (such as grassland), generalizing it to more heterogeneous environments such as heaths and forests has been challenging. A more physical modelling approach is also needed to better explore the parameters governing behaviour related to vegetation, topography, wind, etc. and their relative importance (Morvan et al., 2022).

In contrast to previous fully empirical models, Anderson and Rothermel (1965), Frandsen (1971), and Rothermel (1972) proposed the so-called semi-empirical rate-of-spread (ROS) evaluation methods, which took some physical aspects into account. The models of Andersson and Rothermel were based on wind tunnel experiments, and the effects of slope and wind on ROS were considered with a correction factor. The main advantage of this model is its simplicity, which is why it was adopted in the world's most used fire area simulator tool FARSITE (Finney, 2004), where a fuel model library was added to the topography of the area, which has been continuously supplemented due to the extensive use of the program. The major limitation of the method is that the experiments used to calibrate the model constants were performed at laboratory scale for solid fuel litters with pine needles or excelsior, and for various reasons (fuel bed tightness, low turbulence, low fuel moisture content, vegetation layer dimensions, etc.) the conditions of the experiments covered only a limited set of situations to apply the model to all configurations observed in the field (Morvan et al., 2022). The properties of this semi-empirical model are being improved by adding new data sets from experimental fire tests (Finney et al., 2015).

Experience has also shown that the results of a simplified fire propagation model can be improved by considering the interaction between topography and atmospheric flows (Hanson et al., 2000), which has motivated the development of the coupled atmosphere-wildland fire models (Clark et al., 1996; Filippi et al., 2011; Mandel et al., 2011). For operational applications that require the simulation of wildfire spread at a regional scale, this combined approach is considered very promising. New, more physical fire propagation models are also being developed (Balbi et al., 2009; Balbi et al., 2020).

2.2.2 Physical modelling of wildfires

A self-propagating wildfire follows natural laws that determine its behaviour and spread through living and dead plant fuel. These laws determine the release of energy from burning fuels and the transfer of this energy to and interaction with the surrounding environment. Physical modelling aims to capture the central properties of the phenomenon in the form of governing mathematical equations that enable computer simulation of the modelled system, which helps to understand the behaviour of the system under prevailing conditions and the dependence of this behaviour on critical variables. Physical modelling of wildfires is usually based on computational fluid dynamics (simulating the flow of fluids such as air and water), which is extended to include fuel chemistry and reactions, combustion dynamics, energy release and transfer, and ignition of fuels. Such models are very complex, and their solutions often require simplifying assumptions about the underlying physics and sophisticated numerical computational techniques, often requiring large computational resources. (Williams 1985, Cox 1998).

Significant progress in the physical modelling of wildfires began in the 1980s (Williams 1982), when computing power was sufficiently advanced to provide affordable, sufficiently accurate and extensive numerical solutions to the mathematical equations that form the core of the physical model. The phenomenon being modelled is so complex that its simulations are still limited and simplified to solve the underlying mathematics. The main processes that the fully physical fire model aims to describe are the chemical reactions associated with the heating, dehydration and thermal decomposition of cellulosic biomass fuel, the oxidation of thermal decomposition products and the release of energy from molecular bonds, the transfer of this energy through radiation, convection and conduction to adjacent fuels, and the interaction of these processes with the surrounding vegetation, terrain and atmosphere (Shafizadeh 1982, Williams 1985, Sullivan 2017a, b). In modelling these processes, both the solid phase (such as vegetation) and the gas phase (such as wind and hot gases released during combustion) and their interactions must be taken into account.

The physical model of a wildfire is written as a set of differential equations that describe the behaviour and interactions of the key processes and the change of each dependent variable in relation to another variable, usually in time or spatial dimension. Usually, the equations are non-linear and linked, creating a complex network of variables, coefficients, and parameters necessary to describe the behaviour of a given phenomenon and its evolution over time. However, the original form of a physical process is not necessarily easy to represent as a mathematical equation, and therefore assumptions and simplifications are often used. Due to the inherent non-linearity, the differential equations cannot usually be solved analytically. Instead, solutions are obtained using numerical calculation methods that provide approximate solutions to a set of equations. Physical model validation, testing, and evaluation are perhaps the most critical steps in the model development process (Alexander and Cruz, 2013). Comparing model results

with observation is the basis of validation, which measures the model's ability to accurately represent reality.

3. METHODOLOGY

In our approach, we used two different computational fluid dynamics (CFD) software, namely Fire Dynamics Simulator (McGrattan et al., 2023), and OpenFOAM (CFD Direct, 2024). In the following subsections (from 3.1 to 3.5), we present these tools, compare them in terms of usability and applications and describe the limitations of our approach in modelling wildfires and predicting extreme fire behaviour. Both selected CFD (Computational Fluid Dynamics) software are open-source programmes. FDS is a globally and widely used CFD based on fire simulation software in engineering and research applications, and it is specially designed for different kinds of fire simulations. OpenFOAM is a more general CFD software, and it is widely used for diverse CFD simulation tasks including combustion and fire modelling.

3.1 Computational Fluid Dynamics (CFD)

Computational fluid dynamics (CFD) is the science of using computers to predict liquid and gas flows based on the governing equations of conservation of mass, momentum, and energy. CFD is used wherever there is a need to predict fluid flow and heat transfer, or to understand the effects of fluid flow on a system. Fluid mechanics is a branch of physics that studies the physical behaviour of liquids and gases, i.e. changes in velocities, pressure, density, and temperature. These relationships are expressed mathematically by the Navier-Stokes equations, which are based on the laws governing the behaviour of viscous fluids. On the other hand, heat transfer studies how thermal energy is generated, stored, transported, and transformed. The main mechanisms it analyses are heat conduction, heat convection, thermal radiation, and phase transformations.

Due to the complexity of the Navier-Stokes equations, solving them accurately is possible only in the simplest cases. This is where numerical analysis and computers come into the picture, i.e. simulation. Using numerical approximations, CFD transforms complete differential equations into systems of linear equations, which are then solved at a finite (but often large) number of points in the problem domain, i.e. in the computational grid. In practice, the application of CFD to practical problems is limited by the available computing power.

The complicated nature of fluid flow makes modelling it on a computer inherently difficult. Multiphysics interactions, non-linearity, and unsteadiness are some of the complexities that make analysing fluids so challenging. Multiphysics interactions happen for example between air flow and a structure. Turbulence is an example of non-linearity in fluid dynamics, since turbulence affects other quantities like heat transfer and momentum, which in turn also affect turbulence. Unsteadiness means that the flow quantities at any fixed point in space change with time.

CFD has long been used to study the spread of smoke and fire in buildings, and recently it has been increasingly used to study wildfires as well (McGrattan, 2017). One of the biggest challenges in modelling wildfires with CFD is the characterization of burning

vegetation. For this, the so-called Lagrangian particles can be used, which act as sources and sinks at the subgrid scale, while the scale of the grid used to calculate mass, momentum, and energy can be hundreds or even thousands of meters. Vegetation particles have the advantage of being less sensitive to grid resolution.

CFD models are powerful research tools for studying fire dynamics, but their application requires evaluation against relevant experimental data. There are some studies (e.g. McGrattan, 2017; Mueller et al., 2021) in the scientific literature that show its promising properties, but also that further research and development is needed. In CFD fire modelling, equations that describe fluid flow and heat transfer are solved due to fire growth and spread, and fire behaviour problems may be addressed by fully physical models at different scales (Accary & Morvan, 2024). This approach to wildfire modelling enables the study of many basic physical phenomena that affect the behaviour of wildfires, such as the effect of wind speed, the effect of slope, the effect of fuel interruptions, the effect of the ignition process on fire dynamics, etc.

3.2 Fire Dynamics Simulator (FDS)

Fire Dynamics Simulator (FDS) is a computational fluid dynamics (CFD) model of fire-driven fluid flow. FDS solves numerically a form of the Navier-Stokes equations appropriate for low-speed (The Mach Number < 0.3), thermally driven flow with an emphasis on smoke and heat transport from fires (McGrattan et al., 2023, p. 3.). Fire Dynamics Simulator (FDS) is being constantly developed, and new versions are published regularly. First version was published in 2000. Main developer of the code is the National Institute of Standards and Technology (NIST). Software is meant for both practical fire safety engineering and fundamental fire research applications. FDS can be used to study behaviour of thermally driven flows, fire development and solid heat transfer in different environments. Typical environments include single buildings (varying from residential buildings to industrial), larger urban areas, wildlands, vehicles, and ships. FDS is globally widely used both for engineering and research applications, also in association with nuclear power plants. FDS Validation Guide (McGrattan et al. 2023) includes a large variety of conducted validation studies and their results. Also, extensive verification work has been conducted and documented (McGrattan et al. 2024b). U.S. Nuclear Regulatory Commission (NRC) has included FDS in their validation study of fire models used in nuclear power plant (NPP) applications, which has been documented in the NUREG-1824 report (NRC 2016). Of the studied models, FDS resulted, in general, in the most accurate results. FDS versions that were used for this work are FDS-6.7.7, FDS-6.7.9, FDS-6.8.0, and FDS-6.9.1.

3.2.1 General description of FDS

FDS is a CFD programme that was developed to model fires in built environment. The model has been enhanced so that it is capable of modelling outdoor fires also. FDS deals with the fire phenomena by dividing the problem in two phases: One is the gas phase, and the other is the solid phase. The fire (flame) is a gas phase phenomenon and FDS uses different kinds of reaction schemes to model gas phase combustion as demanded by the user. The gas phase combustion produces heat flow to the solid structures present in the simulation domain. The effect of the heat on the solid material is dealt separately

from the gas phase combustion processes. The pyrolysis reactions in the solid state produce gases (gas phase) and flammable pyrolysis gases are converted to an equivalent amount of the fuel gas(es) of the gas phase combustion process(es). The solid can also produce heat due to exothermic reactions like char oxidation. Exothermic reactions increase the solid temperature and the hot surface (or in depth, if semi-transparent material, i.e., absorption coefficient of the solid state is given as a user input) emits heat radiation to the gas phase domain. Also, the (possibly) hot pyrolysis gases could heat up the gas domain. The gases emitted from a pyrolyzing surface are assumed to have the same temperature as the surface of the solid. The pyrolysis reactions happening in the solid phase can depend on the properties of the gas phase, like the oxygen concentration at the solid surface.

The FDS solid state solver is, by default, one dimensional. There is also a possibility to use 3-dimensional solid solver, but it is not a very practical choice for, e.g., wildland fires, because the grid resolution in the gas phase should be quite fine so that the gridding in the solid state would be good enough. In the 3-dimensional case the solid-state gridding and the gas phase gridding are (somewhat) connected. But in the basic 1-dimensional (perpendicular to the surface) solver, the 1-dimensional heat conduction equation is independent of the gas phase resolution. Just the area of the solid surface in the gas phase gridding has some meaning to the gas phase – solid phase coupling. The solid forming one contact surface in the gas phase grid cell is treated as homogeneous in the horizontal dimensions, and just the perpendicular direction heat conduction equation is solved, i.e., the piece of solid is treated like an infinite planar surface. There can also be solid objects (“particles”) in FDS simulation that have some different kind of surface than an infinite plane. Particles might have cylindrical or spherical shape, i.e., the 1-dimensional solver is able to solve things using cartesian, cylindrical, and spherical coordinates. For example, a wildland fire load can be made from cylindrical particles introduced in the gas phase above the solid obstacle forming the ground to represent the fire load.

FDS software provides a range of simulation models for computation. In this work, Large Eddy Simulation (LES) mode is used in which convective heat flux at the boundary of solid material is defined by:

$$\dot{q}'' = h\left(T_g - T_S\right) \qquad 1$$

where, h is the heat transfer coefficient, T_g is the temperature of the gas, and T_s is the temperature of the solid material. The calculation of heat transfer coefficient, in general, is based on thermal conductivity of gas, Nusselt number, characteristic length of the obstacle, grid spacing etc., see the FDS Technical Reference Guide for further details (McGrattan et al. 2024b, Sec. 7.1.2).

The radiant heat transfer from the flame sheet also has to be accounted for solid material boundary condition. In FDS, to resolve a flame sheet, a very small cell size is required. When large cells are used then the temperatures in the actual reacting flame will not be captured in FDS disallowing the direct use of the source term T^4, where T is the temperature of the cell. The cells where combustion takes place, the radiative source

term I_b must be approximated. According to the technical reference guide of FDS (McGrattan et al. 2024), the source term is approximated as follows:

$$\kappa I_b = \begin{cases} \frac{\kappa\sigma T^4}{\pi}, Outside\ flame\ zone \\ C\frac{\kappa\sigma T^4}{\pi}, Inside\ flame\ zone \end{cases} \quad 2$$

where σ is the Stefan-Boltzmann constant, κ is the mean absorption coefficient and C is a constant that is computed at each time step. The volume integral of equation (4) is done to compute constant C:

$$\dot{q}_r''' = \kappa(x)[U(x) - 4\pi I_b(x)];$$

$$U(x) = \int_{4\pi} I(x, s')ds' \quad 3$$

where, $I(x, s')$ provides solution for the radiation transport equation of non-scattering gray gas, such that it is equal to the volume integral of $\chi_r \dot{q}_r'''$, where $\dot{q}_r'''$ is the heat release rate (HRR) per unit volume and χ_r is the global estimate for a fraction of energy emitted as thermal radiation (radiative fraction). The amount of radiant energy released from a flame typically range from 20% to 40% of total energy released (Karlsson & Quintiere, 1999). Generally, in a FDS simulation, there is only one gaseous fuel type combusted in the fluid domain. When it burns, it releases radiant energy as per the pre-listed radiative fraction (χ_r) already determined for some common fuels. For non-listed fuels, the user must give it as an input or else a default value will be used.

The overall net heat flux $\dot{q}_{net}''$ (convective and radiative) will define boundary conditions for conductive heat transfer to the sample material at its surface $(x = 0)$ and is given by:

$$-k_s \frac{\partial T(x,t)}{\partial x} = \dot{q}_{net}''|_{x=} \quad 4$$

where, k_s is the thermal conductivity of the material and $\frac{\partial T(x,t)}{\partial x}$ is the temperature gradient. Such heat transfer will increase the surface and inside temperature of the sample, resulting in temperature-dependent pyrolysis reaction rates (Torero J., 2016).

A solid sample surface which burns in FDS can be made of multiple layers of different materials. Such layers can consist of multiple material components which can represent one mass loss step in the model (Matala A., 2013). To account for pyrolysis, only the necessary number of effective reactions involving selected components are used in the model to capture the main characteristics of the pyrolysis. For solid materials, software allows to define the reaction rates and reaction mechanisms. For non-oxidative j^{th} reaction of i^{th} material at temperature T_s, the reaction rate (in default mode) is calculated as

$$r_{ij} = A_{ij} Y_{s,i}^{n_{s,ij}} exp\left(\frac{-E_{ij}}{RT_s}\right) \quad 5$$

A_{ij} is the pre-exponential factor, E_{ij} is the activation energy, R is the ideal gas constant, $n_{s,ij}$ is the reaction order and $Y_{s,i} = (\frac{\rho_{s,i}}{\rho_s(0)}$. $\rho_{s,i}$ is the mass of the i^{th} material component of the layer divided by the volume of the layer. $\rho_s(0)$ is the initial density of the layer.

For real materials, A_{ij} and E_{ij} are generally not available. At times, other model parameters like specific heat, heat of reaction, heat of combustion, thermal conductivity, reaction order, density, emissivity, etc. are also needed to be measured or estimated for FDS to carry out the pyrolysis. At least specific heat, heat of reaction, heat of combustion, thermal conductivity and emissivity can be estimated from Cone Calorimeter data using inverse modelling and optimization technique (Matala A., 2013). Others can be either measured or estimated through equipment like thermogravimetric analysis (TGA), microscale combustion calorimeter (MCC), or differential scanning calorimetry (DSC).

3.2.2 Wildland fire load description in FDS

To model the combustion of a solid fire load, one needs a model for the pyrolysis of the materials present in the solid phase. There are many ways of obtaining these model parameters to be used in the inputs of FDS. The FDS User guide (McGrattan et al., 2023) and FDS Validation guide (McGrattan et al., 2024b) contain some (example) models to be used to describe a general vegetation fire load. These pyrolysis reaction parameters are used in this work, i.e., no own pyrolysis model for vegetation is made. Also, some other material models found in the literature are used.

Basically, the wildland fire load description in FDS is like any other fire load that is typically used, e.g., compartment fire modelling. The underlaying pyrolysis reactions are same, the solid-state solver is the same, etc., but there are added some wildfire specific user inputs to help a modeller to model wildland fire cases. There are three different ways to model wildfire fire load. The modeller might choose one according to whatever criteria, but the fact is that the computing resources like the used computational grid resolutions dictate quite much, how accurate the fire load model can be. Also, the application case might have some effect. There might not be much knowledge about the actual fire load and its properties, so a detailed model cannot be used. Some quite average methods might be a first choice in these cases.

It should be noted that FDS simulations typically use a rectilinear computation grid, where the grid cell dimensions are constant in each computational mesh. Different computational meshes can have different dimensions, but they should match each other at the mesh boundaries so that the coarser mesh cells span an integer number of finer mesh cells. The advice given in the FDS documentation is that it would be advisable that the adjacent meshes have a factor of two difference in the linear dimensions of the cells So, there cannot be a fine gridding at the fire load compared to the neighbouring outdoor domain. This means that a compromise should be made on how finetuned the burning vegetation is represented vs. how large part of the burning landscape is considered. For present, a moderate table-top computer might be capable of dealing 10 M cells in reasonable time frame. For example. a domain 1 km in length, 500 m in width and 20 m in height could be covered using 1 m grid resolution. Above this “fine grid” area, there should be more sparce meshes above so that the wind and the fire induced flow (fire plume at least) is captured in the vertical direction. The 1 m grid resolution at the ground level still allows some fire spread modelling to be included, i.e., FDS will predict the fire spread, not just using some empirical correlations. Large supercomputers allow the computation domain to be extended substantially, though.

Outdoor simulations typically span hundreds of metres in the ground direction and tens of metres in vertical direction. Thus, the grid resolution is in the order of metres better than in the order of centimetres for outdoor simulations. And it should be noted that modelling a fire spread (indoor or outdoor) would require a grid resolution of the order of millimetres to have some predictive capacity. For a large outdoor fires, the spread might not need millimetre scale resolutions, because the fire spread is dominated by the large, mainly, radiative heating in front of the fire line and the details of the fire load are not described. And the reality is that every detail of a fire load (each tree, branch, needle etc.) can never be modelled.

The first method to represent the vegetation in FDS simulations uses Lagrangian particles (LP), that are heated by the convection and radiation. The second method, boundary fuel model (BFM), describes the vegetation as a porous solid on top of a solid ground. These two models predict the fire spread rate via the pyrolysis model given by the user. In the FDS User Guide (McGrattan et al., 2023, Sec. 17.1) there is a basic pyrolysis model, that can be used for the vegetation. The third method, level set model (LSM), uses purely empirical rules to set the fire front propagation rate for different wind speeds and vegetation types.

Method 1: Lagrangian particles (LP)

FDS uses Lagrangian particles to represent objects that are smaller than the grid resolution, i.e., they cannot be modelled as normal obstacles. FDS used (typically) rectilinear homogeneous meshing and the basic grid cell is typically a cube or close to it (aspect ratios less than 2), so, it is practically impossible to make the numerical grid fine enough to model the vegetation explicitly. Instead, leaves, grass, etc. vegetation can be represented as Lagrangian particles. Some representative particles can be chosen and modelled, and a weighting factor is used to scale the effect of the modelled particles to the actual number of the real particles. The particles can have similar surface properties like any other solid surface in FDS, e.g., the particle material might undergo pyrolysis reactions.

The drag coefficient, C_d, of particles is used to calculate the force per unit volume, f_b, exerted by the vegetation on the gas flow using equation:

$$f_b = \frac{\rho}{2} C_d C_s \beta \sigma u \|u\| \qquad 6$$

where C_s is the shape factor (default 0.25), ρ is the gas density, β is the packing ratio, σ is the surface area to volume ratio, and u is the gas flow velocity. The packing ratio is the mass per unit volume of the vegetation (=particles) divided by the vegetation material density. The surface area to volume ratio defines the particle diameter, $\sigma = 2/r$ for a cylinder, $\sigma = 3/r$ for a sphere, where r is the radius of the cylinder or sphere, respectively. For a plate, $\sigma = 3/\delta$, where δ is the half-thickness of the plate. Note that the size of the vegetation particle does not change as the moisture content of it changes.

The convention used in forestry for the moisture content is used in FDS, where the MOISTURE_FRACTION, M, is given as user input for the particles (or other surfaces as well). Moisture fraction is the mass of moisture (=water) divided by the mass of dry vegetation. The mass fraction of moisture, Y_m, is:

$$Y_m = \frac{M}{1+M} \quad 7$$

Method 2: Boundary fuel model (BFM)

If the vegetation layer of top of the ground surface is thin compared to the computational mesh of FDS used to solve the fluid flow, the fire load might be represented using the so-called boundary fuel model. The ground surface in BFM consist of a hard ground on top of which is a porous layer of vegetation and air. The porous layer exerts a drag on the fluid flow by a special boundary condition, and convective heat transfer in the porous layer is accounted using a source term in the heat conduction equation. The porous layer is assumed to be semi-transparent for thermal radiation and this is treated by the 1-D radiative transport equation similarly as for normal solid surfaces in FDS.

The drag coefficient, C_d, (default 2.8) is used to calculate the force per unit volume, f_b, exerted by the vegetation on the gas flow using equation:

$$f_b = \frac{\rho}{2} C_d C_s \beta \sigma \frac{h_b}{\delta z} u \|u\| \quad 8$$

where C_s is the shape factor of the subgrid-scale vegetation (default 0.25), ρ is the gas density, β is the packing ratio, σ is the surface area to volume ratio, u is the gas flow velocity, h_b is vegetation thickness, and δz is the height of the grid cell. Note that the LP and BFM could be intermixed, they can be given for same wildland fire area, e.g., the ground shrub and litter might be modelled using BFM and Lagrangian particles might be added to represent large trees on top of the BFM surface.

Method 3: Level set model (LSM)

Simulating wildland fires that occupy large areas are difficult with above mentioned FDS vegetation models. The computation domain cannot be gridded finely enough for large areas and the ability of FDS to predict the fire front spread is lost. In these kinds of cases, a solely empirical level set model can be utilized. This empirical model based on level sets reproduces the approach used in the Lagrangian-based fire front-tracking model FARSITE (Finney 2004). The Rothermel-Albini (Rothermel 1972, Albini 1976) fire spread rates are used, and each fire front point is a starting point of an ellipse-shaped fire front that evolves according to the wind, slope and vegetation conditions.

3.2.3 Wind simulation in FDS

There are different ways to model wind in outdoor simulation in FDS as mentioned in FDS User Guide (McGrattan et al. 2023). In this report, just the so-called Wall-Of-Wind (WOW) method and the Monin-Obukhov similarity theory (MO) are used. The third option would be geostrophic wind and let the wind to develop naturally. This would utilize a domain that spans kilometres and, thus, are too large for the present purposes, where the wildland fire load is wanted to be modelled closer to “each tree” level. The fourth option would be just specifying a wind speed and direction, but this was not utilized, because the MO method is basically doing the same thing, but in a better way, e.g., including the atmosphere stability class and aerodynamic roughness information. The WOW method is closer to a wind tunnel type scenario, but the wind speed can have a power law profile at the external boundary. The drawback of the WOW method is that the other methods use more natural boundary conditions on the lateral boundaries than the WOW method.

The WOW method is used despite of this drawback in this work because it is checked how well this quite simple method performs. The WOW method might be better suited for situations like microburst, where a strong, quite homogeneous flow hits a part of a forest, i.e., the situation is not like an ordinary wind.

Wind method 1: Monin-Obukhov similarity theory (MO)

Monin-Obukhov similarity theory has vertical wind speed and temperature profiles that are based on surface and atmospheric conditions. The aerodynamic roughness length, z_0, describes the landscape like "sea", "roughly open" according to Davenport-Wieringa roughness length classification. The Obukhov length, *L*, describes the thermal stability of the atmosphere like "Very Unstable", "Neutral", "Stable". The wind profiles are set on the exterior boundary of the computational domain so the domain should be about flat at these boundaries. The domain could have features "in the middle", i.e., away from the domain boundaries. This includes also the +z (sky) boundary. And this applies also to the fire plume since it should not rise too strongly upwards at the sky boundary. At least the good practices for domain size selection recommended in (Wegrzynski W., 2018) are suggested to be followed. It should be stated that even though the modeller knows the good practices, it might not be straightforward to follow these due to the limitations on computational resources, thus, some compromise between good practices and computational efficiency is typically needed.

Wind method 2: Wall-of-wind method (WOW)

The wall-of-wind method just describes the incoming wind as a power law wind profile at an external boundary of the computational domain. The wind will be along *x* or *y* axis of the simulation geometry, and this could be a problem in some cases, e.g., wind direction changing with time, typical rectangular building geometries that are best constructed matching the *x* and *y* axis to match the rectilinear computational grid used in FDS. But for the present study, this limitation does not matter because the object of current simulations is to study the fire front propagation in the downwind direction.

3.3 OpenFOAM

3.3.1 General description of OpenFOAM

Abbreviation OpenFOAM stands for Open Field Operation And Manipulation. OpenFOAM is an open-source C++ toolbox for the development of customized numerical CFD. OpenFOAM has an extensive range of features to simulate for incompressible, compressible, laminar, and turbulent flow regimes. OpenFOAM can be used in various applications such as process engineering, environmental engineering, automotive, marine, wind power, nuclear, fires, combustion, chemical reactions, heat transfer, liquid sprays, films, and many others. Additionally, it allows to implement any modifications and introduce any additional sub models.

3.3.2 OpenFOAM modelling of the grass fires

OpenFOAM is a general-purpose software that does include facilities for fire and combustion modelling, but it does not include specific models for outside fire simulations. For the grass fire simulation, the following sub models were implemented:

- Non uniform boundary condition for the wind velocity (where the wind velocity is modelled as a function of height)
- Source term for k and omega due to drag caused by forest canopy
- Prescribed ignition of the grass
- Weighted-sum-of-grey-gases radiation model

Grass is modelled as Lagrangian particles. For different type of vegetation physical and fuel properties are declared, such as specific surface area, fuel moisture, volatile matter, fuel composition, calorific value, etc. Several classes of Lagrangian particle clouds with different properties can be declared. Initialisation of Lagrangian particles is done in one or several computational cells. Computational meshes for the cases considered below were typically adapted in the lower area depending on the vegetation height. Typical size of the computational mesh in the upper part of the domain (atmosphere) was ranged from 1 to 4 meter, while in the bottom the mesh size was matching the prescribed height of the grass. If mesh size was smaller than the height of the grass, Lagrangian particles were set uniformly in each computational cell of the grass.

A sub-model for the line grass ignition was introduced. Ignition of the grass was modelled as a forced high temperature in the prescribed area. With the line ignition, the width and ignition speed were prescribed as model parameters representing two persons walking in the opposite direction and igniting the grass. High (1000 K) temperature was forced for a prescribed time interval (10 s) (these parameters are chosen), while the position of the ignition is defined by parameter of the validation case (described later).

The turbulence model used in the simulations was a scale adaptive version of k-omega-SST which is a hybrid RANS-LES model (Egorov et al. 2008). For the combustion of volatile gases, a standard eddy dissipation concept combustion model was utilized (Magnussen 2005).

3.3.3 Developing a method for analysis of OpenFOAM simulation results

During the project more than hundred OpenFOAM CFD simulations were conducted. Therefore, an effective method for an analysis and comparison of the simulation results should be selected. One of the main characteristics of fire propagation is the rate of spread, i.e. the speed with which the fire front is propagating forward. Assuming the domain is large enough, fuel distribution is uniform, and the wind does not change in time, the rate of spread can be constant for each simulated case. It should be noted that the simulation should be well developed in time along with the similar conditions for the fire front propagation to have constant rate of spread. Thus, each simulated case can be characterized with one value of the rate of spread and these values can be easily compared.

Figure 3a shows an illustration of the simulated result at some point of time. Simulations was started with the uniformly distributed fuel. Consider a cross-section plane inside the grass area (constant height with h<grass height, in the illustration h=1.2m while the

height of the grass is 1.5 m). The presence of the fuel (tangerine colour) in the certain part of the computational domain indicates the unburned grass, violet colour means ground without the grass (if grass is burned or was not presented at all). Isosurface in *Figure 3a* illustrates the surface with constant temperature. This means that the air temperature on this surface is constant and equal to prescribed value, in this case 700°C=973K.In each of the time moment the fire front position and the amount of unburned grass is different. The goal was to develop a method for evaluating the rate of spread from these simulation results. Two options of the fire front propagation speed were developed.

- ROS based on temperature.
- ROS based on unburned grass.

The evaluation of the fire front position is demonstrated in *Figure 3*. Fire front position can be either defined as largest distance of the temperature iso surface (*Figure 3b*), or as a line, where grass is already burned (*Figure 3c*). Fire front position as a function of time from ignition is presented in *Figure 4* for both methods. The slope of the curve corresponds to the derivative of the position by the time [d (m)/d (s)], namely the speed of propagation of the fire front in m/s, which is the rate of spread. Sensitivity of the fire front propagation to the selected iso value of the temperature is investigated. *Figure 4a* presents simulation results with various iso-surface temperature. As it can be seen, the fire front propagation is very similar. Their difference can be seen better in *Figure 4b*, which shows the same pictures at a different scale.

Even if the iso-surface of the temperature is always located further than unburned grass, the speed of their propagation is very similar. Therefore, one method can be selected for the further use. Since the implementation of burned grass method requires considering (e.g. the areas, where the grass was cut by purpose around the measuring towers), the method of the iso-surface seems to be easier. Several numerical tests demonstrated the close agreement of calculated rate of spread, therefore, only one method will be used in the further study.

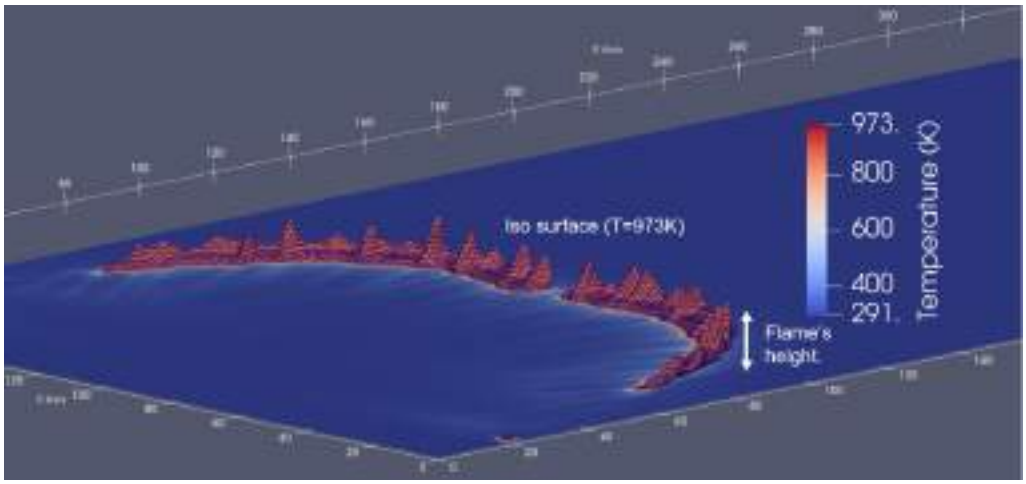

Figure 1. OpenFOAM simulation results. Illustration of the fire front and fire flame's height.

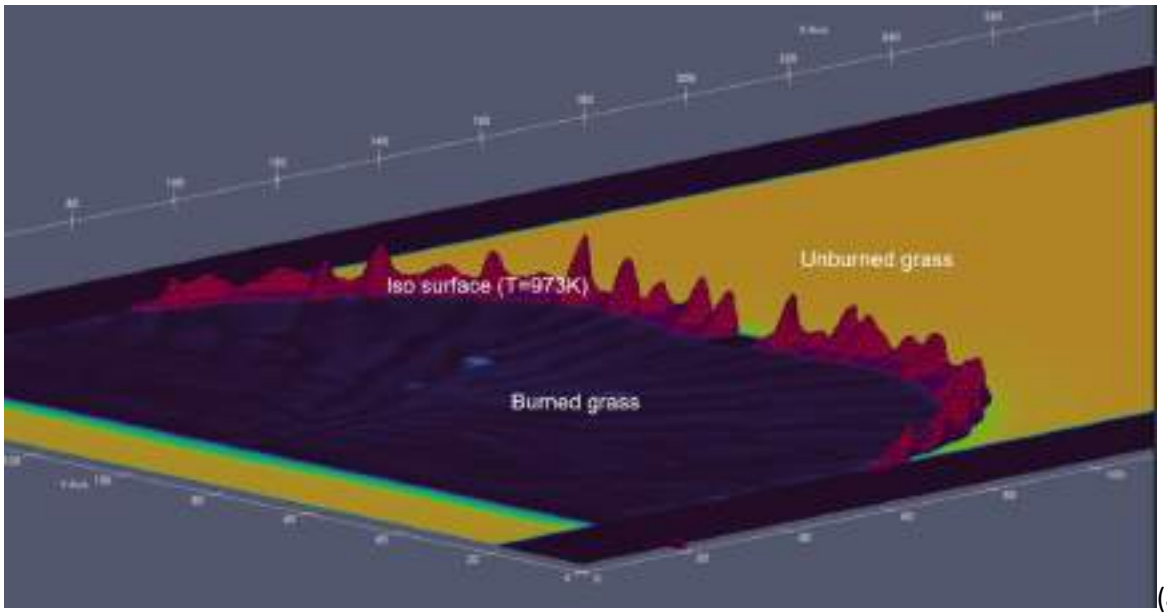

(a)

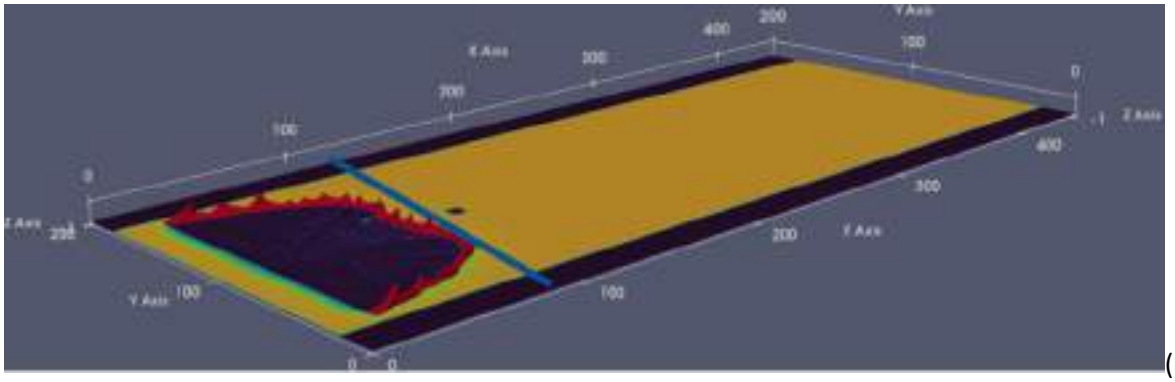
(b)

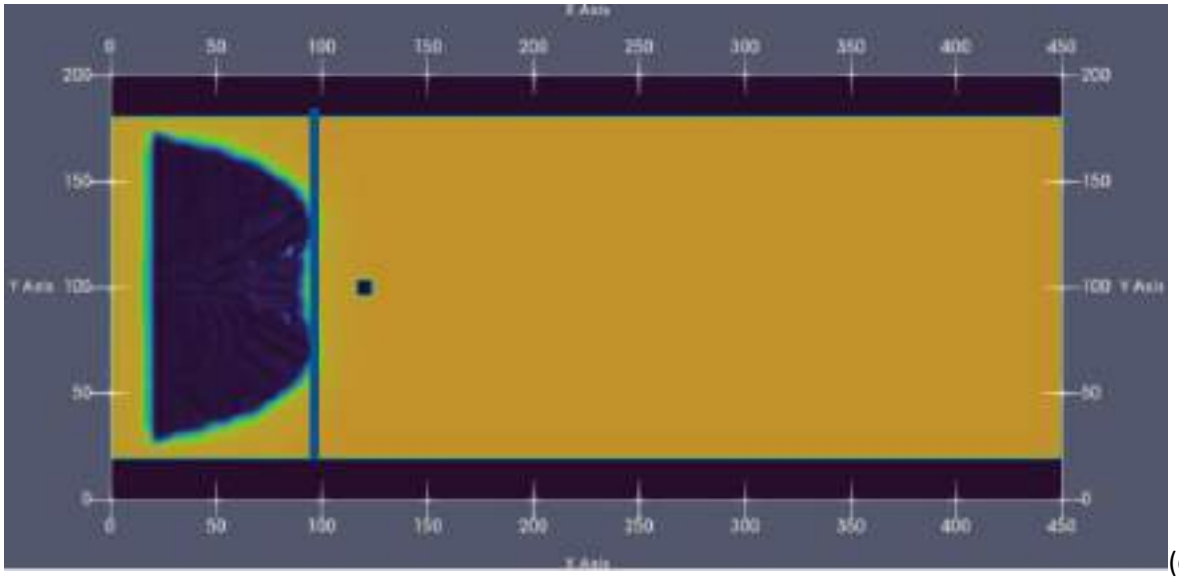
(c)

Figure 2. OpenFOAM simulation results. Illustration of fire front propagation (a), evaluation of the rate of spread based on temperature (b) and based on burned grass (c)

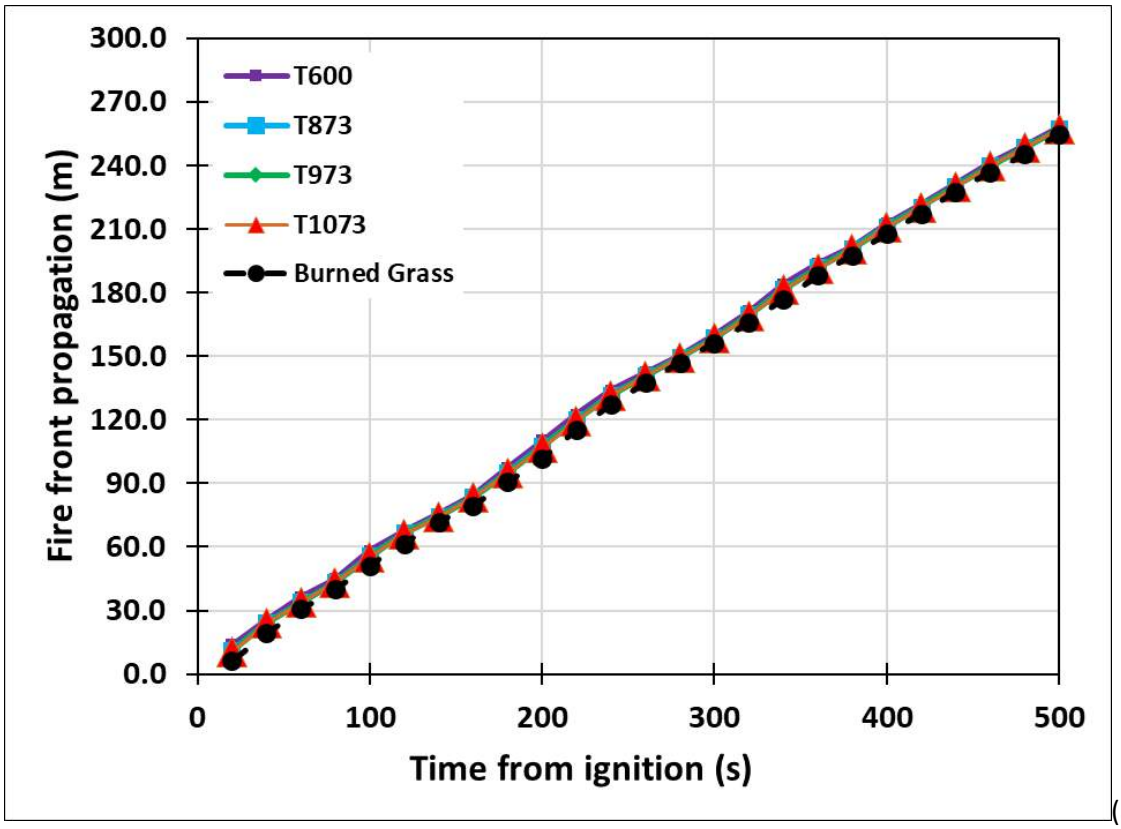

(a)

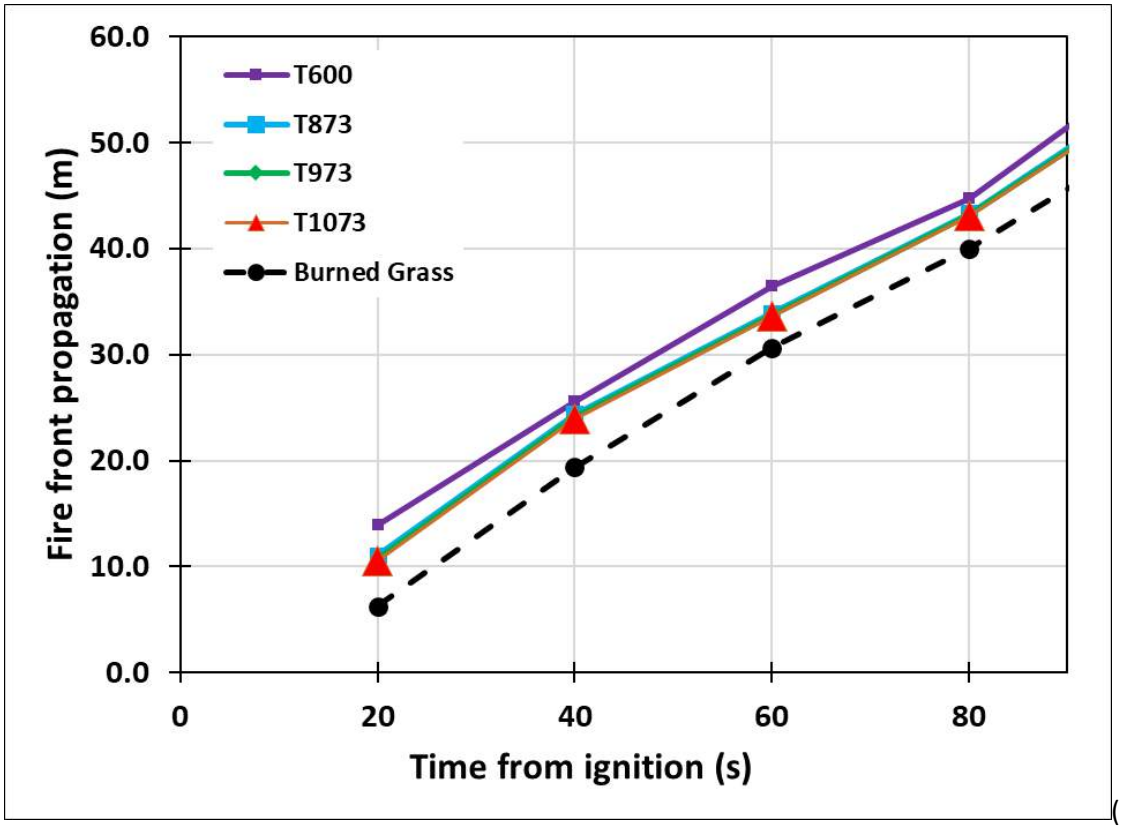

(b)

Figure 3. OpenFOAM simulation results. Calculation of the rate of spread based on different temperature iso-values and based on burned grass. Scale 0–500 s (a) and zoomed 0–90 s (b).

Moreover, from the simulation results the flames heights can be estimated as a height of the peaks of temperature surface see *Figure 2*. Typical temperature value characterising the flames can be considered 700-800°C = 973-1073 K. The flame lengths are not uniform along the fire front and as a function of time. Due to random nature and not strictly defined method this is only indicative value. In the current research it was selected to estimate flame's heights from the temperature surface with value 700°C=973K.

3.4 Differences between the tools

The main difference between FDS and OpenFOAM lies in the implementation of the software and the various sub-models required for fire modelling. FDS is a specialized combustion CFD tool with models adjusted specifically for fire simulation. This specialization provides FDS with a broad array of built-in sub-models and a wide range of preset fuel properties, which simplifies the setup of new cases, as long as the required sub-models are available.

OpenFOAM is a general purpose CFD software which is very capable and widely used. However, despite the wide application areas, it may not include all the desired sub models for fire simulations and some features may need to be implemented by the user. This does require certain experience from the user for coding the new sub models and coding of result pre/postprocessing.

In principle, the two software codes can use the particle model to represent wildland fire load, and, with the certain selection of sub models and model parameters, they should provide identical results. However, not all the sub models are comparable, therefore, there are differences observed in the simulation results.

Some current differences in implementations are listed below. These are presented in the current implementation of FDS/OpenFOAM.

- The basic numerical approaches, such as finite volume discretization, linear solvers and turbulence modelling approaches are different even though the basic approach is similar. There was no attempt to harmonise the approaches and instead the default or readily available settings and models of both software were used.
- OpenFOAM implementation does not include any possible burn of the ground below the grass as well does not consider heat capacity of the ground.
- For the grass fire simulations presented in the report, the meshes in FDS are not adapted, but they are uniform in all the areas. In general, OpenFOAM is more flexible with respect to the mesh. The mesh cell sizes used in the current OpenFOAM simulation are generally larger in the upper part of the model (atmosphere) and smaller near the ground where the fuel is located. In the case of low grass, the grid was adjusted so that the height of the grass is divided into several calculation cells. Thus, the aspect ratio of the most cells with vegetation is far from one (i.e. cells with aspect ratio e.g. up to 40 can

appear), whereas in the FDS simulations cubic cells were always used. The FDS documentation states that aspect ratios larger than 2 should not be used.

- Lagrangian particles initialisation is different in the current simulation of the grass fires. In grass simulations, FDS simulation typically includes only one cell in the vertical direction, where the Lagrangian particles representing the fire load are placed. Moreover, it is common to use larger cell height than the grass height. In OpenFOAM several different initialisation strategies were considered.
- Fuel ignition is implemented differently in FDS and OpenFOAM. The first one brings the gaseous fuel source with prescribed power that is instantly ignited if there is available oxygen present at a mesh cell, while the second uses a sub model that introduces high temperature constrain for in the prescribed area and time. However, both ways can well represent the validation experiments and consider prescribed ignition speed and ignition areas.
- Lagrangian particles pyrolysis is treated using one-dimensional heat conduction equation in FDS utilizing either cartesian, cylindrical, or spherical coordinates according to the user inputs. The vegetation undergoes an Arrhenius type pyrolysis reaction that evaporates the moisture, pyrolyzes the dry vegetation to char, and oxidates the char to ash. OpenFOAM has a similar approach, but the particles are treated as zero-dimensional spherical particles.

In addition to these differences, post processing, result collection and visualisation are different in FDS and OpenFOAM. For FDS there is a specific software (Smokeview; Forney, 2007) for the visualisation of the simulation results. OpenFOAM does not have any graphical interface at all. ParaView software is used for visualisation and all visualisation does not include any specific properties unless they are computed in the simulations or evaluated based on the known properties.

3.5 Limitations of the methodology

The CFD simulation approaches are mainly limited on how the fire load and the pyrolysis reactions are described and by the computational resources available for the simulations. In general, the accuracy of simulations depends quite heavily on the accuracy of the underlaying computational grid. This grid resolution sets the ultimate limit on how detailed the outdoor fire load description can be and increasing grid resolution quickly scales up the computational cost of the simulations.

However, besides the computational cost, often a more limiting factor is the availability of data on the detailed fire load of a specific fire case. Typically, there is no exact information on the level of each tree, each bush, etc., so the more general information on the (generic) forest fire load should be interpreted somehow to the level allowed by the simulation grid resolution. Also, when modelling the pyrolysis reactions and combustion, both software could use sophisticated models. However, usually there is only very limited amount of data available and thus the modelling approaches need to be quite simplified and generic so that they can be practically applied.

Also, the size of the practical simulation domain brings additional limitations regarding how the wind and atmosphere can be modelled. Both FDS and OpenFOAM can simulate some effects that should be included in the modelling of natural wind, but they are not meteorological software, so their ability to describe wind might be incomplete.

Typically, for example, when using FDS, the scope of outdoor simulations is very limited, so the wind cannot be described on an atmospheric scale, nor can the interaction between fire and the atmosphere or cloud formation caused by fire (pyrocumulonimbus) be simulated. There were some tests made to find out the limitations of FDS for present use in this project. They are summarized shortly in the next section.

3.5.1 Preliminary tests of outdoor simulations using FDS

Different ways to model outdoor fires using FDS were tested for some fire scenarios. Some limitations of FDS became apparent, most pronounced is the need to use relatively large computational domains to simulate natural wind scenarios to some accuracy. This means that the number of simulations is limited due to the required computing time restrictions. The description of the burning fire load has also restrictions, some of which arise from the used computational grid resolution. The fire load cannot be described in more detail than is the underlaid computational grid used for the CFD calculation. There are also other than computational limitations regarding to outdoor fire simulations, most notably the available data on the fire load and its properties as well as the meteorological and landscape related information. But the emphasis of the test simulations was related to the computational parameters of FDS.

The test simulations were addressing following aspects:

- The wind modelling methods of FDS:
    - Monin-Obukhov similarity theory (MO) for natural wind
    - Wall-Of-Wall (WOW) method for wind tunnel type situation
- The computational domain size effects and applied boundary conditions at the exterior boundaries:
    - Lateral and vertical dimensions of the domain
    - Periodic boundary conditions for the side boundaries
- Modelling a forest fire like scenario using a “tree trunk forest” as an example:
    - This allowed much larger fire line intensities than grass fires and, thus, the resulting fire plume was rising much higher and affecting the wind flow much more.
    - This case was also used to estimate how large domain could be simulated in a forest fire scenario, where each individual tree is resolved in the numerical grid.
- Outdoor heptane pool fires were simulated with different wind speeds:

- The "CPR 14E Yellow Book" (van den Bosch & Weterings, 2005) has empirical correlations for outdoor oil tank fires. These were used to check the validity of FDS (and the present modeller) to reproduce these experimental findings.
- To give insight on the required computational domain size and effects of boundary conditions at the exterior boundaries.

3.5.2 Preliminary tests of outdoor simulations using OpenFOAM

The focus of the preliminary OpenFOAM simulations was on the development, coding, and testing of the submodels needed in outdoor fire simulations, as well as the postprocessing of the results.

Preliminary test simulations with OpenFOAM dealt with the effect of the following factors on the functionality and results of the simulations:

- Dimensions of the calculation domain,
- Mesh size and mesh adaptation,
- Velocity boundary condition (3 different velocity inlets were implemented for wind simulation),
- Model parameters and fuel properties,
- For the forest fire several options of introducing the trees were tested (various Lagrangian particles initialisation, Lagrangian particles properties, porous region declaration etc).

4. VALIDATION OF THE METHODOLOGY

Numerical models, such as CFD models, are increasingly used in safety and consequence analyses, and the validity of these models is usually determined by benchmark testing. This is done quantitatively by measuring the agreement between the predictions given by the model and the observations made in the real world. In this approach, it is essential that all variables relevant to a specific study are sufficiently monitored in experiments representing the real world and, in the predictions, made by the model (Borg et al., 2014).

Since the modelling interest of the Living Labs of the FIRE-RES project was mainly focused on the regional scale, it was not possible to obtain sufficiently accurate experimental data from the areas in question for the validation of the CFD models. Therefore, we were looking for applicable data in the scientific literature. The fire tests that we used to test the suitability of the CFD models presented above for the simulation of wildfires were originally and specifically designed for the validation of simulation models and have been used for that purpose in the past.

One of the selected cases was the tall grass fire in prairie. The corresponding experiment took place in 2006 at Houston Coastal Centre, Texas, USA. Simulation results demonstrated that the fire line intensity ranges from 3000 kW/m up to more than 10000 kW/m depending on the conditions of the case, such as wind velocity and the amount of

growing grass. According to wildfire events classification based on Tedim et al. (2018), presented in *Figure 1*, typically a prairie grass fire belongs to category 4, which is a strong normal fire event. In certain conditions, a grass fire can be classified as a category 5 fire, which is already an extreme fire event.

The burning of Douglas fir tree was selected as another validation case. Experimental results for the mass loss rates of fir trees are available in Mell et al. (2009) for the cases with different tree sizes and combustion parameters. Validated FDS model for the fir trees is essential for the further forest fire simulations.

4.1 Validation simulations of grass fires (with FDS and OpenFOAM)

Two different CFD based simulation methods, FDS and OpenFOAM, are used in this work to conduct outdoor fire simulations of burning wildland fire loads. Three validation cases were chosen for the model validation.

Two cases are derived from the Commonwealth Scientific and Industrial Research Organisation (CSIRO) grass fire scenarios (case F19 and C064), which are typically used for the FDS validation (McGrattan et al., 2024b). The third case is Fireflux described in (Clements et al. 2007 and Clements et al. 2008). Unlike the previous cases, not any validation results from this case were used to optimise the FDS simulation parameters. Therefore, it can be considered as a good validation simulation for FDS.

To the best of our knowledge, none of these cases were simulated in OpenFOAM before, or at least these results are not reported in the literature. During the project several specific submodels were custom made in OpenFOAM for the outdoor fire modelling of grass fires and these are not available in the general OpenFOAM installation.

4.1.1 CSIRO grass fire experiments

During summer 1986 controlled grassland fire tests were performed in Australia by CSIRO. Two of those tests were used in the FDS Validation Guide (McGrattan et al. 2024b) as validation cases. Those two tests are also used as validation cases in the present work. The experiments were conducted in a warm and dry weather in the middle of the dry season with fully cured (dried) fire loads. The test C064 had 100 m × 100 m area of kerosene grass, the test F19 had 200 m × 200 m area of kangaroo grass. The measured properties during the tests are summarized in the FDS Validation Guide (McGrattan et al. 2024b: *Table 3.6*) and they are represented in *Table 1*.

Table 1. The CSIRO grassland fire case properties (taken from McGrattan et al. 2024b: Table 3.6).

	F19	C064
Wind Speed (m/s)	4.8	4.6
Temperature (°C)	34	32
Surface-area-to-volume (SAV; 1/m)	12240	9770
Grass Height (m)	0.51	0.21
Moisture Fraction (%)	5.8	6.3
Bulk Mass per Unit Area (kg/m^2)	0.313	0.283

4.1.1.1 FDS simulations of the CSIRO F19 experiment

In *Figure 4* the FDS simulations of the CSIRO test F19 are compared to the experimental fire front positions. The FDS results are in reasonable agreement with the experiments. The FDS results shown are practically the same as in the FDS Validation guide (McGrattan et al., 2024b) because the same input files are used (FDS version 6.9.1 was used). The three different ways to describe the wildland fire load are used in the simulations: "LP" Lagrangian particles are used to describe the fire load, "BFM" Boundary fuel model is used, and "LS" empirical Level set model. The FDS simulations were using three different computational grid resolutions "crude", "mid", and "fine". Note that not all grid resolutions were used in each different fire load options in the present simulations. Some of the fine gridded simulations would have needed considerable large computational resources and there was no actual need to conduct these simulations as the same outputs are already reported in the FDS Validation Guide.

The experimental grass fire front in CSIRO test F19 can be seen in the FDS Validation Guide (McGrattan et al., 2024b: *Figure 3.7*). From *Figure 5* to *Figure 7* show snapshots of the FDS simulations at times 56 s, 86 s, and 138 s.

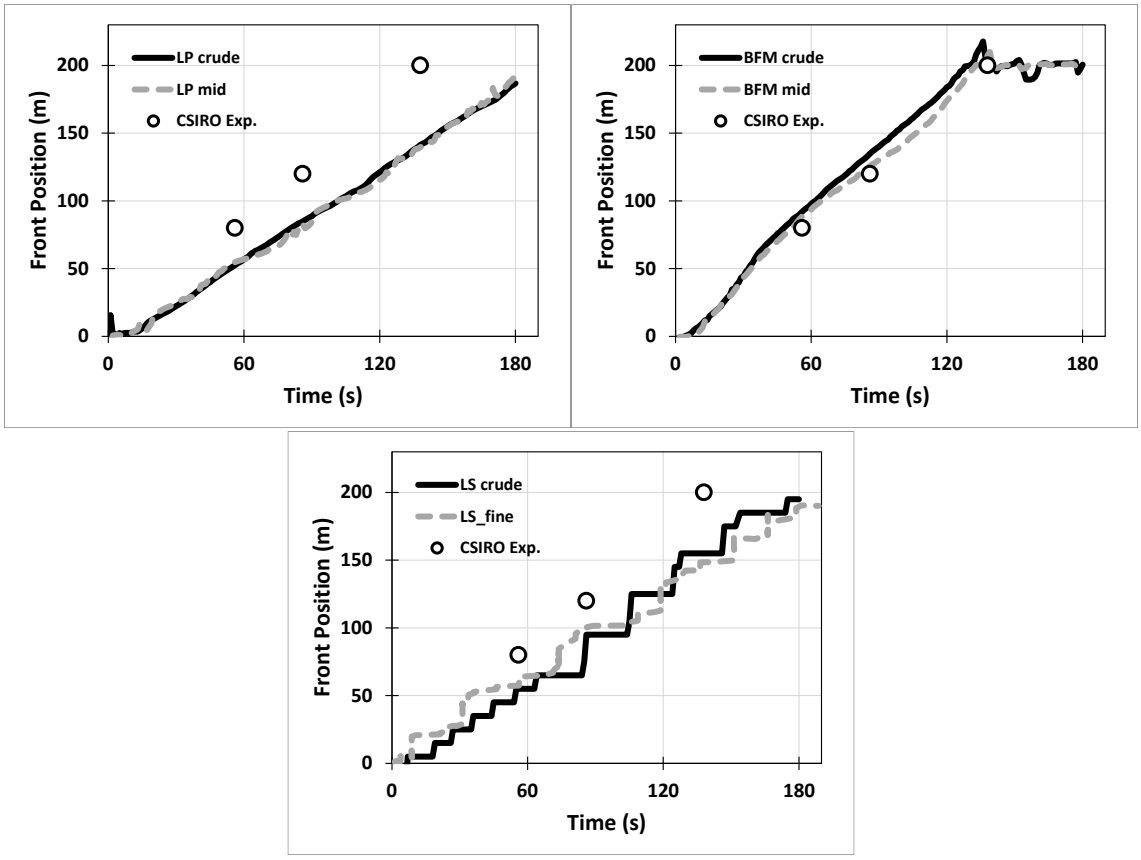

Figure 4. FDS simulations of CSIRO grass fire test F19 compared to experimental fire front position. Shown are results of FDS models, where the fire load was described as Lagrangian particles (LP), as Boundary Fuel Model (BFM), and as a Level Set model (LS) for different computational grid resolutions (crude, mid, fine).

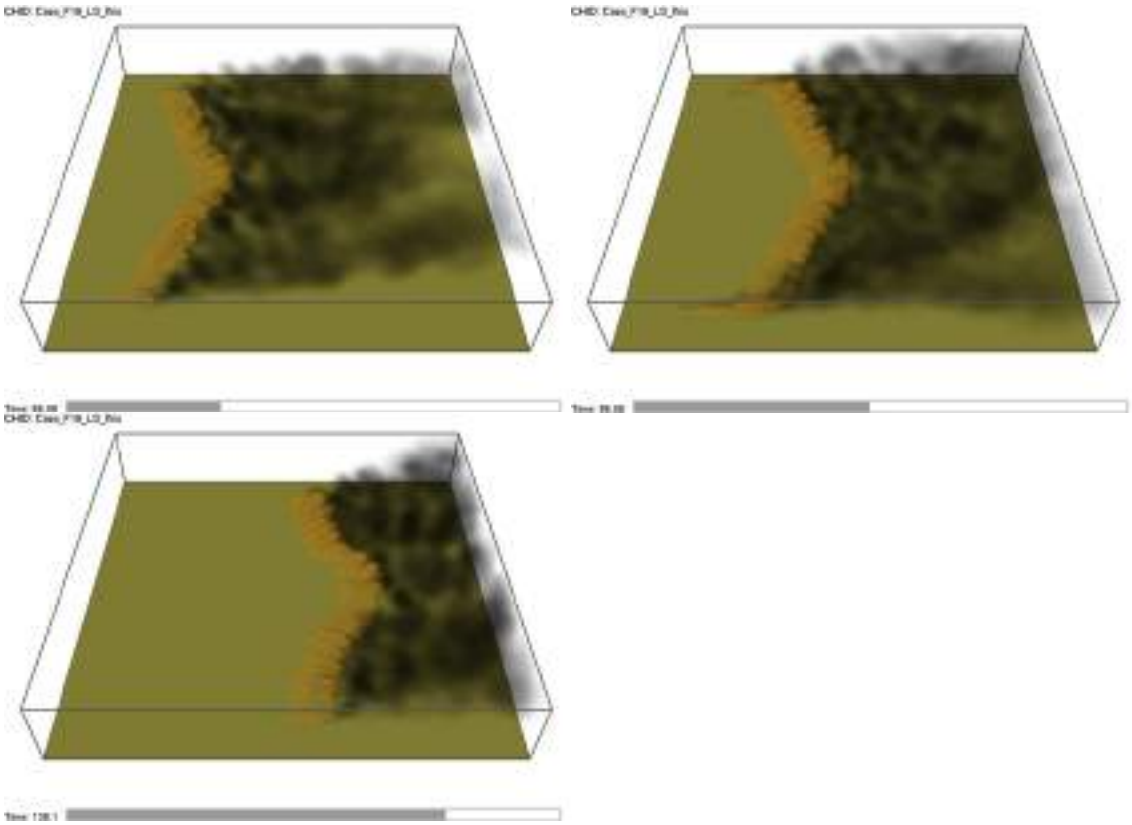

Figure 5. Snapshots of the FDS simulation of CSIRO test F19 using the empirical level set method to describe the fire load.

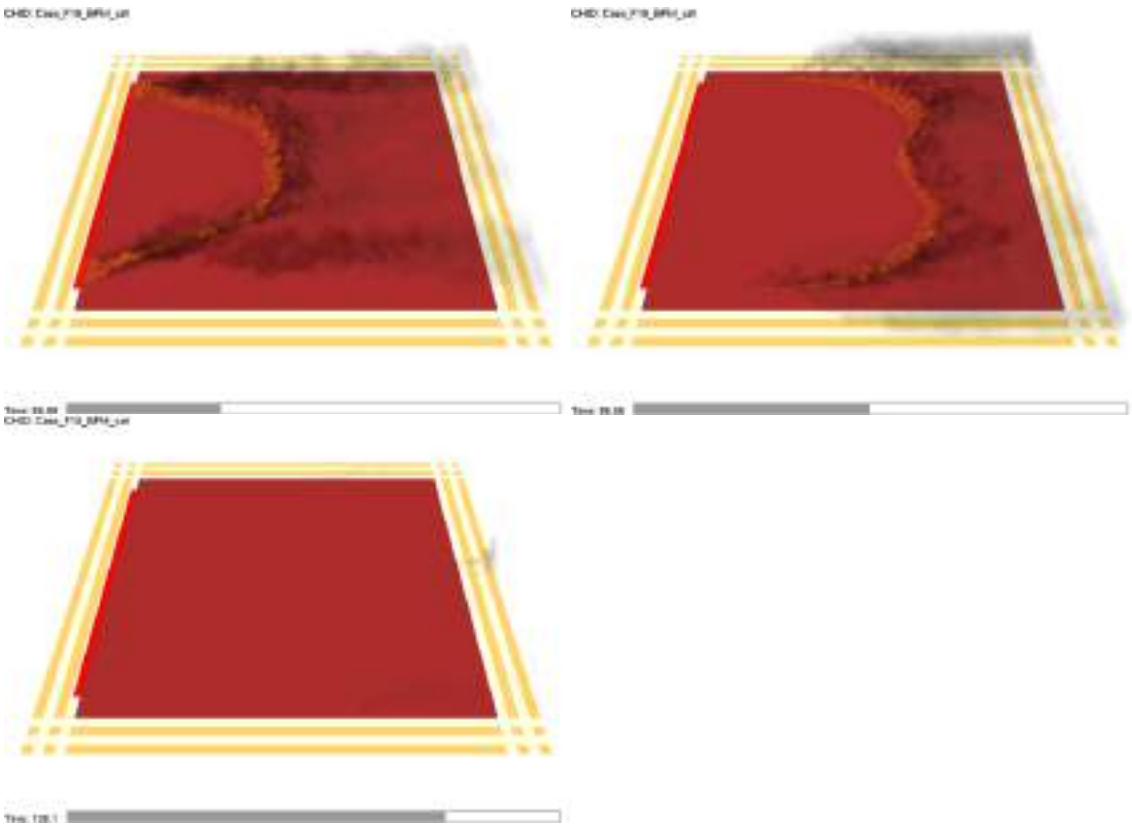

Figure 6. Snapshots of the FDS simulation of CSIRO test F19 using the boundary fuel model to describe the fire load.

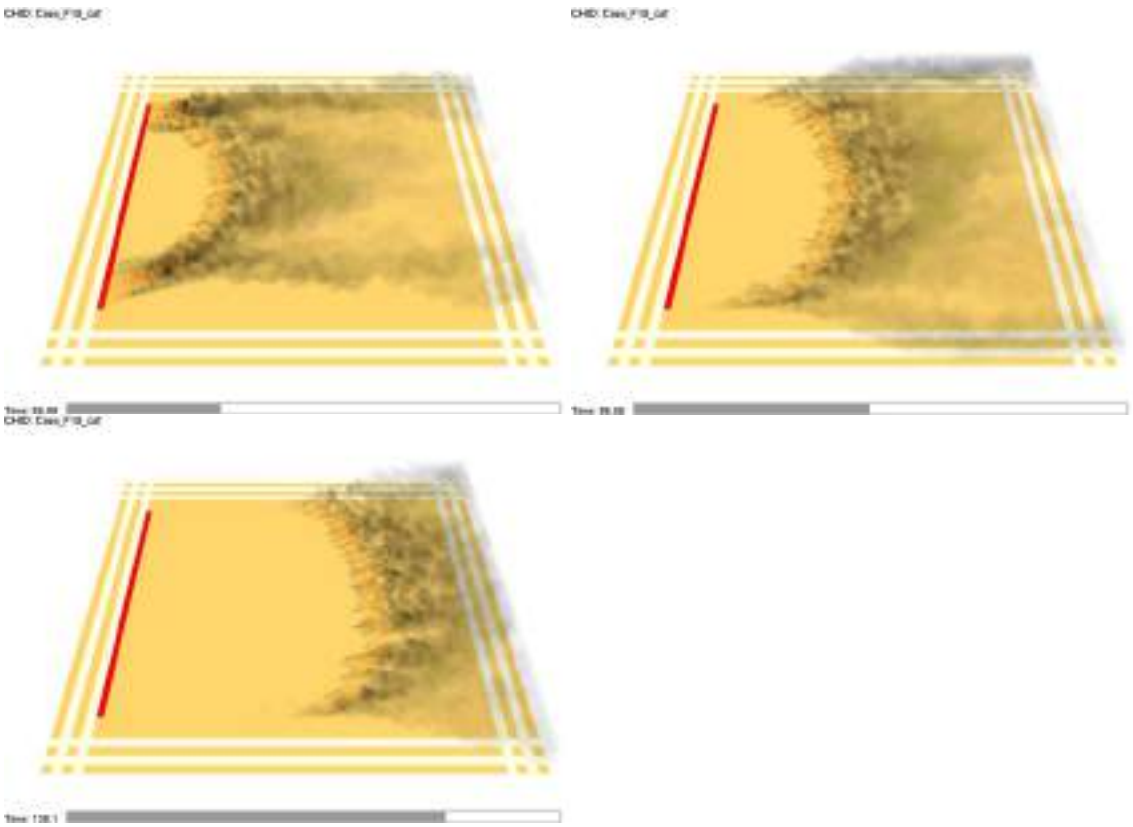

Figure 7. Snapshots of the FDS simulation of CSIRO test F19 using Lagrangian particles to model the fire load.

4.1.1.2 OpenFOAM simulations of the CSIRO F19 experiment

Simulation parameters for OpenFOAM simulation for the case F19 are presented in *Table 2*. Several computational meshes were tested. Mesh for the simulations were adapted in the lower area. Thus, top part of the mesh includes cubical cells with size of 4 m. Lower part of the domain includes cells with 1 m cubical cells. The grass surface and small area above the grass was set up with rectangular blocks with smaller heights, at the same time horizontal coordinates of the mesh were kept constant at 1m sized. The height of the grass in the case of F19 was 0.51m. This was divided either in 1 block (i.e. mesh cell dimensions was 1*1*0.51m, Case 4), 2 blocks (i.e. mesh cell dimensions was 1*1*0.255m Case 1 and Case 3), or 4 blocks (i.e. mesh cell dimensions was 1*1*0.1275m, Case 2). Case 3 includes more smaller blocks above the grass area.

OpenFOAM simulation results for the validation case F19 are presented from *Figure 8* to *Figure 9*. *Figure 9* illustrates the comparison with validation data. At the beginning fire front propagates in a close agreement with the validation data, while in the later stage the speed of the fire front propagation is underestimated. The best agreement is achieved in Case 1. Figure 8 illustrates that the simulated fire front in this case is not symmetrical. Horizontal component of velocity is observed to the direction of the fire front.

Estimated typical heights of the flames range from 2 to 3 meters, with few higher fire flames reaching up to 4 meters. This is 4–5 times larger than the height of the grass.

Table 2. Parameters used in OpenFOAM simulations of the CSIRO grassland fires (cases F19 and C064).

	Case F19	Case C064
Domain in CFD simulations	**240m * 240m * 200m grass 200m * 200m**	**140 * 140m * 200m grass 100m * 100m**
Height of the grass	**0.51 m**	**0.21 m**
Mass of the grass	**0.313 kg/m2**	**0.283 kg/m2**
Surface to volume ratio	**12240 (1/m)**	**9770 (1/m)**
Velocity inlet	**Constant value 4.8 m/s**	**Constant value 4.6 m/s**
Speed of ignition	**1.56 m/s**	**1 m/s**
Ignition area	**(20-23.3) * (33-187) * 0.51**	**(20-21.6) * (45-95) * 0.21**
Temperature	**307 K**	**305 K**
Fuel composition:		
Fuel moisture	**5.8 %**	**6.3 %**
Volatile matter	**80 %**	**80 %**
Solid mass fraction	**0.1884**	**0.1874**
Solid C	**0.98**	**0.98**
Solid ash	**0.022**	**0.022**
Net calorific value, dry	**15.6 MJ/kg**	**15.6 MJ/kg**

Figure 9 also includes fire front propagation of the Case 4. In this case, grass area includes only one computational cell in z direction. The results demonstrate large underestimation of the rate of spread. Moreover, heights of the fire flames for this case are the grass height, up to 0.55m only. Thus, in OpenFOAM simulations the mesh size can significantly affect the simulation results. However, it should be also noticed that variations on the meshes did not significantly change the rate of spread, provided that the mesh in the grass area contains at least several computational cells. Considering that none of the model parameters were adjusted based on the validation results, the OpenFOAM simulation results represent the case quite well.

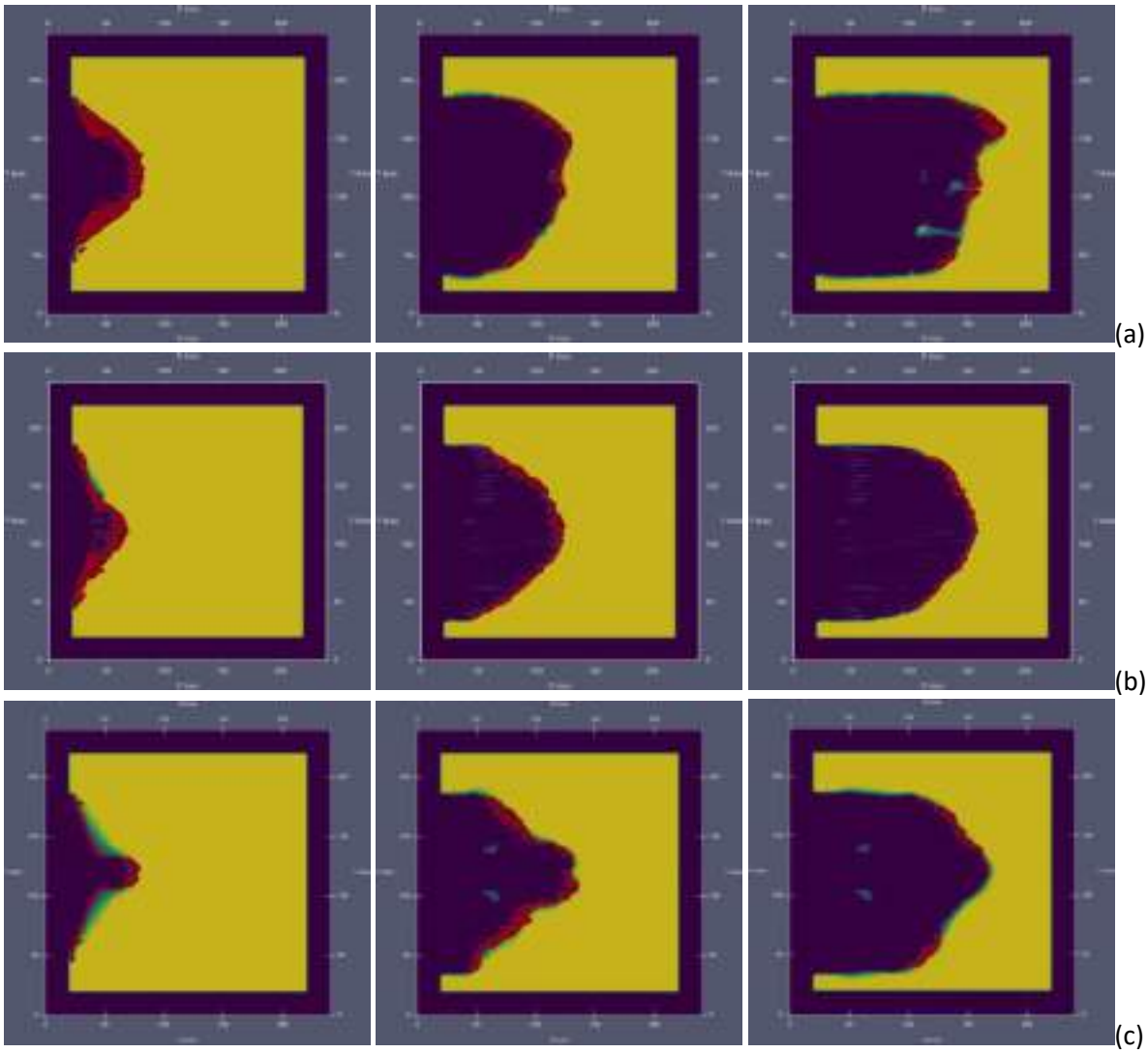

Figure 8. OpenFOAM simulation results of CSIRO cases F19. Fire front propagation and unburned grass illustration for the simulated cases with 3 different meshes and Lagrangian particle locations (Case 1(a), case 2 (b), case 3 (c)). Time moments 50 s, 100 s, 150 s from the ignition.

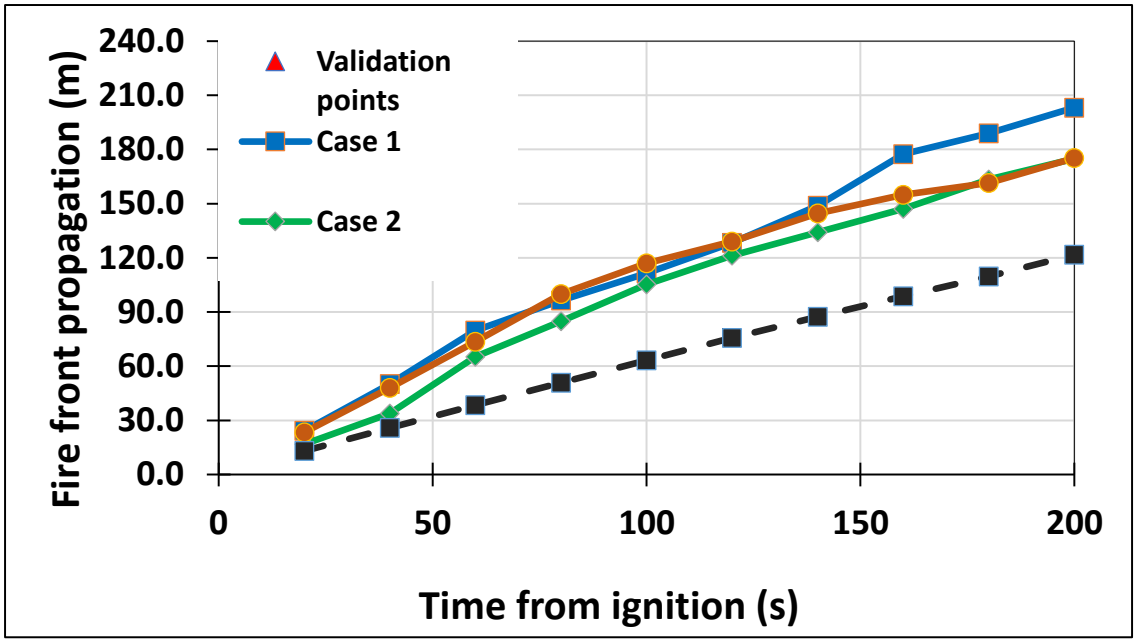

Figure 9. OpenFOAM simulation results of CSIRO cases F19. Fire front propagation of the simulated cases.

4.1.1.3 FDS simulations of the CSIRO C064 experiment

In *Figure 10* the FDS simulations of the CSIRO test C064 are compared to the experimental fire front positions. The FDS results are in reasonable agreement with the experiments. The FDS results shown are practically the same as in the FDS Validation guide (McGrattan et al., 2024b) because the same input files are used (FDS version 6.9.1 was used). The three different ways to describe the wildland fire load are used in the simulations: "LP" Lagrangian particles are used to describe the fire load, "BFM" Boundary fuel model is used, and "LS" empirical Level set model. The FDS simulations were using three different computational grid resolutions "crude", "mid", and "fine". Note, that not all grid resolutions were used in each different fire load options.

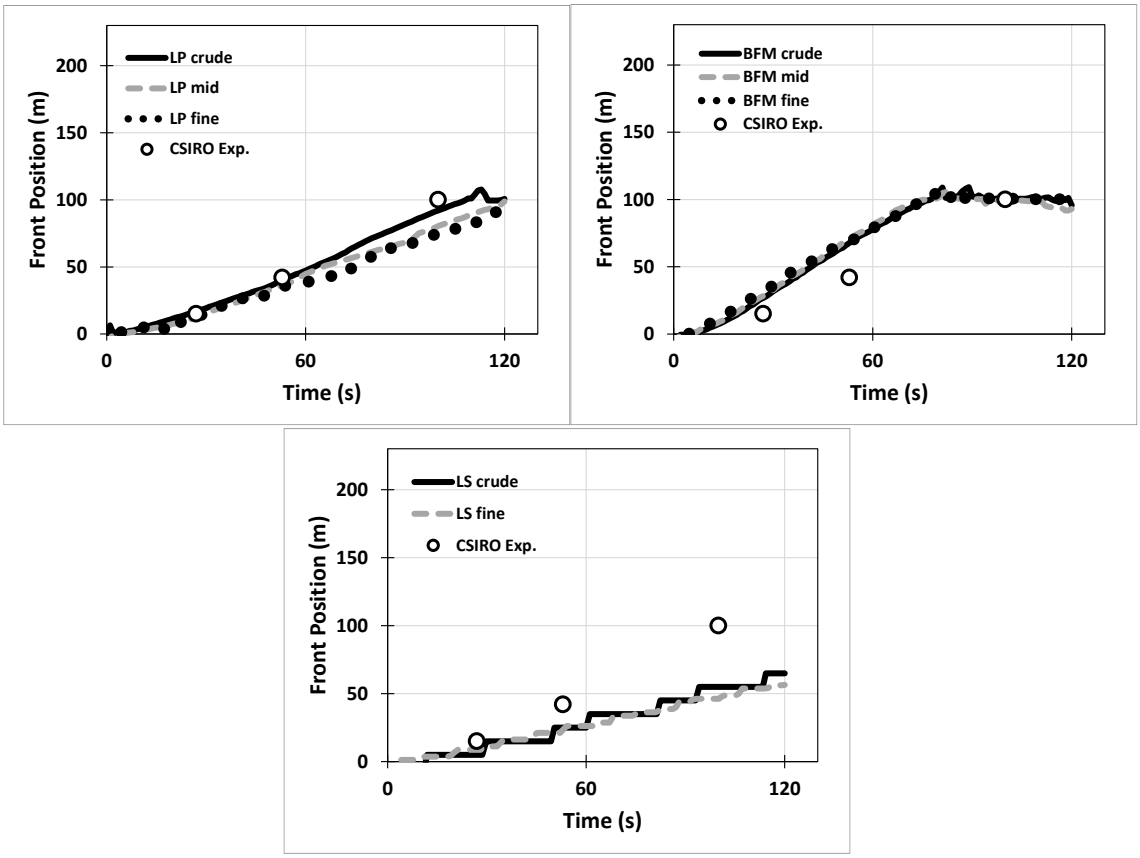

Figure 10. FDS simulations of CSIRO grass fire test C064 compared to experimental fire front position. Shown are results of FDS models, where the fire load was described as Lagrangian particles ("LP"), as Boundary Fuel Model ("BFM"), and as a Level Set model ("LS") for different computational grid resolutions ("crude", "mid", "fine").

The CSIRO case C064 was studied a little bit more using FDS simulations. The properties of the grass and the environment were varied and the changes in the simulated ROS were recorded. The case C064 was simulated using the LP method to describe the fire load and computational grid resolution "fine" was used. Four parameters were modified by giving them a value above and below the value that was used above, when the actual experiment was simulated. Wind speed was increased and decreased by 1 m/s from the 4.6 m/s, the ambient temperature was increased and decreased by 10 °C from the 32 ˚C., the fuel moisture fraction was increased and decreased by 4% units from the 6.3%. and the fuel mass was increased and decreased by 0.3 kg/m^3 from the 1.33 kg/m^3. Note that the mass per volume is a FDS input for a description of wildland fire load. The fuel load mass per area is obtained multiplying the mass per volume by the height of the described fuel in the FDS simulation, which was 0.21 m. Moisture fraction is the mass of moisture divided by the mass of dry vegetation in FDS inputs.

The results of the parametric studies are shown in *Table 3*. The reference case is labelled as "C064" and the cases, where the ROS is assumed to be increased are labelled as "C064 fast", and label "C064 slow" is for the cases, where the ROS should be decreased due to the change of parameters. So, it is expected that the ROS will increase when there is more fire load (mass per volume), higher wind speed, higher temperature, or less moisture

(grass is drier). The ROS values are estimated from the plots of the position of the fire front vs. time by fitting a straight line to the data starting at 10 s after the ignition. As it can be seen, the ROS behaves as it is expected to.

Table 3. The effect of different parameters on the simulated ROS in the CSIRO grassland fire case C064.

	C064 slow	C064	C064 fast
Wind Speed (m/s) ROS (m/s)	3.6 0.7127	4.6 0.8260	5.6 0.9335
Temperature (°C) ROS (m/s)	22 0.8136	32 0.8260	42 0.8837
Moisture Fraction (-) ROS (m/s)	0.103 0.7378	0.063 0.8260	0.023 1.0159
Mass per Volume (kg/m^3) ROS (m/s)	1.03 0.8214	1.33 0.8260	1.63 0.8851

The results show that FDS is predicting a ROS behaviour that is intuitive. There is no experimental data to compare these predictions, but qualitatively it can be compared to the forest fuel models like the Scott and Burgan (2005) forest fuel model. The models GR1, GR2, GR4, and GR7 could be used for the CSIRO case short grass as they are for arid and semiarid climate (rainfall deficient in summer). The properties of these fuel types are listed below (Scott & Burgan 2005). Note, that Scott & Burgan use imperial units, they are converted to SI units using following conversion factors: 1 ch/h = 0.005588 m/s, 1 t/ac = 0.2471 kg/m^2, 1 1/ft = 3.28084 1/m, 1 mi/h = 0.44704 m/s.

- GR1: Grass is short, patchy, and possibly heavily grazed. Spread rate moderate, flame length low. Fine fuel load 0.40 t/ac = 0.099 kg/m^2, surface-area-to-volume (SAV) 2054 1/ft = 6739 1/m, packing ratio 0.00143.
- GR2: Moderately coarse continuous grass, average depth about 1 foot. Spread rate high; flame length moderate. Fine fuel load 1.10 t/ac = 0.27 kg/m^2, SAV 1820 1/ft = 5971 1/m, packing ratio 0.00158.
- GR4: Moderately coarse continuous grass, average depth about 2 feet. Spread rate very high; flame length high. Fine fuel load 2.15 t/ac = 0.53 kg/m^2, SAV 1826 1/ft = 5991 1/m, packing ratio 0.00154.
- GR7: Moderately coarse continuous grass, average depth about 3 feet. Spread rate very high; flame length very high. Fine fuel load 6.4 t/ac = 1.58 kg/m^2, SAV 1834 1/ft = 6017 1/m, packing ratio 0.00306.

The C064 case fire load properties are SAV = 9770 1/m, grass height (fuel depth) 0.21 m, moisture 6.3%. and bulk mass per unit area 0.283 kg/m^2, so it is somewhere between GR2 and GR4 fuel types. The ROS vs. mid-flame wind speed values is given as graphs in Scott & Burgan. The ROS values for wind speed 4.6 m/s are read from these graphs and the following values are found:

- Type GR2: Dead fuel moderate moisture ROS = 0.46 m/s, low moisture ROS = 0.55 m/s, very low moisture ROS = 0.65 m/s.
- Type GR4: Dead fuel moderate moisture ROS = 0.95 m/s, low moisture ROS = 1.1 m/s, very low moisture ROS = 1.3 m/s.

The FDS results are within the range of GR2 and GR4 values. The effect of moisture seems to be quite identical to type GR2 and GR4 fuel values, but there is not exact relationship between the moisture values used in FDS simulations with respect to the "moderate", "low", and "very low" moisture used in the literature values. The effect of wind speed is not as strong in FDS simulations than in the literature values, but it is in the right order of magnitude, though. Some differences might arise due to the wind speed definitions, literature values use mid-flame wind speed whereas the FDS simulations used MO similarity method wind speed with the reference height at 2 m above the (solid) ground.

4.1.1.4 OpenFOAM simulations of the CSIRO C064 experiment

Model parameters used in the OpenFOAM simulations of the case C064 are presented in *Table 2*. The results of the simulations are presented in *Figure 12* with comparison of the validation data. Current simulations demonstrate underestimation of the rate of spread.

Simulation cases with low grass C064 were done with many various computational meshes. The simulations with the only one cell in the grass area did not demonstrate fire front propagation. The cell size either corresponded to the height of the grass or exceeded it. Thus, many trials were made to divide the grass area in the vertical direction. The smallest computational cells were as small as 1 m × 1 m × 0.02625 m. Simulation results are presented in *Figure 12*.

Low grass and low grass mass did not create the sufficient fire flame and did not create high plume able to introduce velocity variation in the domain. On the other hand, uniform wind velocity boundary condition resulted in quite uniform velocity distribution during the simulation. This decelerates fire propagation. Simulation results demonstrate typical heigh of the flames only slightly higher than the height of the grass (up to 0.3-0.35m). During the ignition the flame heights in the vicinity of ignition were higher, which can be seen in *Figure 12* (initial larger fire front propagation and decreasing around 30 s after the ignition). In some cases, fire front propagated in a non-symmetrical way. It can be seen from *Figure 12* and *Figure 13* that propagation of the fire front in one part of the computational domain affects the overall rate of spread value.

In all these cases there was very little fire spread perpendicular to the primary propagation direction.

From the CSIRO cases simulation with OpenFOAM it can be concluded that the approach seems to work better when the grass is higher. In the low grass case, the simulation results demonstrate lack of flow caused by the fire and related velocity variations. Moreover, the simulation results are sensitive to the mesh in the grass area and positions of Lagrangian particles.

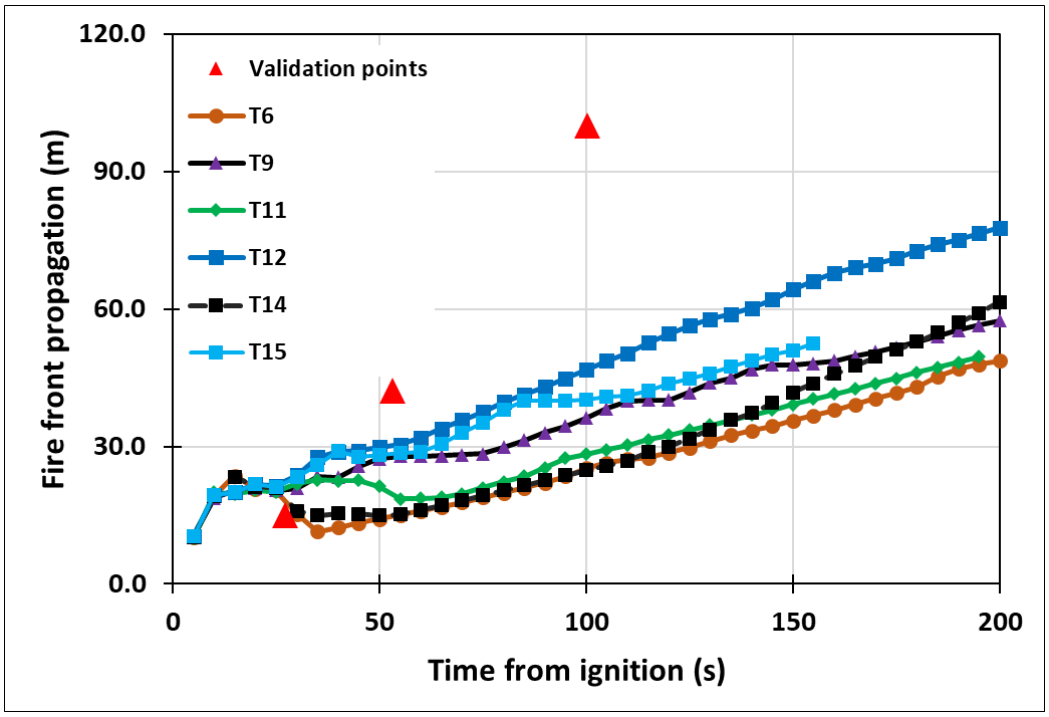

Figure 11. OpenFOAM simulation results of CSIRO cases C064. Fire front with several different meshes and Lagrangian particle's location. Comparison from the validation data.

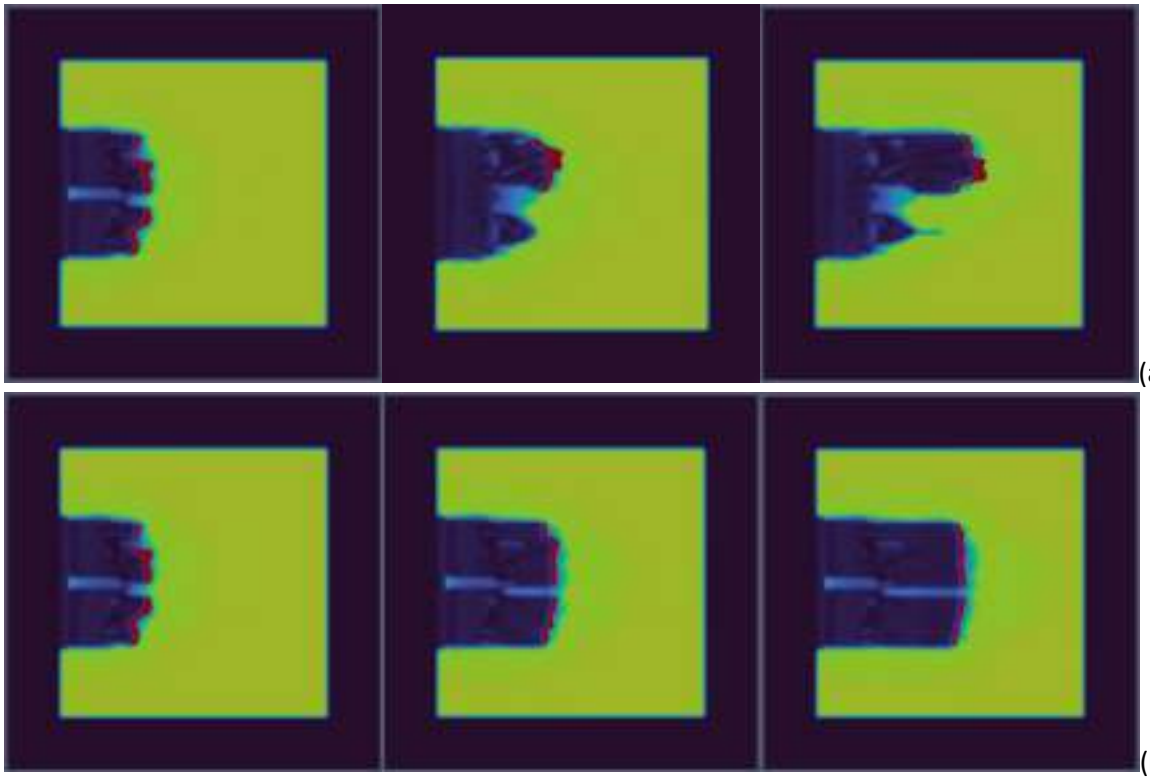
(a)

(b)

Figure 12. OpenFOAM simulation results of CSIRO cases C064. Fire front propagation and unburned grass illustration for the simulated cases with 2 different meshes and Lagrangian particle's location (Case T12(a), case T9 (b)). Time moments 50 s, 100 s, 150 s from the ignition.

4.1.2 Fireflux grass fire experiments

The Fireflux grass fire experiments (Clements et al. 2007, 2008) were used to validate the used simulation tools (FDS and OpenFOAM) and the modellers.

Fire flux experiment took place in 2006 at Houston Coastal Centre, Texas, USA. Experimental prairie had a size of 400 m × 970 m. The prairie was burned the year before the experiment; therefore, the grass was one year old and mainly consists of native species. The main goal of the experiment was to achieve conditions similar to wildfires. The grass was supposed to be dry, and the fire propagation should be driven purely by the side wind.

Two towers with measuring sensors at 100 and 400 meters from the ignition point. Grass was cut away 5 meters around the towers to avoid the damage of the observation towers. Area around the prairie was also mowed for safety reasons.

Ignition was done from the upwind side of the area; no back burn was done. Ignition of the area was done from the central point of the ignition line simultaneously in both direction with the speed of 0.5 m/s.

During the Fireflux experiments sensor in the towers were recording various properties, such as velocity, temperature, net radiation, heat flux, water vapour, etc. Some of the measurements are reported in Clements et al. 2007, 2008. In addition, two doppler sodars were operated in the experiments for measuring the wind profiles. The evolution of the fire behaviour and fire line propagation was documented with time lapse photography.

Average mass of the grass and its moisture was calculated from ten samples of 38 × 38 cm^2 cut from random parts of the prairie. A uniform grass mass of 1.08 kg/m^2 and constant dry moisture of 5% is used in the further simulation.

The FDS simulations were mainly done to check the ability of FDS to produce a representative fire without much emphasis on the fuel load description and other aspects of the model inputs. The model used grass fire data found from the FDS User Guide (McGrattan et al. 2023) and on the FDS validation Guide (McGrattan et al. 2024b). The fire load models were used “as is”, just the amount (kg/m^2) and the moisture content, among others, were modified to match the Fireflux experimental conditions. The FDS simulations were not used to do any parametric studies, like the effect of wind speed on the ROS. The OpenFOAM simulations were conducted in more detail and parametric studies were also performed.

4.1.2.1 FDS simulations of the Fireflux grass fire experiment

The Fireflux grass fire experiment used a large area of grass, so the computational mesh used in the FDS simulations is relatively coarse. This means that there is no way to treat the burning grass as individual particles, so the BFM of FDS was chosen to describe the fire load.

To model the Fireflux grass fire using FDS, the modeller needs to choose many different parameters that describe the fire load and some other simulation parameters. Some of this information was found on the documents that are describing the Fireflux

experiments (Clements et al. 2007, 2008), some from other wildland fire literature and others from the FDS documentation.

The wind was modelled using the MO method in FDS and wind speed of 3 m/s at a reference level of 2 m above ground was used. The relative humidity was set to be 63 % and the ambient temperature at 17.7 ˚C. The wind direction was set to be along the long side of the grass field (from left to right in the simulation domain). The MO parameters for the wind were roughly open (z_0 = 0.1) and unstable stability class (L = -500). The computational domain size was 1000 m × 480 m × 40 m. The fire load area dimensions were at the largest 817 m long and 384 m wide. A numerical mesh of 2 m spatial resolution was used for most simulations, although one simulation used 1 m spatial resolution. Due to the relatively coarse spatial resolution of the numerical mesh, the grass fire load was described using the BFM vegetation model of FDS (McGrattan et al. 2023).

A fire load density 1.08 kg/m^2 was assumed and the grass was presumed to be "GR7" grass fire load type according to Scott & Burgan (2005). The GR7 has characteristic SAV of 1834 1/ft (6017 1/m) and a dimensionless packing ratio of 0-00306. It has somewhat larger fuel load density than the 1.08 kg/m^2 measured for Fireflux grass, but it is close enough (6.4 t/ac = 1.6 kg/m^2), so that GR7 grass model can be used to set those FDS fire load parameters that cannot be found from the Fireflux documentation. Thus, the FDS model for the burning surface was the one with 1 m thick layer of vegetation (with material name "GENERIC VEGETATION") with moisture fraction of 0.10, mass per volume 1.08 kg/m^3, SAV 6017 1/m, and drag coefficient of 2.8. Below the grass was 0,1 m layer describing unpaved roads on grass fields (with material name "DIRT"). The "DIRT" and "GENERIC VEGETATION" material and burning properties were directly taken from the "vegetation_model.txt" of the FDS validation cases "Crown_Fires" and "CSIRO_Grassland_Fires" (FDS Github repository revision FDS-6.9.1-752-g115fc2734, McGrattan et al. 2024b).

Figure 13 through *Figure 26* show the snapshots of FDS simulations at 1-minute intervals until the end of the fire. FDS simulations were done using two different computational mesh resolutions, one was using a 2 m grid resolution ("coarse"), the other a 1 m grid resolution ("fine"). The fine mesh fire simulation has slightly faster spread rate than the coarse mesh. The fine mesh fire ended within 14 minutes and the coarse mesh fire ended within 15 minutes after ignition. It is seen that the fire develops and travels qualitatively similarly in both simulations.

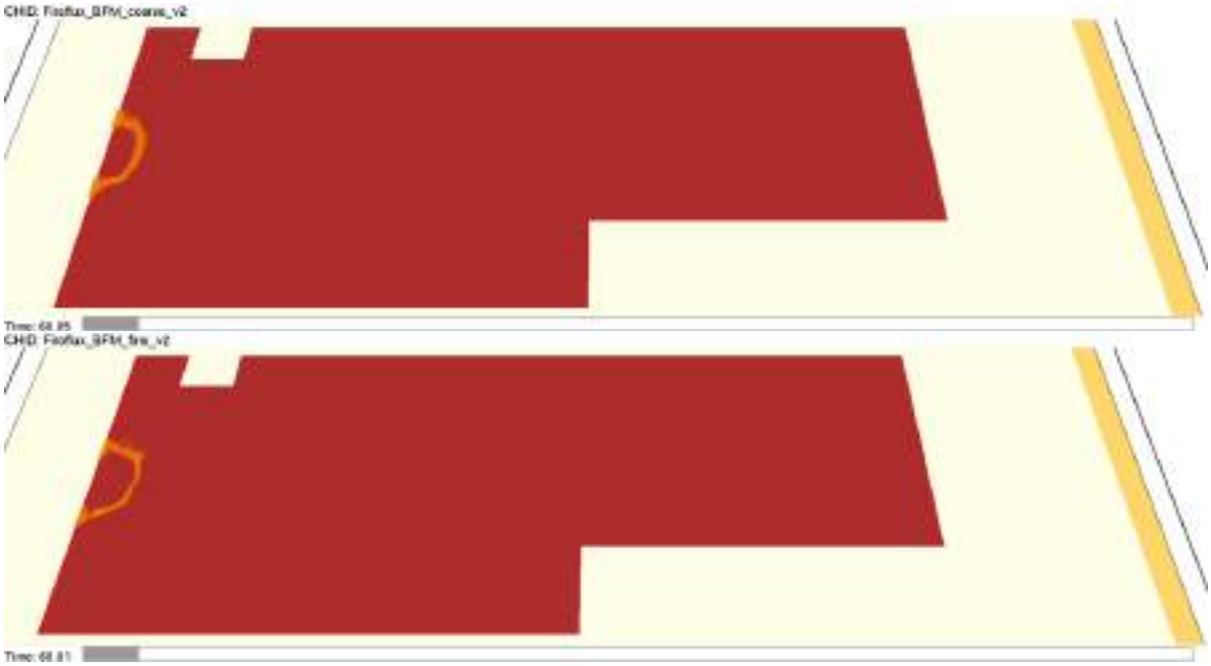

Figure 13. Snapshot of FDS simulation at 1 minute after the ignition in the Fireflux grass fire. Shown are the results of two simulations using a coarse (top) and a fine (bottom) computational mesh.

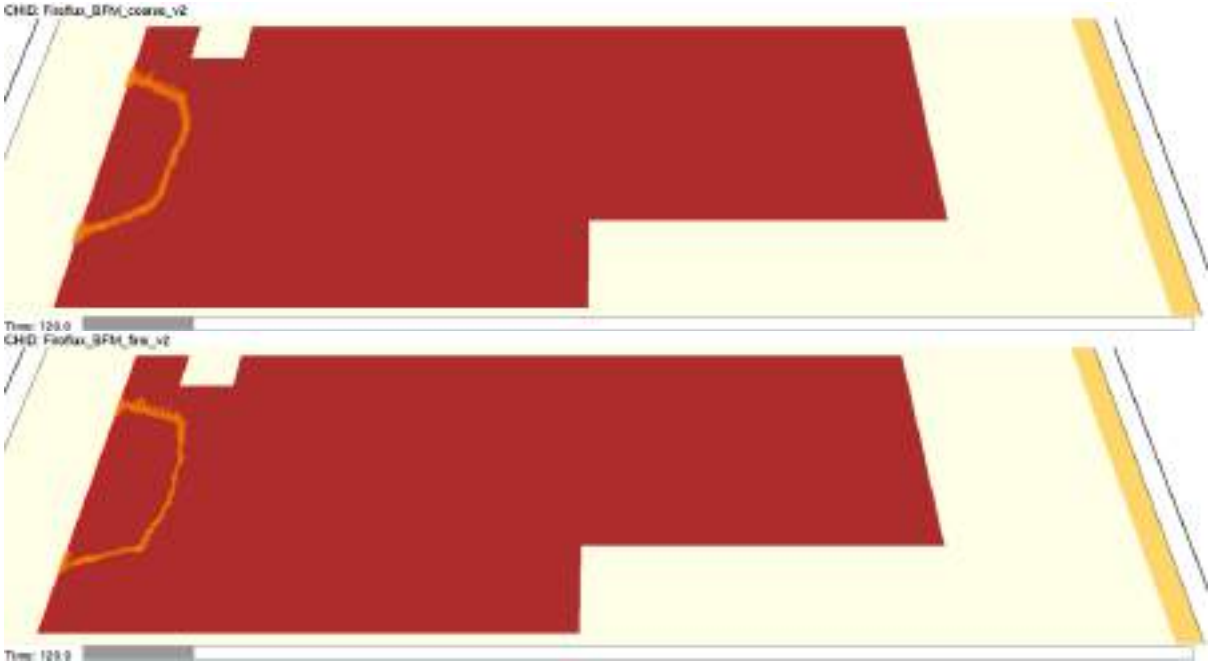

Figure 14. Snapshot of FDS simulation at 2 minutes after the ignition in the Fireflux grass fire. Shown are the results of two simulations using a coarse (top) and a fine (bottom) computational mesh.

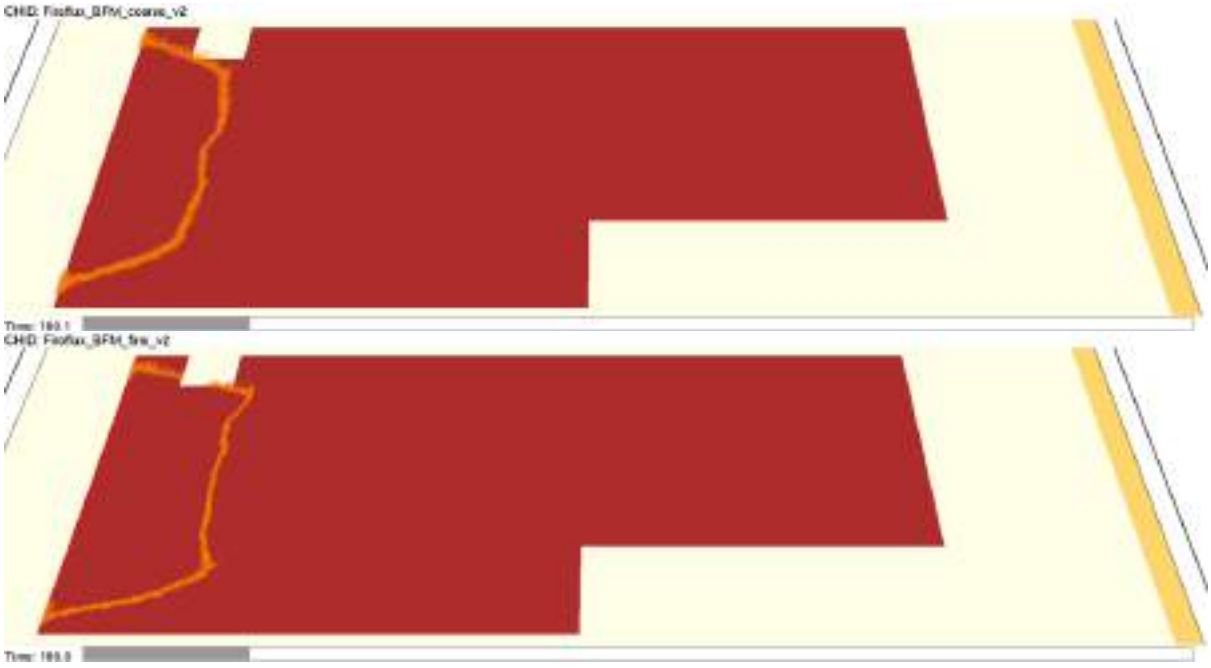

Figure 15. Snapshot of FDS simulation at 3 minutes after the ignition in the Fireflux grass fire. Shown are the results of two simulations using a coarse (top) and a fine (bottom) computational mesh.

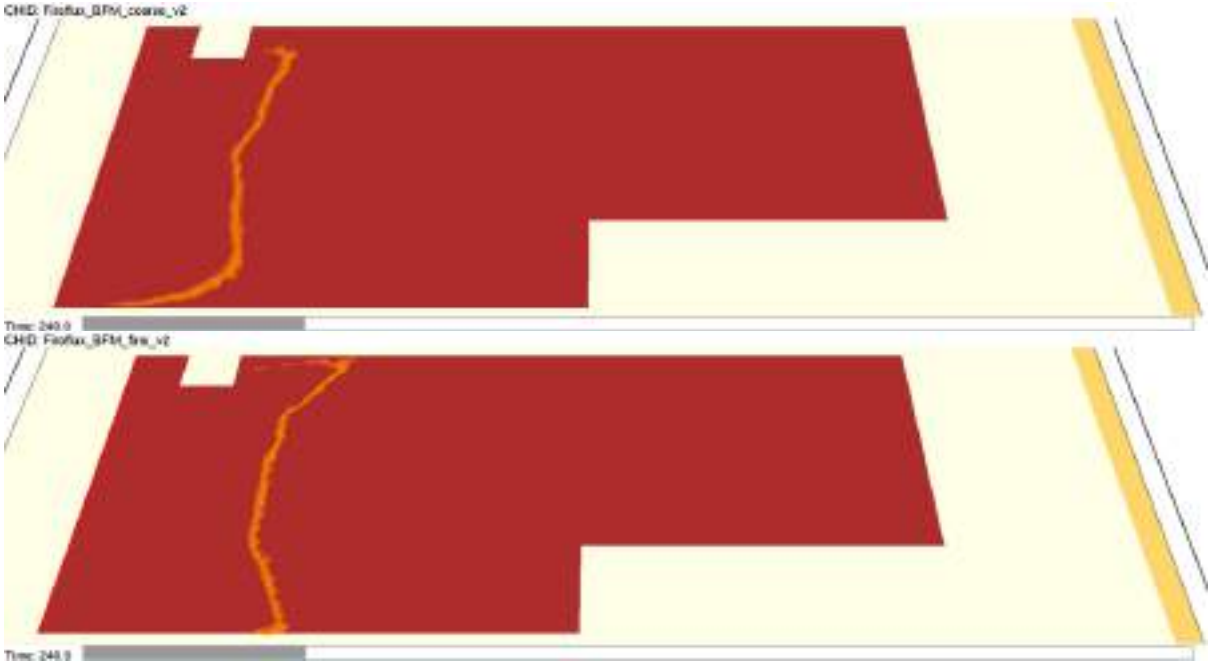

Figure 16. Snapshot of FDS simulation at 4 minutes after the ignition in the Fireflux grass fire. Shown are the results of two simulations using a coarse (top) and a fine (bottom) computational mesh.

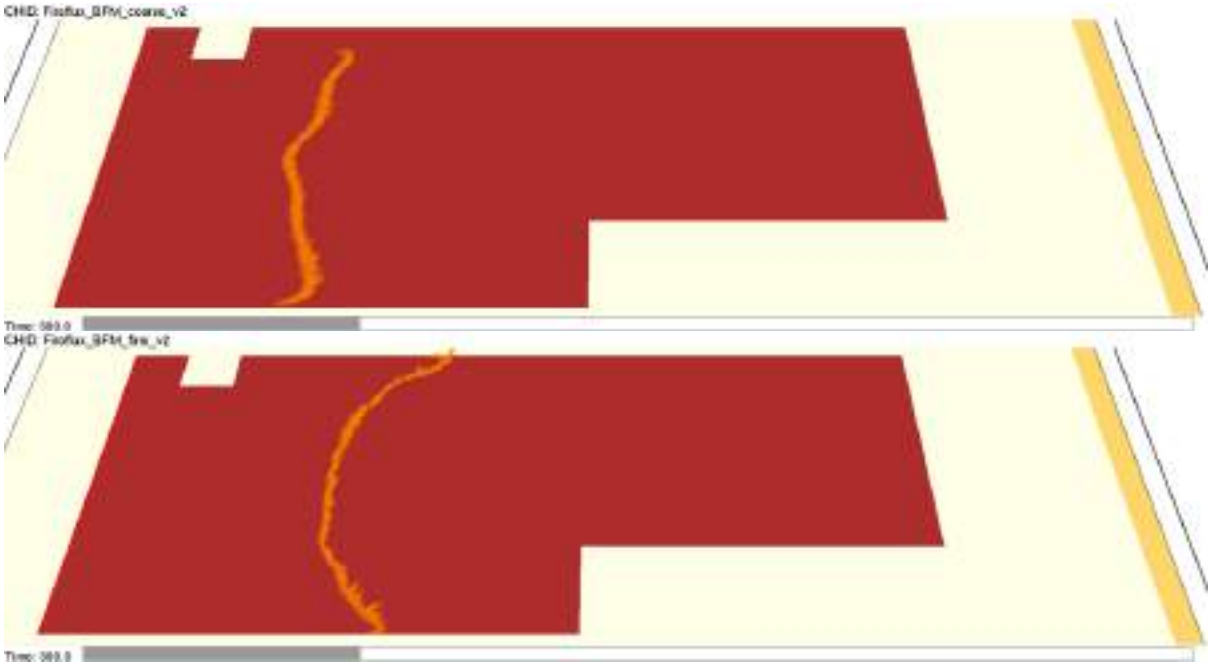

Figure 17. Snapshot of FDS simulation at 5 minutes after the ignition in the Fireflux grass fire. Shown are the results of two simulations using a coarse (top) and a fine (bottom) computational mesh.

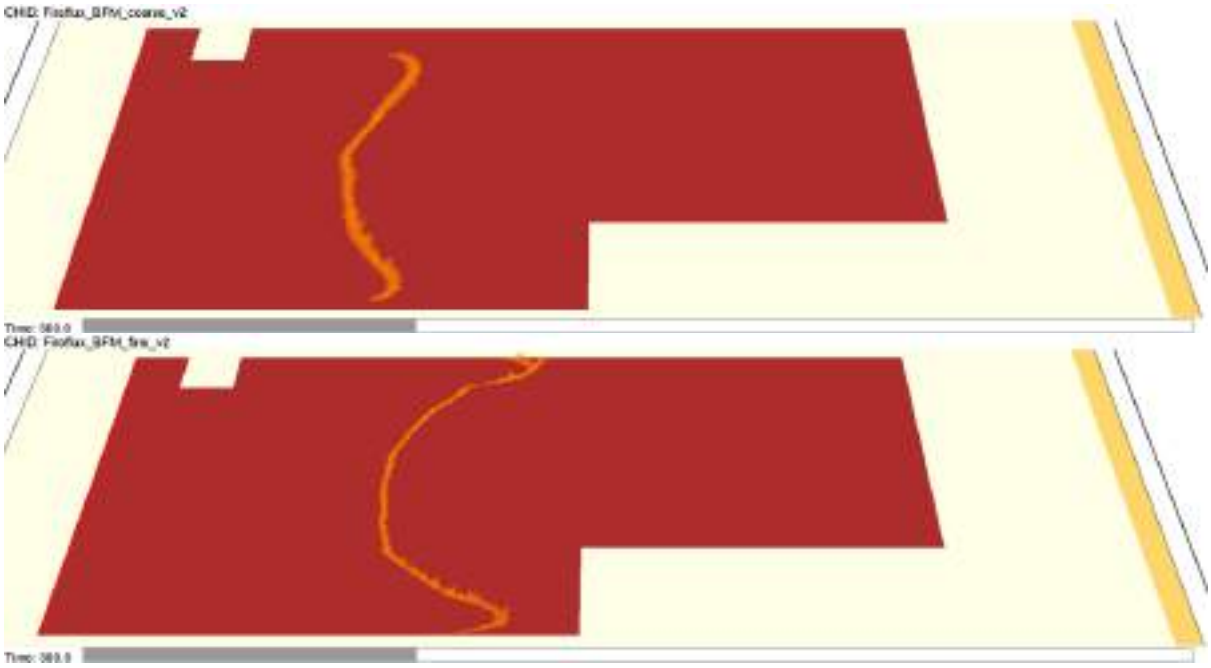

Figure 18. Snapshot of FDS simulation at 6 minutes after the ignition in the Fireflux grass fire. Shown are the results of two simulations using a coarse (top) and a fine (bottom) computational mesh.

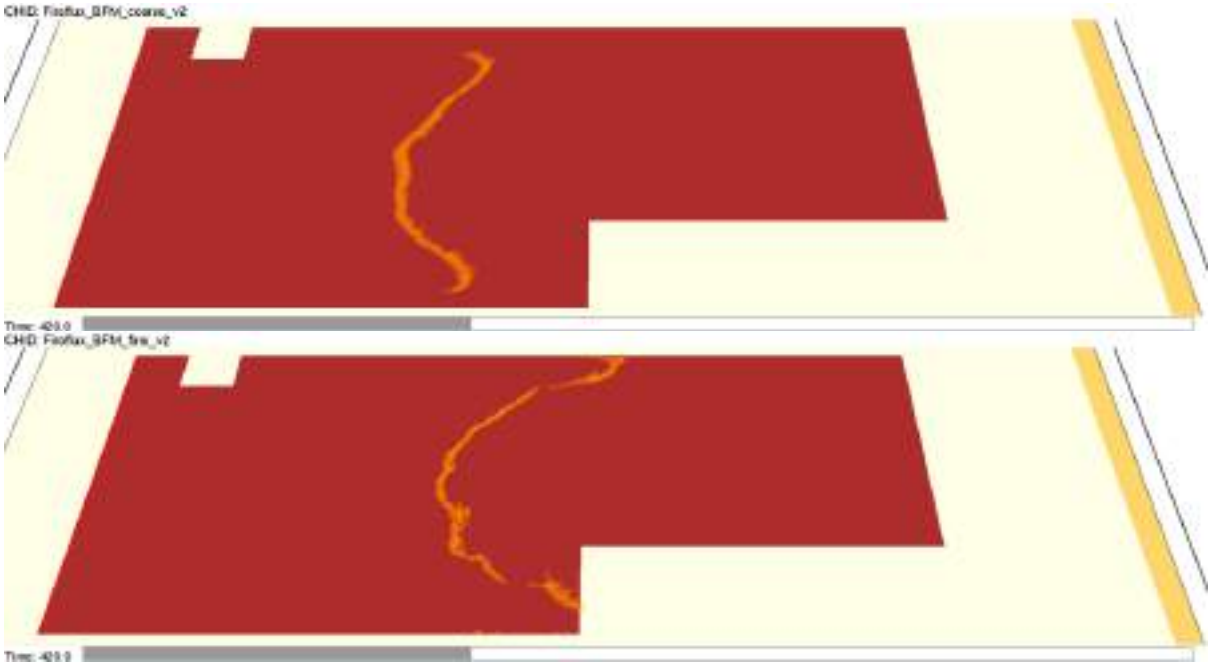

Figure 19. Snapshot of FDS simulation at 7 minutes after the ignition in the Fireflux grass fire. Shown are the results of two simulations using a coarse (top) and a fine (bottom) computational mesh.

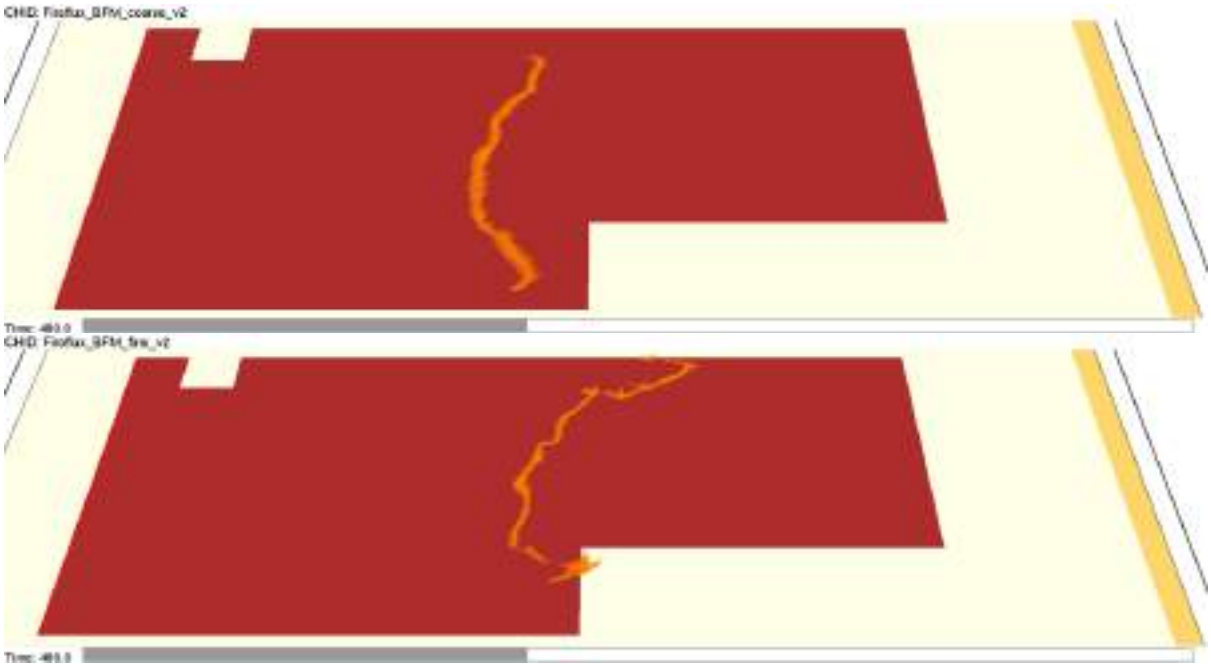

Figure 20. Snapshot of FDS simulation at 8 minutes after the ignition in the Fireflux grass fire. Shown are the results of two simulations using a coarse (top) and a fine (bottom) computational mesh.

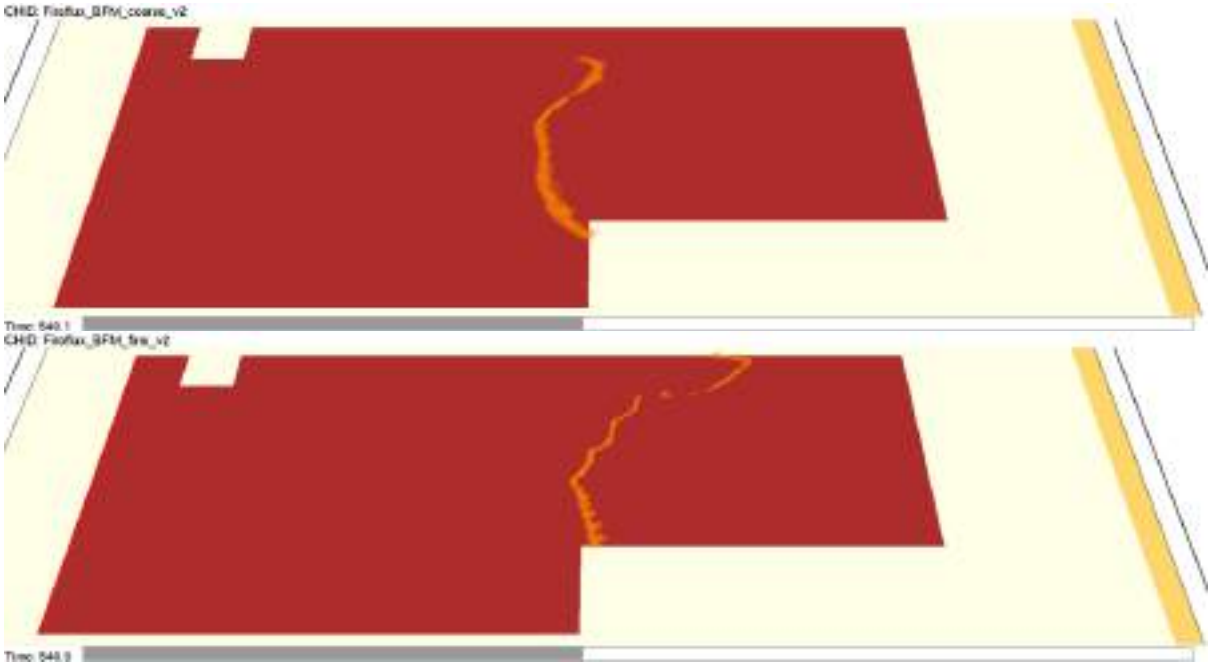

Figure 21. Snapshot of FDS simulation at 9 minutes after the ignition in the Fireflux grass fire. Shown are the results of two simulations using a coarse (top) and a fine (bottom) computational mesh.

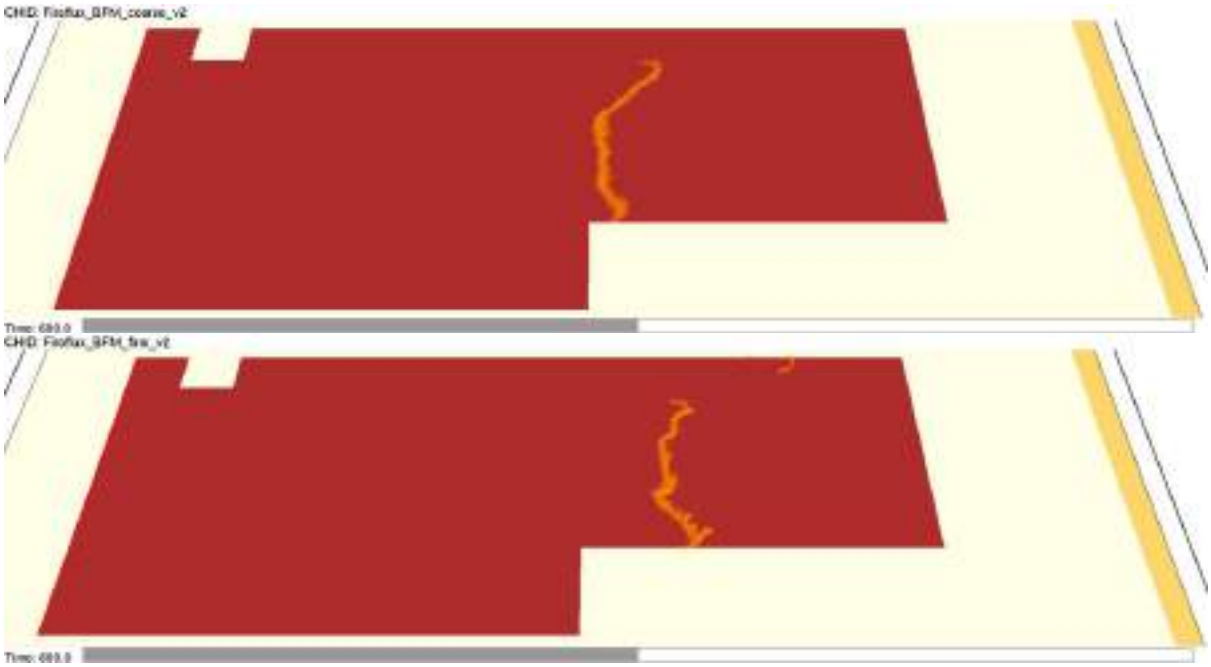

Figure 22. Snapshot of FDS simulation at 10 minutes after the ignition in the Fireflux grass fire. Shown are the results of two simulations using a coarse (top) and a fine (bottom) computational mesh.

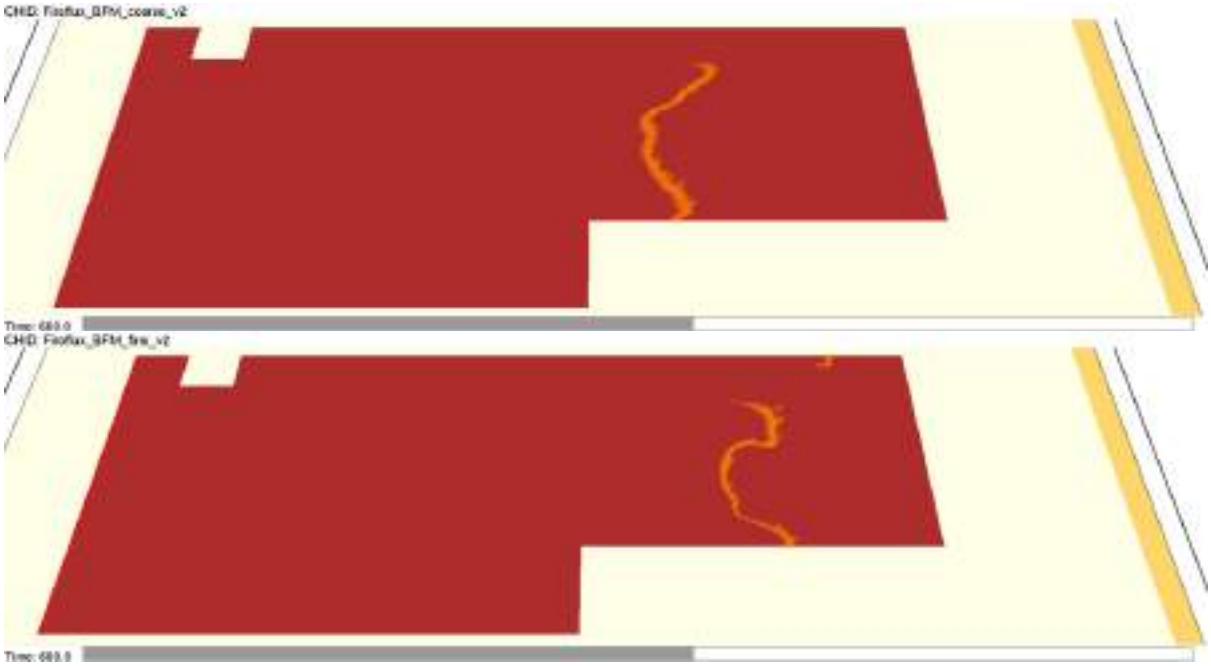

Figure 23. Snapshot of FDS simulation at 11 minutes after the ignition in the Fireflux grass fire. Shown are the results of two simulations using a coarse (top) and a fine (bottom) computational mesh.

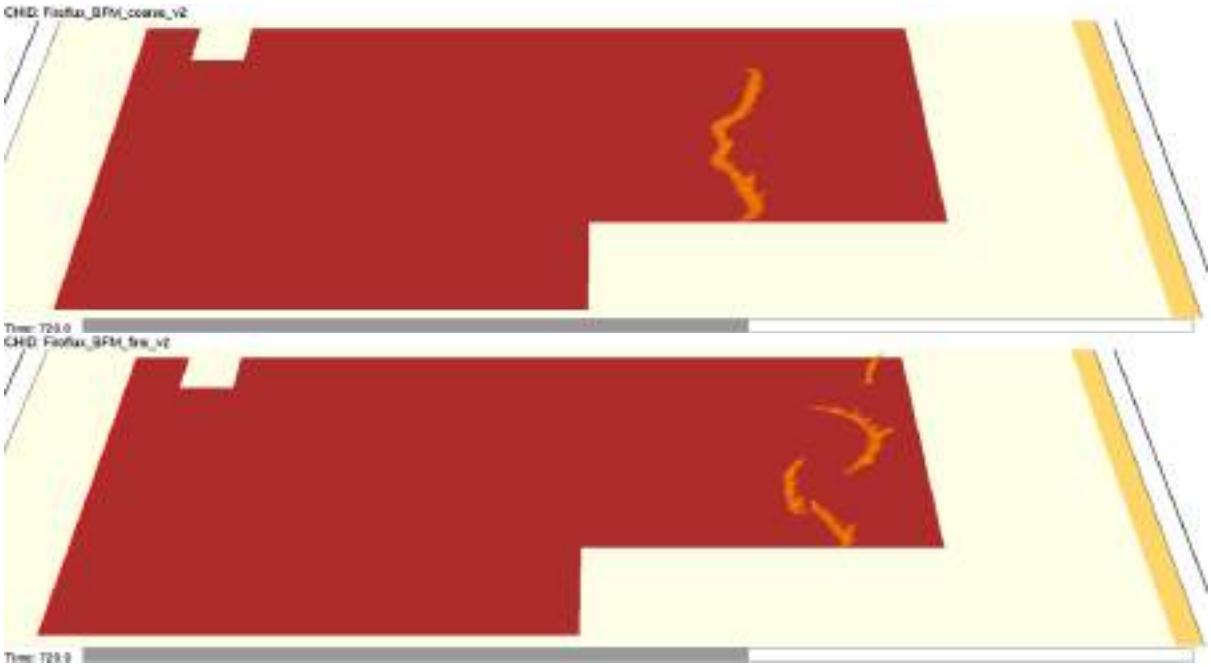

Figure 24. Snapshot of FDS simulation at 12 minutes after the ignition in the Fireflux grass fire. Shown are the results of two simulations using a coarse (top) and a fine (bottom) computational mesh.

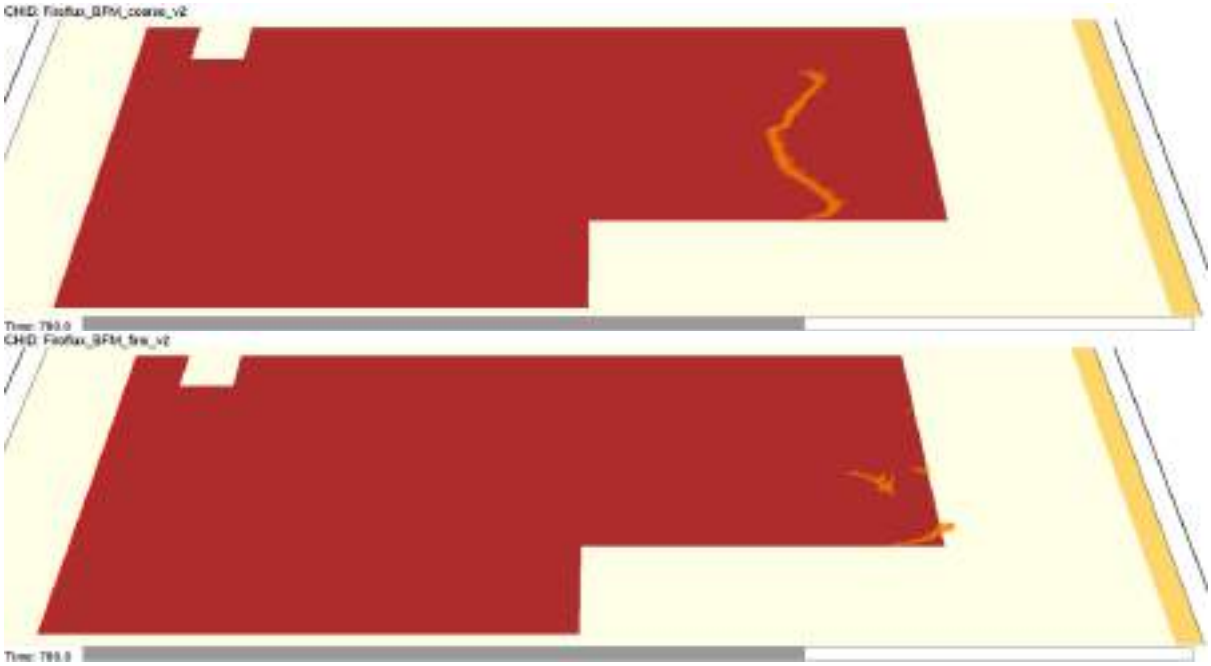

Figure 25. Snapshot of FDS simulation at 13 minutes after the ignition in the Fireflux grass fire. Shown are the results of two simulations using a coarse (top) and a fine (bottom) computational mesh.

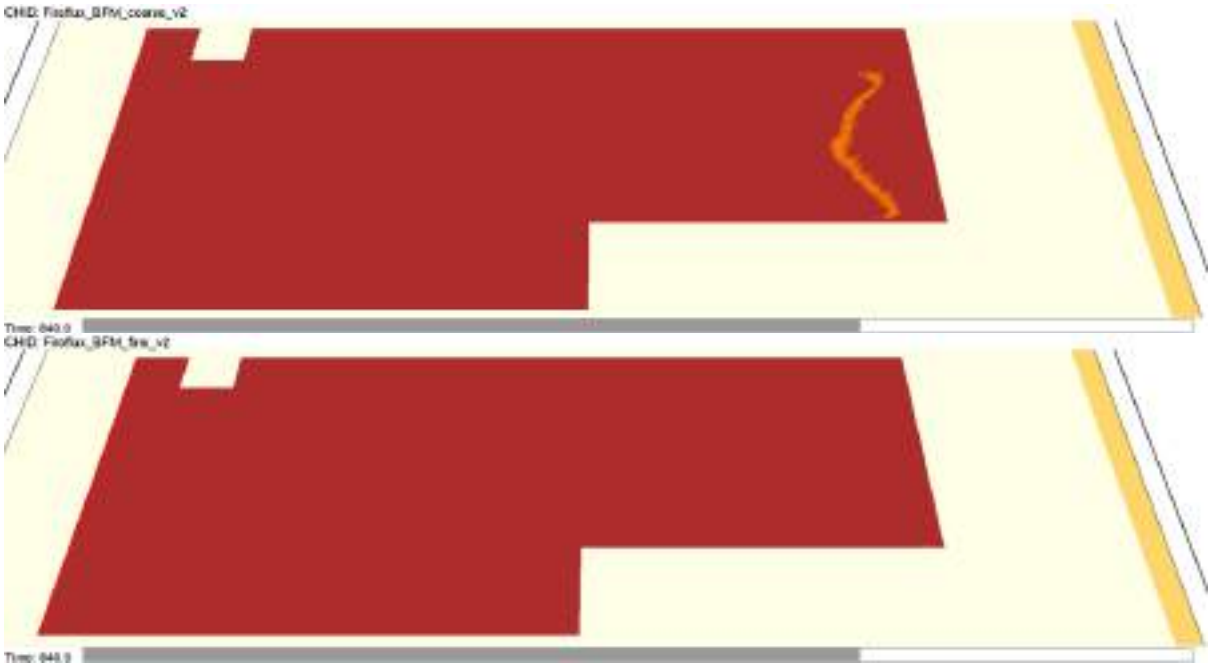

Figure 26. Snapshot of FDS simulation at 14 minutes after the ignition in the Fireflux grass fire. Shown are the results of two simulations using a coarse (top) and a fine (bottom) computational mesh.

Due to the relatively coarse computational mesh, the fire load definition in FDS used a keyword that controls the burnout of a single burning mesh cell at the burning surface. The effect of this keyword value, MINIMUM_BURNOUT_TIME, was studied using the coarse mesh so that the values of 1 s, 4 s, 8 s, and 16 s were tested. The fine mesh case was simulated just once, and it used 4 s for the burnout parameter.

Table 4 collects the estimated ROS values found in the performed different simulations. Four of these used a coarse mesh and one fine mesh. Four different values were used for the burnout time keyword. The ROS was estimated visually looking the fire front progress in the simulation by checking the times, when the fire front reached the main tower at 126 m and the short tower at 486 m. The ignition line was at 0 m (left side of the grass in the above snapshot figures). There is some ambiguity in the estimated ROS due to this procedure, as the fire front is not progressing homogeneously, as it has a curved shape, and the shape evolves over time. The "tower crossing times" were taken when the middle (vertical direction in above snapshot figures) part of the fire front passed the (horizontal) location of the towers.

Table 4. Estimated ROS in the FDS simulations of Fireflux grass fire experiment.

	Minimum burnout time (s)	Mesh resolution (m)	ROS (m/s) MT - ST	ROS (m/s) Ign.line – MT
Case 1	8	2	0.76	0.52
Case 2	4	2	0.98	0.57
Case 2 fine	4	1	1.02	0.68
Case 3	1	2	1.06	0.63
Case 4	16	2	0.50	0.42

Two different ROS values are tabulated in *Table 4*, one ("MT- ST") uses the fire front travel time from main tower to the short tower and the other ("Ign.line – MT) from the ignition line to the main tower. The later one might be a more reliable value and it should be compared to experiments and OpenFOAM simulations. As can be seen from the snapshots of the fire front propagation, the fire front shape might not be good at 5 minutes or later in the simulation. The reason for this might be the relatively small domain, i.e., the boundary conditions might affect the fire development. In *Figure 27* the velocity component along the wind direction and the gas temperature are at the same moment when the fire front has reached the main tower. It can be seen that the computational domain is not optimal, at least the sky boundary should have been higher. This issue was not addressed more in this context, as there were many other cases where the domain size and boundary condition effects to simulation results were addressed. The main emphasis of the current work was not to study grass fires, the main goal of the current project is to study extreme wildland fires. The grass fire scenarios presented in this report were done mainly for verification and validation purposes of the used methods.

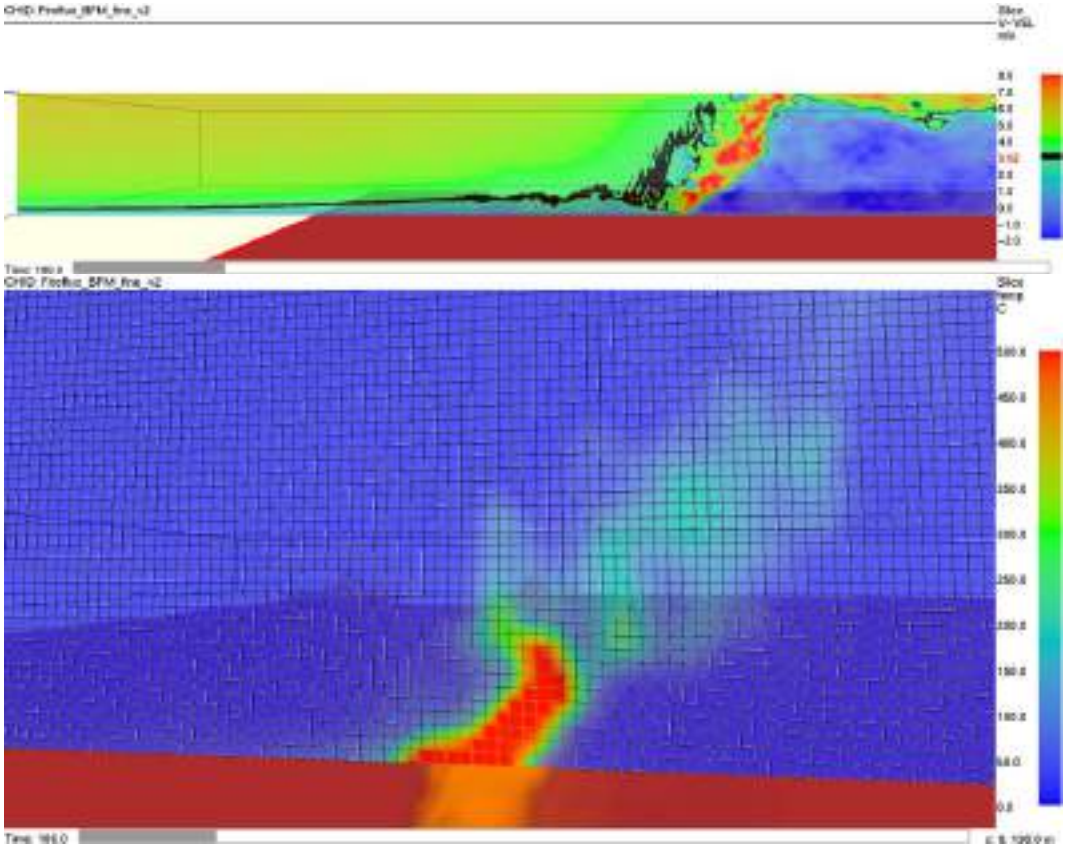

Figure 27. Snapshots of the FDS simulation "Case 2 fine" of Fireflux grassfire experiment. Shown are the velocity component along the wind direction (top) and the gas temperature (bottom) at 186 s, when the fire front has reached the main tower. The computational mesh had 1 m spatial resolution that is shown in the temperature figure.

It can be seen that FDS was able to qualitatively reproduce the experimental case. The calculated ROS is reasonable, especially as there was no optimization of the FDS input keywords, i.e., the result might be stated to be a "blind simulation", where the results of the experiment are not used to guide the simulation parameters at all. In this regard, the FDS simulation results can be considered to represent the case quite well.

4.1.2.2 OpenFOAM Simulation of the Fireflux case

OpenFOAM simulation parameters for the Fireflux case are presented in *Table 5*. The domain size was reduced to save computational time. Simulation results with smaller domain demonstrate similar rate of spread to the simulation results for the larger domain. The mesh cell sizes were ranged from 1 m × 1 m × 0.5 m in the grass area, 1 m × 1 m × 1 m in the area above the grass and coarse 4 m × 4 m × 4 m cell in the top of the domain.

According to the measurement (Clements et al 2007), the wind velocity in the lower 200 meters increases as a function of the height above the ground. A simple linear fit to the measured data was made and the corresponding boundary condition model was implemented. In the literature atmospheric model is commonly used as a wind boundary condition. The dependence of the height above the grass has a logarithmic shape

presented in *Table 6*. The log-model was also implemented as velocity boundary conditions. In the current research, parameters of the log-model were adjusted to reproduce the measured wind velocity (see *Table 6* and *Figure 29*). Here the log model was limited from below to the constant value of 3 m/s, which was reported as a value at height of 2 m above the ground.

Table 5. Parameters used in OpenFOAM simulations of the Fireflux case.

	Parameters
Domain in CFD simulations	**200 m*450 m*200 m**
Height of the grass	**1.5 m**
Mass of the grass	**1.08 kg/m²**
Surface to volume ratio	**6000 (1/m)**
Velocity inlet	**Constant value4 m/s; linear model; log-model**
Speed of ignition	**0.5 m/s**
Ignition area	**(20-22)*(0-200)*1.5**
Temperature	**290.7 K**
Fuel composition:	
Fuel moisture	**5%**
Volatile matter	**85.5%**
Solid mass fraction	**0.1378**
Solid C	**0.972413793**
Solid ash	**0.027586207**
Net calorific value, dry	**18.65 MJ/kg**

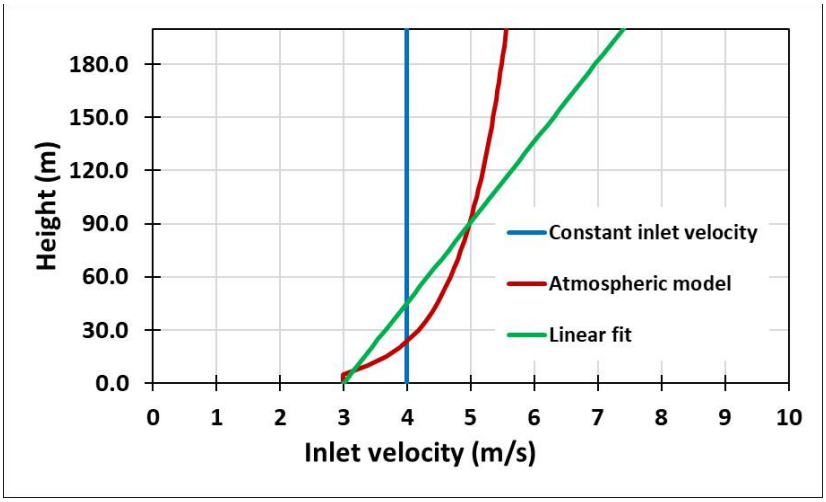

Figure 28. Boundary condition models for inlet velocity

Table 6. Boundary condition models for inlet velocity

	Linear model	Log model
Inlet velocity	$u = u^* + bz$	$u = \frac{u^*}{\kappa} ln\left(\frac{z - d + z_0}{z_0}\right)$
$\boldsymbol{u^*}$	3.0	0.3
b	0.022	-
κ	-	0.41
d	-	0.0
$\boldsymbol{z_0}$	-	0.1
$\boldsymbol{u_{lim}}$	-	3.0

OpenFOAM simulated results are presented from *Figure 30* to *Figure 34*. Simulated results for the cases with three various inlet velocities are presented in *Figure 30*. Linear model for the inlet wind has the largest velocity variation at the inlet. However, otherwise, the simulated results are similar. Propagation of the fire front is the fastest in the case of the constant velocity since it has the highest wind velocities near to the ground level.

Simulated results of the case with linear boundary condition for the inlet velocity are presented in *Figure 31* and *Figure 32*. Formation and propagation of the fire plume is illustrated by the velocity magnitude (which mainly consists of the vertical velocity component) and temperature propagation. Similar phenomena are described in the articles of Clements at al. 2007 and Clements et al. 2008.

Simulated flame height typically ranges between 5 and 6 meters with few higher flames up to 7 meters. This agrees well with the validation measurements of 5.1 meter reported in the paper of Clements at al. 2007.

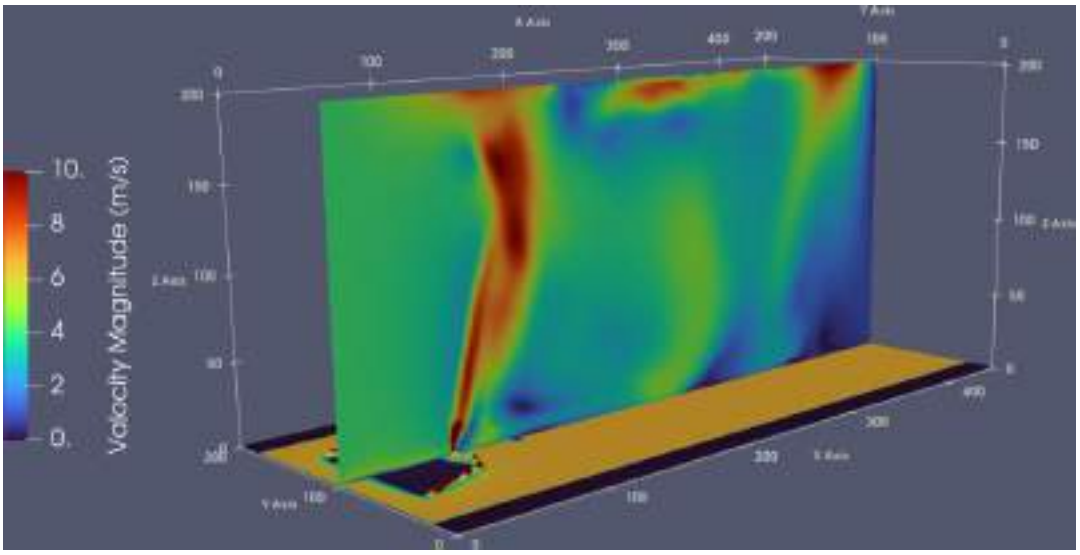

(a)

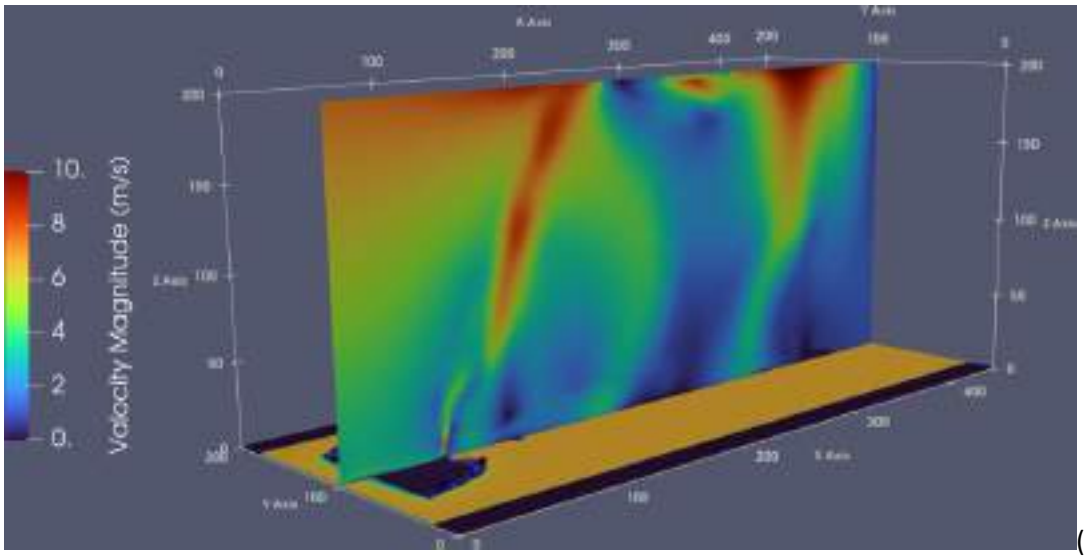

(b)

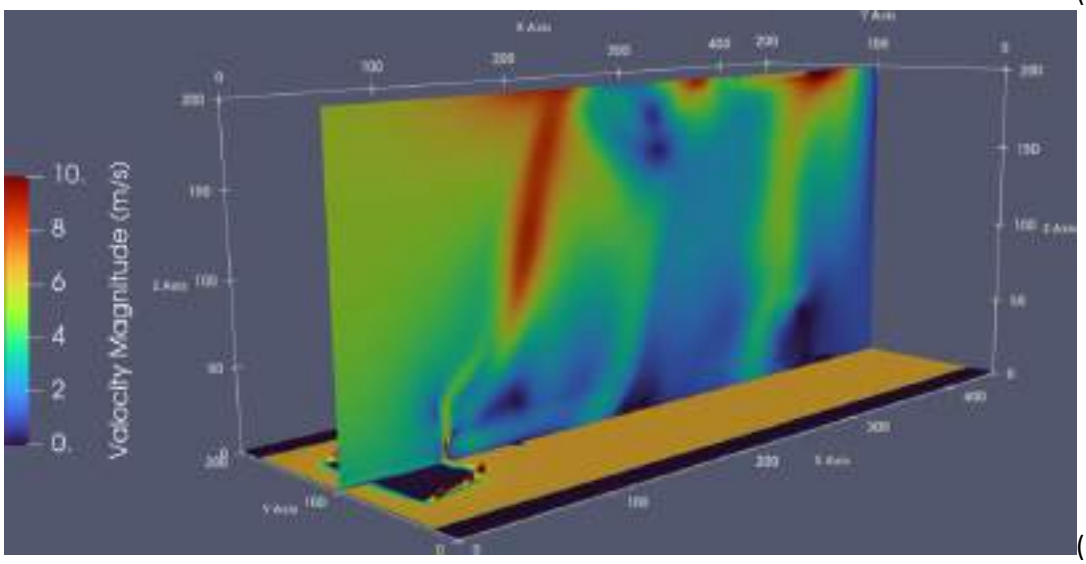

(c)

Figure 29. OpenFOAM simulation results of Fireflux case. Velocity magnitude at 100 s after ignition. Simulation results with different velocity boundary conditions: (a) constant velocity, (b) linear inlet velocity; (c) log model for inlet velocity.

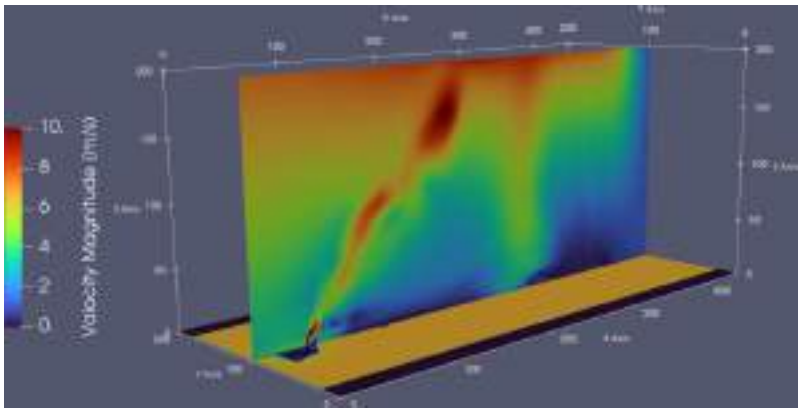

(time =50s)

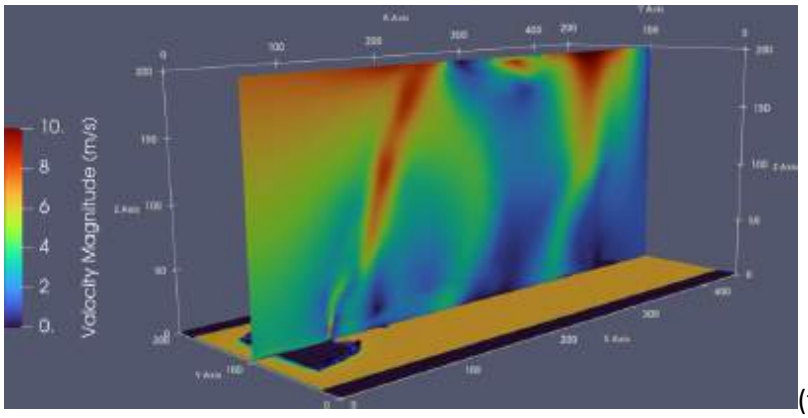

(time=100s)

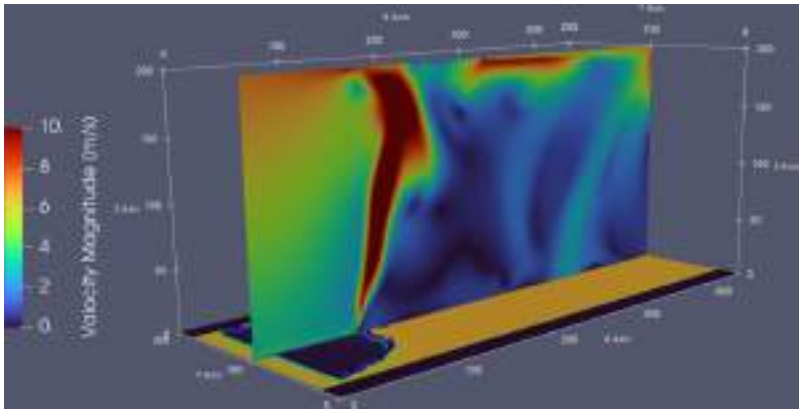

(time=150s)

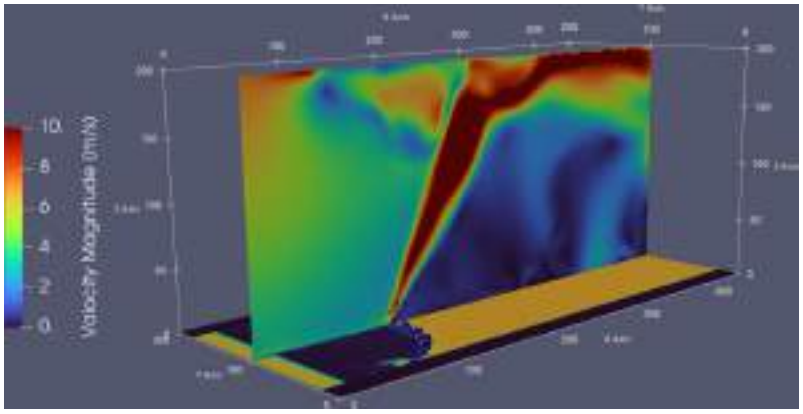

(time=200s)

Figure 30. OpenFOAM simulation results of Fireflux case. Velocity magnitude at time moments 50 s, 100 s, 150 s and 200 s after ignition. Case with linear velocity boundary condition.

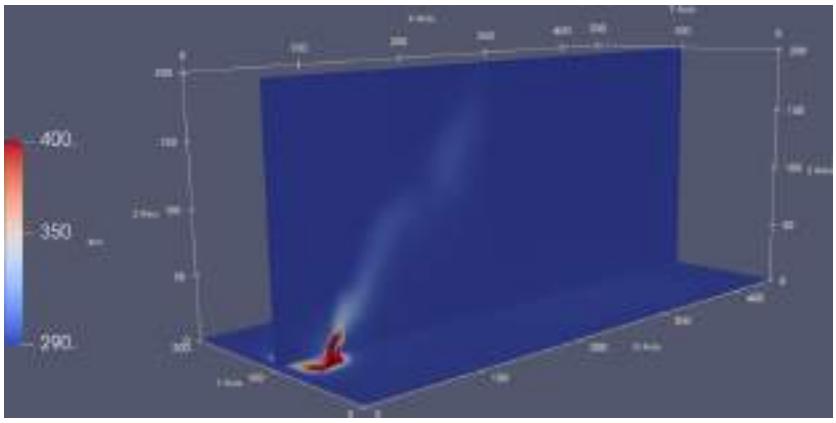

(time=50 s)

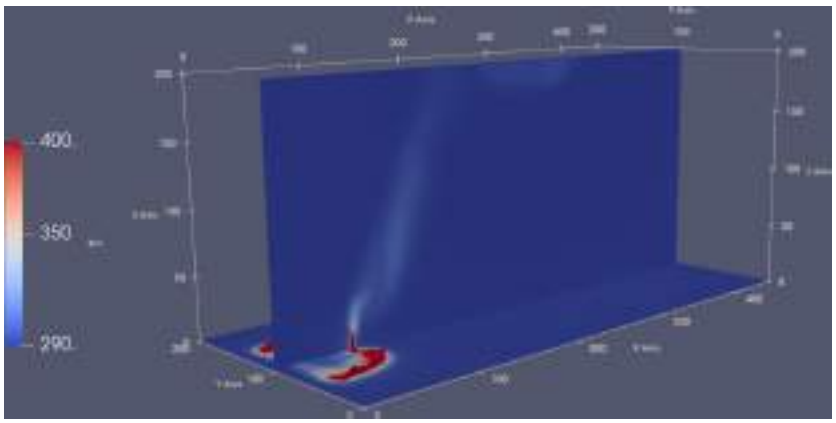

(time=100 s)

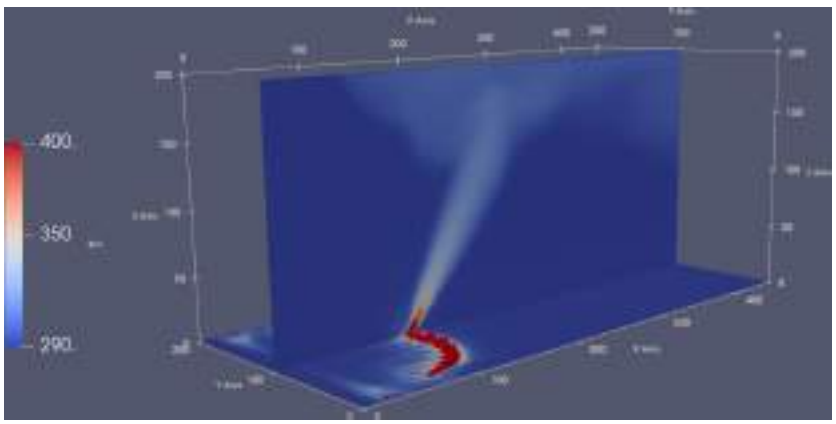

(time=150 s)

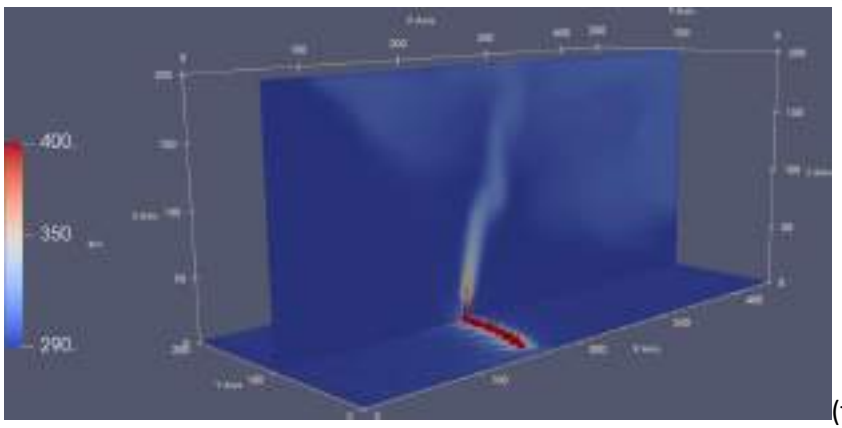

(time=200 s)

Figure 31. OpenFOAM simulation results of Fireflux case. Temperature at time moments 50 s, 100 s, 150 s and 200 s after ignition. Case with linear velocity boundary condition.

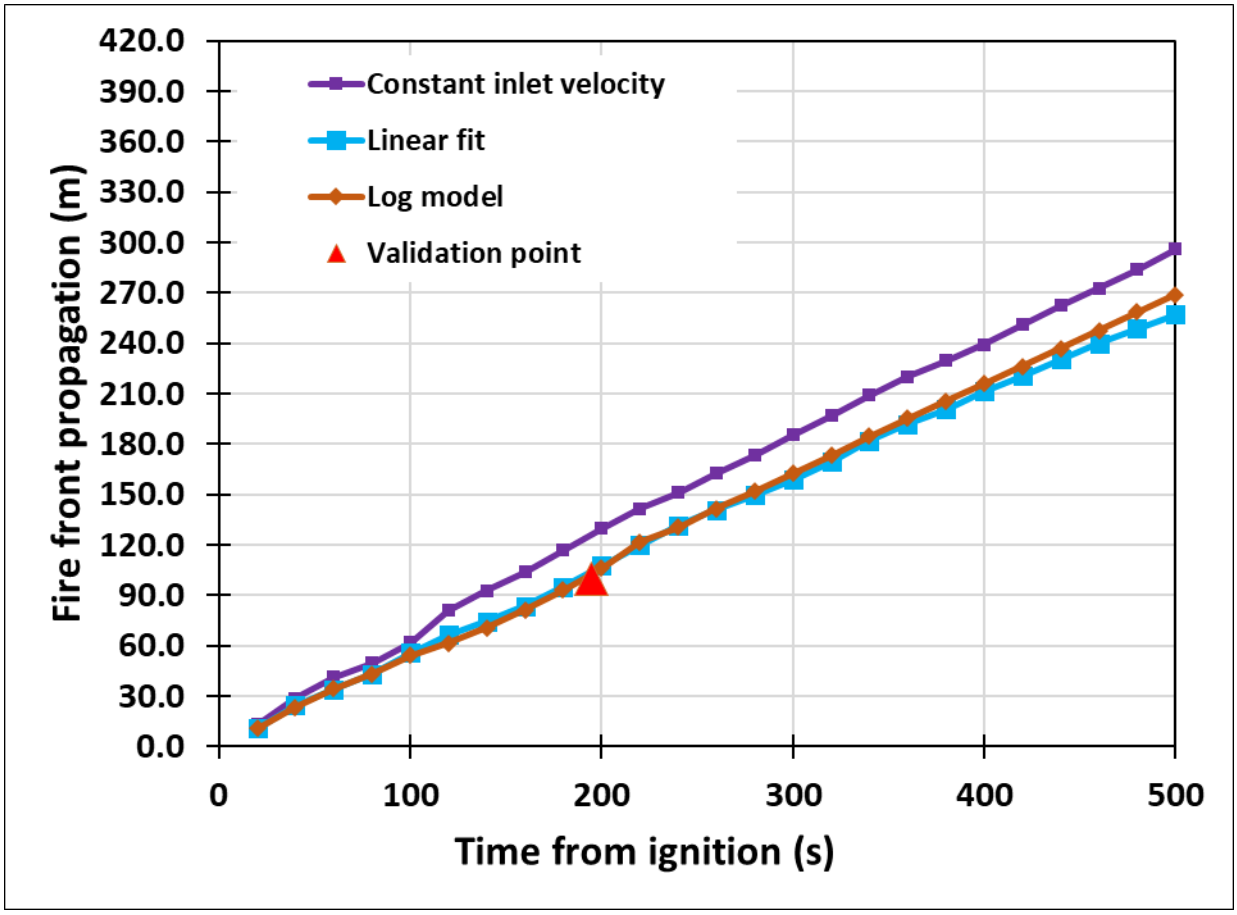

Figure 32. OpenFOAM simulation results of Fireflux case. Comparison of the fire front propagation with the validation data. Validation data point is obtained from Clements et al. (2007.

The only measurement point of the fire front propagation is presented in *Figure 33*. Simulated results for the fire front propagation are in good agreement with the validation data.

Figure 34 presents the comparison of the simulated temperature against the measurements at different heights at the main tower. Similarly to the measured data, heat of the tilted fire plume first reaches the sensors located in the higher levels of the main tower, and later for the lower levels. The simulated data is in good agreement with the validation measurements. It reaches the peak values at the same time and the values agree well.

The simulated results demonstrate the same phenomena of the plume development and fire propagation, both quantitatively and qualitatively, as described in the works of Clements et al 2007 and 2008. A sensitivity study for the Fireflux case is presented in the section 5.3.2.

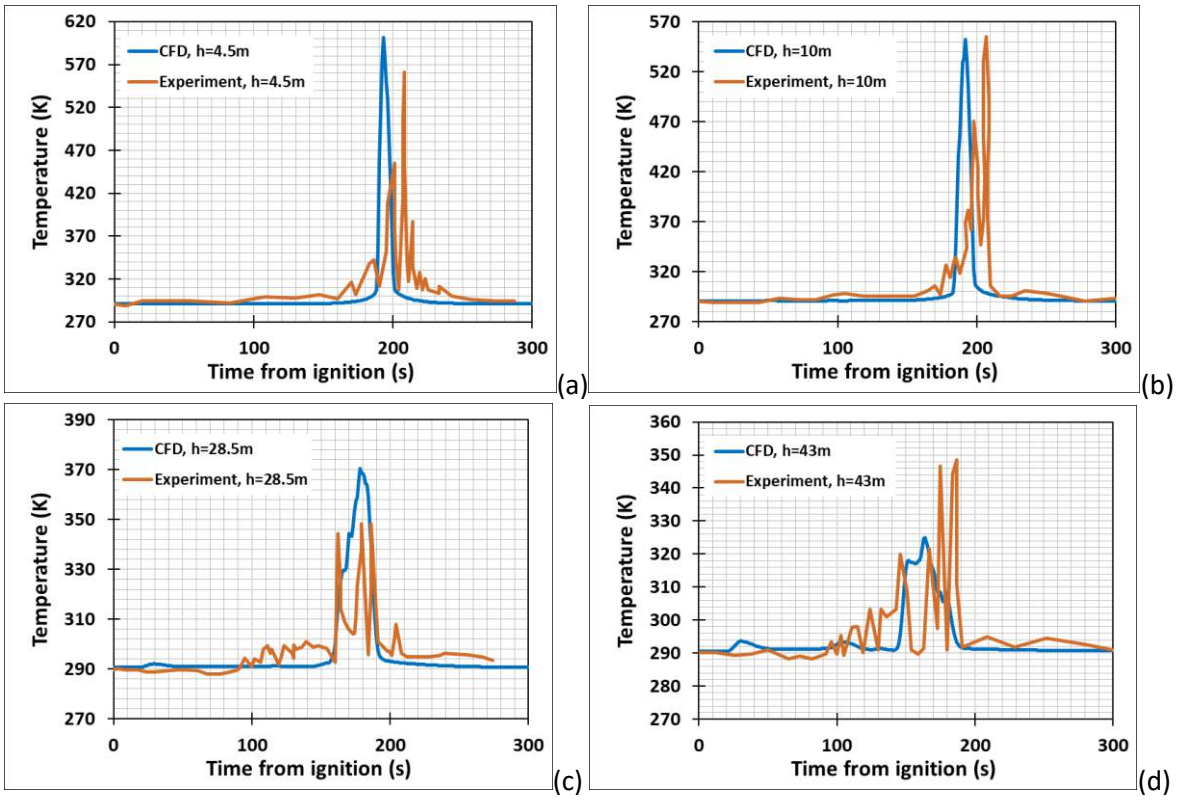

Figure 33. OpenFOAM simulation results of Fireflux case. Comparison of the simulated temperature with the measurements at the main tower at height 4.5m (a); height 10 m (b); height 28.5 m (c) and h=43 m (d).

4.2 Validation simulations of burning Douglas fir trees (with FDS)

Burning of Douglas fir trees was simulated with FDS, and the results were compared with the experimental results of Mell et al. (2009). The goal was to assess the accuracy of FDS in capturing fire behaviour in single tree fire tests by examining mass loss rates from simulations and experiments to determine if the trees model could also be used in larger scale simulations.

4.2.1 Description of the experiments of burning Douglas fir trees

In the study about Douglas fir trees (Mell et al. 2009), NIST conducted controlled burning experiments on 12 Douglas fir trees: nine 2-meter trees and three 5-meter trees. The 2-meter trees were categorized into dry and moist trees with average moisture contents of 14% and 49%, respectively. 5-meter trees had only one category and those trees had 26% average moisture content.

Two types of custom gas burners were used for ignition:

- For the 2-meter trees, an 80 cm circular burner with a heat release rate of 30 kW was used. The igniter was turned off after 10 seconds for the driest trees (average

moisture content (MC) = 14%) and after 30 seconds for trees with larger moisture content (average MC = 49%). The vertical distance from burner to the tree crown base was between 10 and 20 cm.

- For the 5-meter trees (average MC = 26%), a larger hexagonal burner with a span of 122 cm and a heat release rate of 130 kW was used, and the igniter was shut off after 30 seconds. Here, the vertical distance from burner to the tree crown base was 30 cm.

Load cells measured the mass of the trees throughout the burning process, and video recordings documented the ignition and burning phases. The tree trunk and biggest branches were not completely burned during the experiments in any of the trees and with trees with 49% moisture content the tree crown was not completely burned either. Modelling was mainly based on the actual mass loss measured during the experiments.

Figure 34 A snapshot from a 2 m tall tree experiment showing the igniter and load cell configuration (Mell et al. 2009).

In addition to mass loss tracking, also the radiant heat flux was tracked at different distances from the tree base. Radiant heat flux was measured at 2-metre and 3-metre distances at heights of 0.2 m, 1.2 m, 2.3 m, 3.4 m and 4.5 m for all trees.

4.2.2 Modelling and simulation of the experiments

In the article of Mell et al. (2009) some fire models have already been constructed by the researchers. These models were made with Wildland Urban Interface Fire Dynamics Simulator (WFDS), which is an extension of FDS version 5.2 to outdoor fire spread and smoke transport problems. This time the models were tested using FDS version 6.8.0.

Fire models are from FDS Validation files (McGrattan et al., 2024b) and have the same model inputs as described in the article of Mell et al. (2009). The most important parameters are described in the table below (*Table 7*).

Table 7. Parameters used in the simulations, HRR meaning Heat Release Rate.

	2-meter-tall tree with 14 % moisture content	2-meter-tall tree with 49 % moisture content	5-meter-tall tree with 26 % moisture content
Heat of Combustion	17 425 kJ/kg	17 425 kJ/kg	17 425 kJ/kg
Simulation time	30 seconds	60 seconds	60 seconds
Ignition with particles	Circle with 80 cm diameter, total HRR 30 kW	Circle with 80 cm diameter, total HRR 30 kW	Circle with 120 cm diameter, total HRR 129.4 kW
Ignition time	10 seconds	30 seconds	30 seconds

Figure 35 and *Figure 36* show the two simulation domains used in FDS. In both figures the black circle represents the ignition area. Green and brown dots in cone shape are the fuel particles that the tree model is using. Yellow dots next to the cone are measurement devices for gauge heat flux.

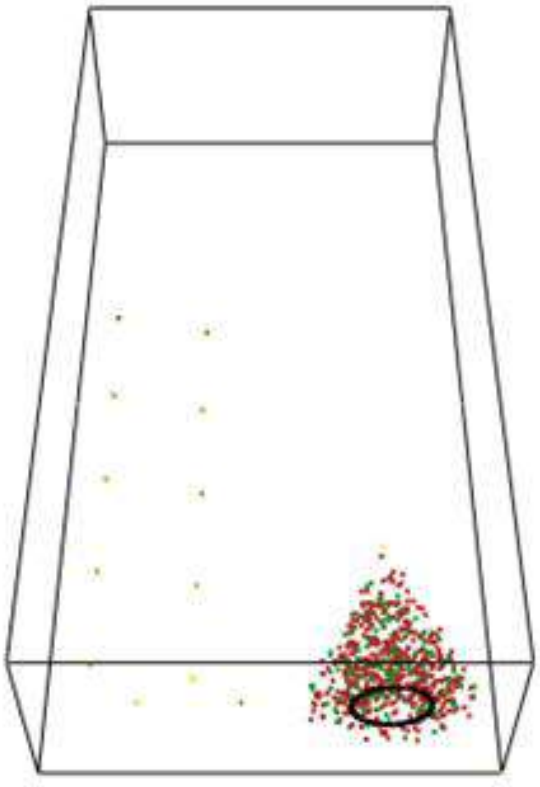

Figure 35. Simulation domain in FDS for the 2-meter-tall trees.

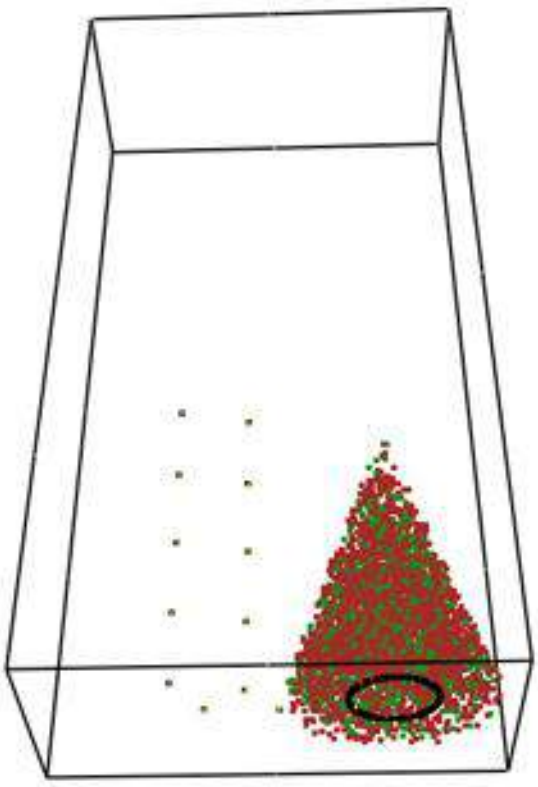

Figure 36. Simulation domain for the 5-meter-tall tree.

4.2.2.1 Mass loss validation

Mass loss simulated with FDS was compared to the experimental values and the WFDS simulation values from the research paper of Mell et al. (2009). Average initial total mass for each tree type from Mell et al. (2009) and mass in FDS are presented in *Table 8*.

Table 8. Initial total mass in the experiment compared to mass loss and FDS initial total mass in simulations.

The height and moisture content of the burned tree in the experiment	Initial total mass in the experiment	Average dry mass loss during the experiment	Initial dry mass in the FDS model
2 m tall, 14% moisture content	9.7 kg	3.9 kg	3.7 kg
2 m tall, 49% moisture content	13.5 kg	3.0 kg	5.9 kg
5 m tall, 26% moisture content	57.9 kg	18.8 kg	19.5 kg

In the experiment dry mass loss was acquired by measuring the total mass loss and using the following formula to calculate the dry mass loss:

$$\Delta m_{dry} = \frac{\Delta m_{total}}{1+M},$$

M = moisture content (in percentage), Δm_{dry} = dry mass loss and Δm_{total} = total mass loss.

Similarly, Δm_{total} can be obtained by the following equation:

$$\Delta m_{total} = \Delta m_{dry} * (1 + M)$$

The drier 2-metres and 5-metres tall trees (see *Table 8*) were modelled according to the mass losses in the experiment, so that in the FDS simulation the whole fuel load can burn, and unburnt wood can be left out of the simulation. The burnt mass was divided into 4 categories: foliage, round wood of diameter ≤ 3 mm, round wood of diameter ≤ 3−6 mm and round wood of diameter ≤ 6−10 mm. Foliage and round wood up to 10 mm in diameter dominated the mass losses and, to simplify the model, these parameters were chosen.

The distribution of dry mass in these size classes was approximately 64%, 11%, 10%, and 15%, respectively. A similar distribution of mass was found in the 5-metres tall trees from sampling five branches of one tree. The mass distribution for the 5-metres tall tree was: 60%, 17%, 12%, and 11%.

In the research paper (Mell et al., 2009) it is stated that for 2-metres trees with 49% moisture content, foliage, and round wood less than 10 mm in diameter, are not completely consumed throughout the crown in the MC = 49% burned trees. For this reason, it was not possible to use the total dry mass loss as a first approximation to the mass of vegetation in the tree crown that is 10 mm in diameter or smaller.

However, from post-burn observations of the MC = 49% burns, it was estimated that the burned region occupied the entire upper 2/3 of the crown and a cylindrical region in the bottom about 1/3 of the crown with a diameter approximately equal to the burner diameter. In this burn region, to a first approximation, the mass loss was predominately from completely consumed foliage and relatively little round wood was consumed. From the volume of the burned region, the volume of the entire crown, the measured mass loss and the assumption that only foliage was consumed, we estimate the mass of foliage to be 3.75 kg. This allows for an approximate determination of the mass of vegetation in the crown that is less than 10 mm in diameter (since from bioassays 64% of this crown mass is foliage). This gives 5.86 kg. As with the MC = 14% case, this mass is portioned into four size types (Mell et al., 2009).

Differences between average dry mass loss during the experiment and the initial dry mass in the simulation are:

- 5.6% for 2-meter-tall trees with 14% moisture content
- 65.3% for 2-meter-tall trees with 49% moisture content
- 3.5% for 5-meter-tall trees with 26% moisture content

Differences between total mass loss in the experiment and in the simulation are:

- 16.5% for 2-meter-tall trees with 14% moisture content
- 55.9% for 2-meter-tall trees with 49% moisture content

- 8.7% for 5-meter-tall trees with 26% moisture content

Equation used for calculating the difference:

$$\frac{|a-b|}{\left(\frac{a+b}{2}\right)}$$

, where a = experimental value and b = simulation value.

The difference between average dry mass loss and initial dry mass in simulation was calculated as follows, *a* is the average of the initial masses of the trees before burning and *b* is the initial mass used as input for the simulation. Exact values can be seen in *Table 8*.

For the difference between total mass loss in the experiment and in the simulation, *a* is an integral calculated from the experimental mass loss data points and *b* is integral of mass loss obtained from simulation. Exact values for *a* are 4.26, 4.31, 24.77 and for *b* they are 3.61, 7.65, 22.71 for 2 m (MC = 14%), 2 m (MC = 49%) and 5 m (MC = 26%) trees, respectively.

Graphs comparing the experimental and simulated mass loss are presented in figures below (*Figures 38 and 41*).

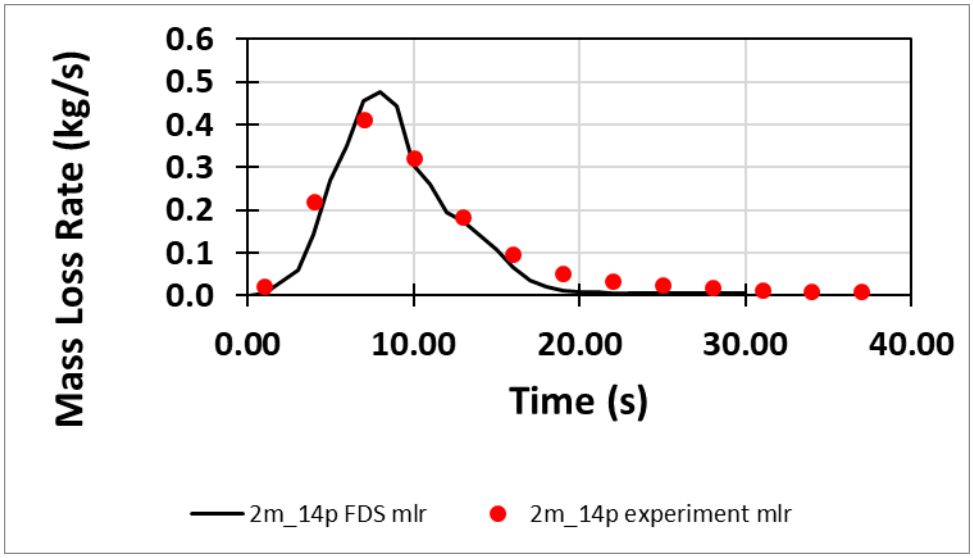

Figure 37. Comparison of 2-meter trees (MC = 14%) in simulation and experimental measurements. Experimental mean values are marked with red dots and the FDS simulation values for 2-meter-tall trees with 14% moisture content are marked with black line.

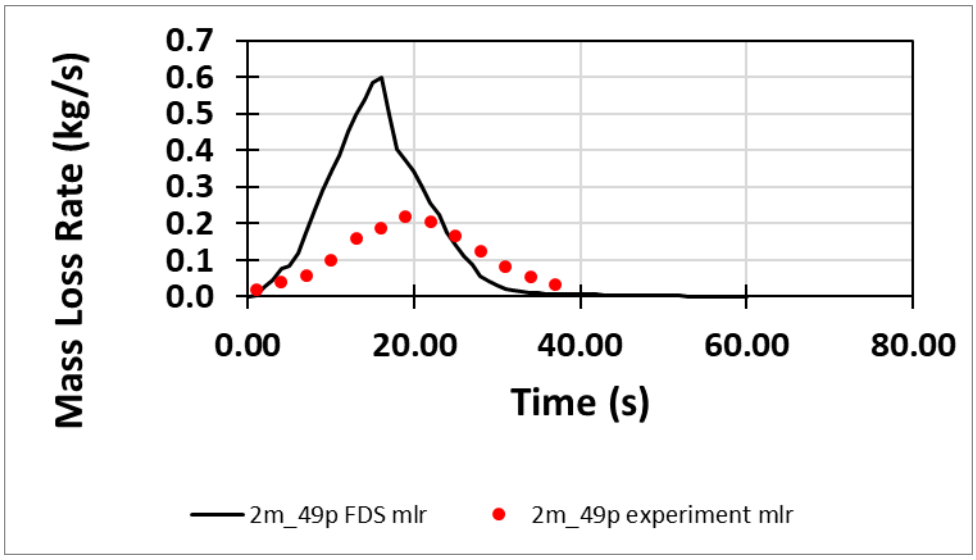

Figure 38. Comparison of 2-meter trees (MC = 49%) in simulation and experimental measurements. Experimental mean values marked with red dots and the FDS simulation values for 2-meter-tall trees with 49% moisture content marked with black line.

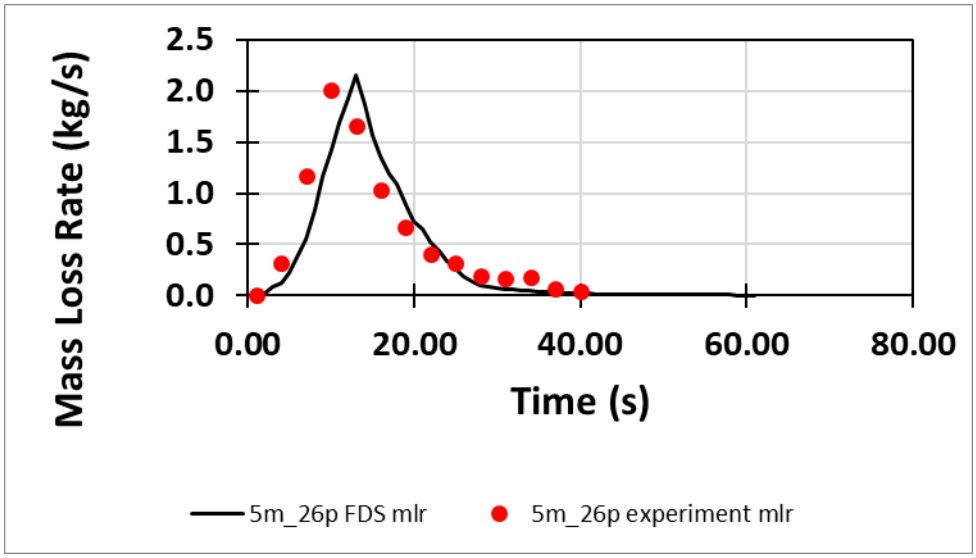

Figure 39. Comparison of 5-meter trees (MC = 26%) in simulation and experimental measurements. Experimental mean values marked with red dots and the FDS simulation values for 5-meter-tall trees with 26% moisture content marked with black line.

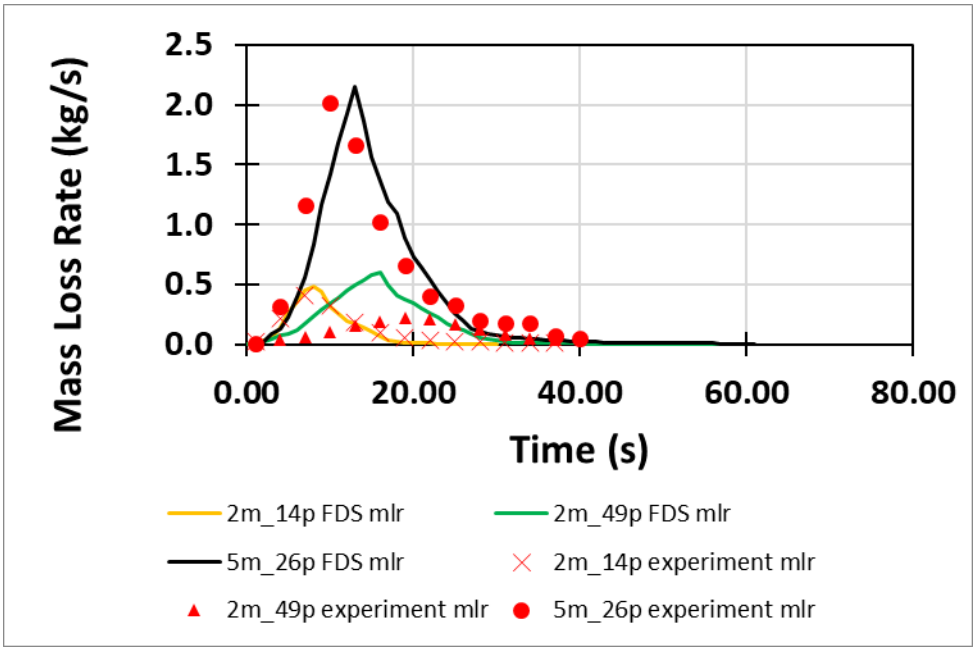

Figure 40. All experimental means and comparison to FDS mass losses.

In *Figure 42* and *Figure 43* there are some interpolated input values to understand better why certain events occur.

In *Figure 42*, moisture content was varied between experimental values of 14% and 49% moisture content. Chosen values were 26%, 33% and 41%. This was done to see how the mass loss rate develops differently with different moisture contents because at first only 14% and 49% cases were seen and 49% wasn't close to experimental values. As can be seen from the figure, the curves with 33%, 41% and 49% are at similar heights and curves with 14% and 26% are closer to the experimental mass loss with 14% trees.

In *Figure 43*, three-meter-tall tree was also simulated, and the mass, height and cone radius were interpolated from 2 m and 5 m tall trees. Moisture content was chosen according to 5 m tall trees (26%) and 2 m tall trees had also realistic mass loss rates, so the interpolated 3 m tall tree had also the same 26% moisture content.

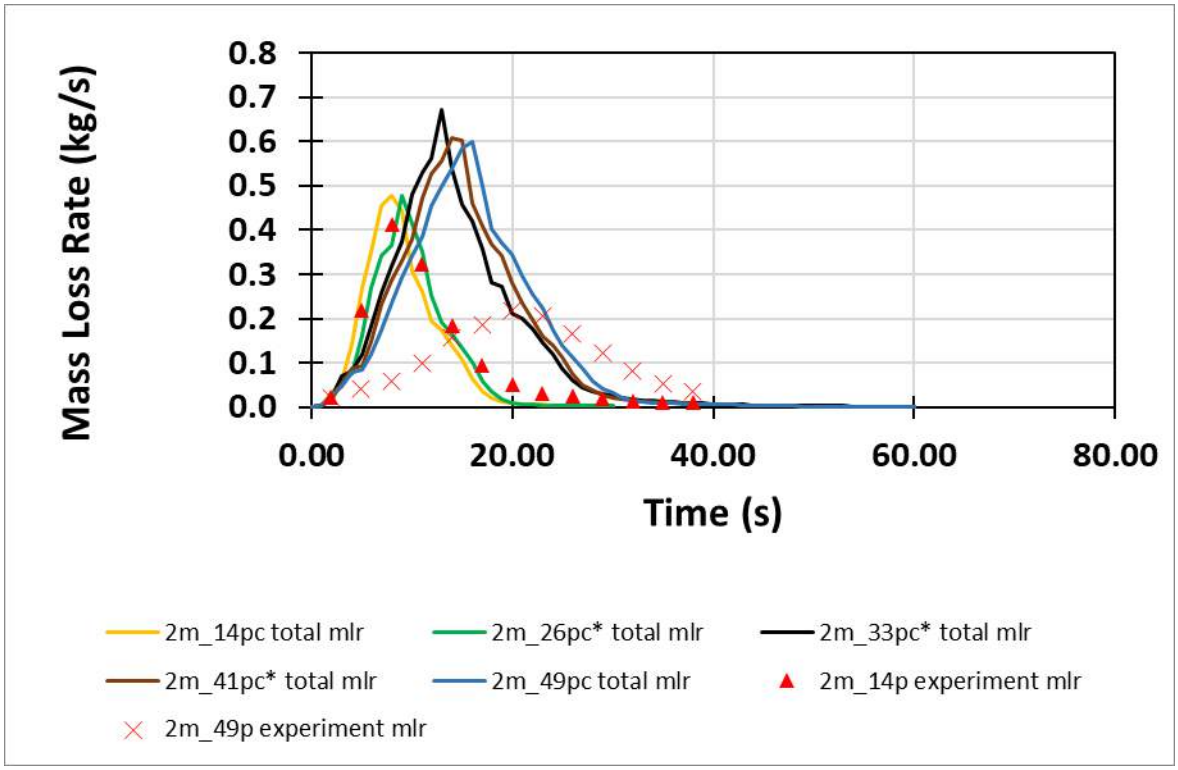

*Figure 41. All 2-meter-tall trees. Graphs marked with * don't have comparison with experimental values. For 2-meter-tall trees, experiments were done only for trees with 14% and 49% average moisture content.*

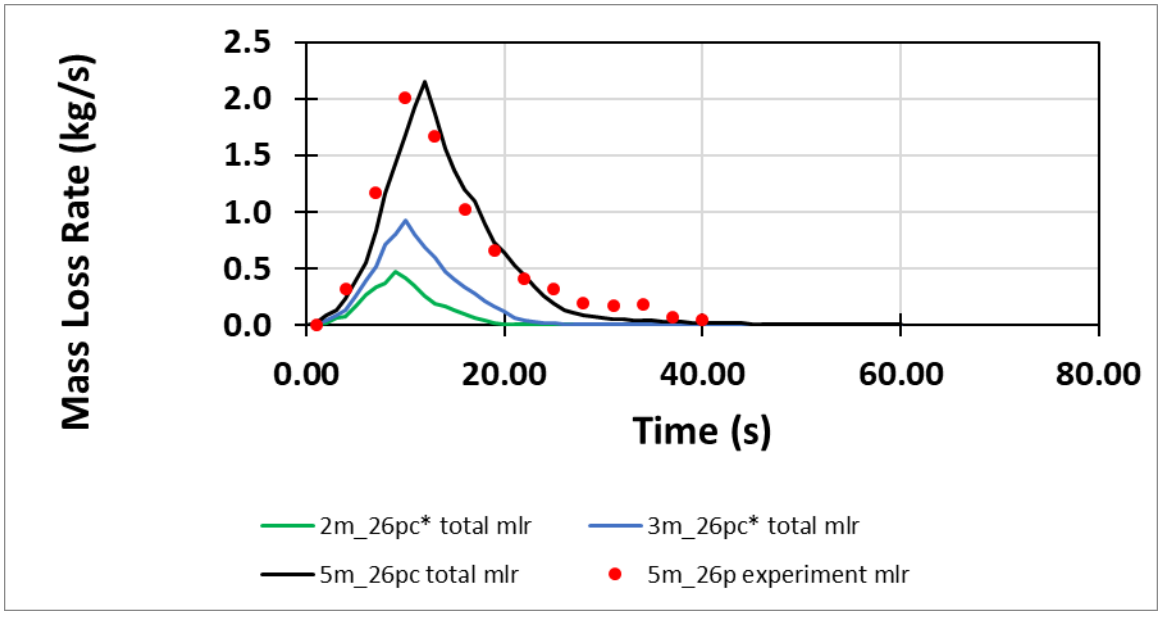

*Figure 42. All trees with 26% moisture content. Graphs marked with * don't have comparison with experimental values. For trees with 26% moisture content experiments were done only for 5-meter-tall trees.*

4.2.2.2 Heat flux validation.

Heat flux in FDS was compared to the experimental values and to the WFDS simulation values in the research paper (Mell et al., 2009). There were sensors in 10 places to measure radiation in experiment and in simulations the heat flux was measured at respective places. In the graphs below all heat flux measuring devices are placed 2 meters away from the base of the tree.

Validation about heat flux was done for the 2-meter trees with 14% moisture content. Result can be seen from *Figure 44* and *Figure 45*.

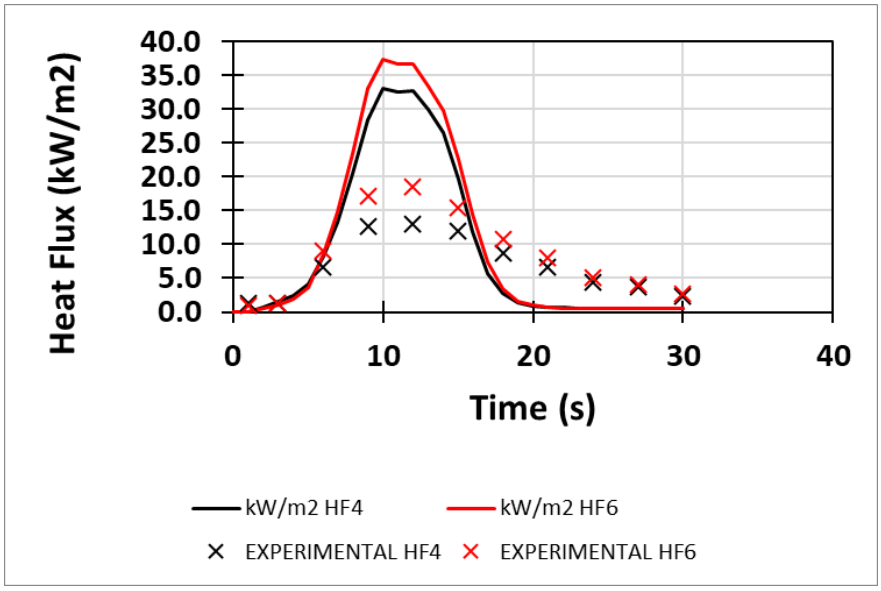

Figure 43. Comparison between Heat Fluxes of experimental mean and FDS simulation results. HF4 is placed at 0.2 m height and HF6 is placed at 1.2 m height.

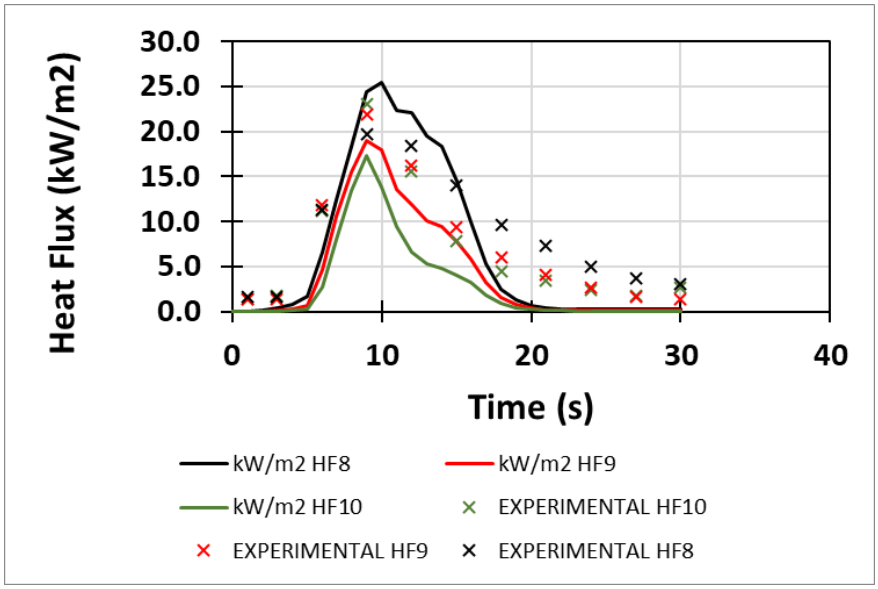

Figure 44. Comparison between Heat Fluxes of experimental mean and FDS simulation results. HF8, HF9 and HF10 are placed at heights 2.3, 3.4 and 4.5 meters respectively.

From *Figure 44* and *Figure 45* can be seen that heat flux is higher on lower heights in FDS, whereas in experiments it is lower. This will result in higher fire spread in simulation than in real life, so the simulations are conservative by nature.

4.2.2.3 Test with coarser mesh

Simulations with 2 m 14% and 5 m 26% were repeated with coarser mesh size: 0.2 m side length compared to originally 0.1 m side length. No big differences were found in neither mass loss rates nor heat fluxes between 0.2 m and 0.1 m mesh sizes.

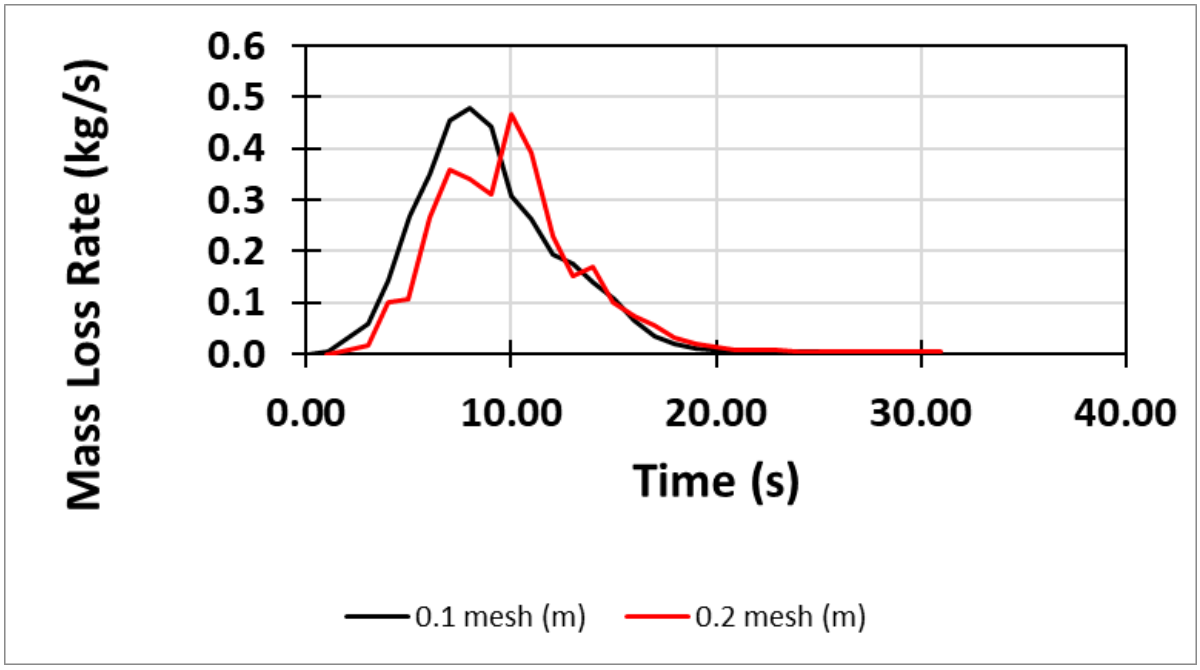

Figure 45. Differences between mass loss rates for coarse and fine mesh in 2-meter trees.

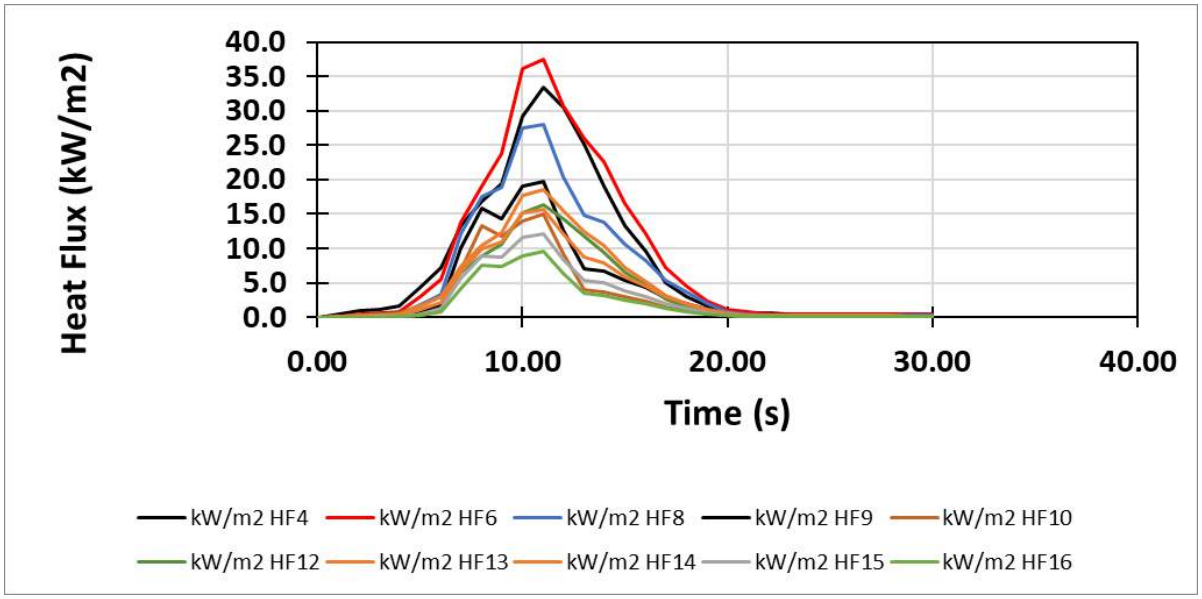

Figure 46. Heat Flux in 0.2 mesh size.

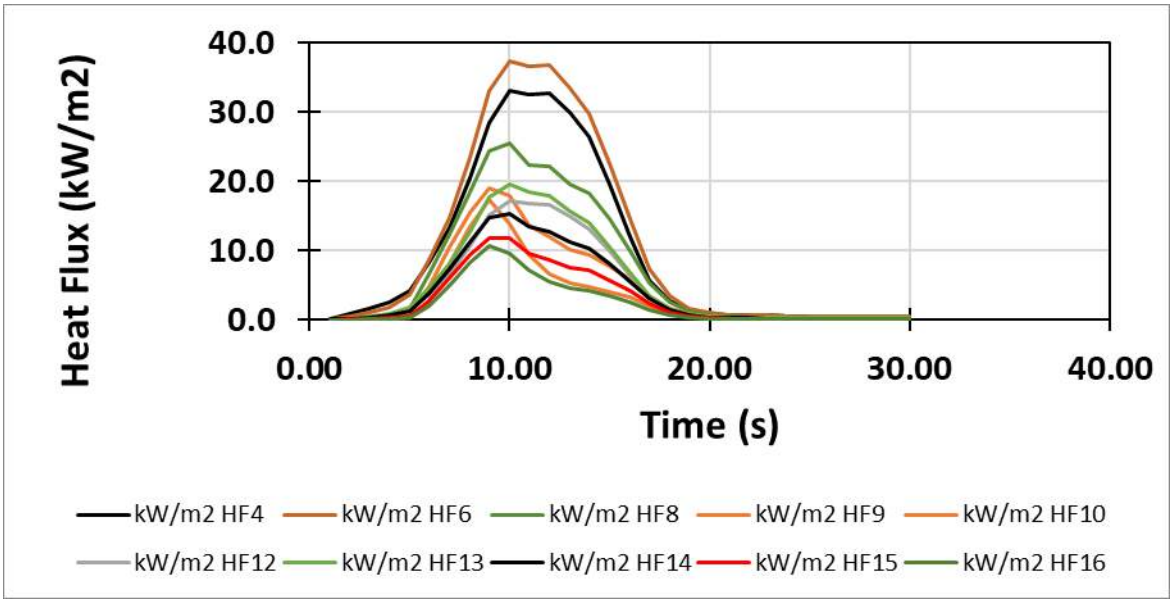

Figure 47. Heat Flux in 0.1 mesh size.

Table 9. Differences in total mass loss compared to experimental values.

	0.1 mesh	0.2 mesh
2 m 14 % mass loss difference	4.1%	6.5%
5 m 26 % mass loss difference	2.1%	3.2%

4.2.2.4 Conclusions

Models created in the research (Mell et al., 2009) for trees with 2 meters of height and 14

% moisture content and trees with 5 meters of height and 26% moisture content can be used for further studies in FDS. Trees with 2 meters of height and 49% of moisture content should not be used in FDS, because of unrealistic mass loss rates.

Heat fluxes were in all cases unrealistic, but conservative, so the decision which trees to use in further simulations were done on basis of mass loss rates only.

5. APPLICATIONS

Once an understanding of the applicability and calculation accuracy of the models was obtained in the validation cases, some applications were made and the simulations were extended by interpolating and extrapolating; with the aim of sensitivity analysis to determine fire behaviour under different conditions, including conditions where extreme fire behaviour is typically observed.

5.1 Combustion of pine needles

The modelling capabilities of FDS were applied to the combustion of pine needles, for which Norway-Sweden LL provided us with measurement data related to the boreal pine forest.

5.1.1 Measurements for (milled) pine needles

The Norway-Sweden LL has collected some information on the ground fire load in Northern hemisphere pine forest. They have examined the burning behaviour of pine needles. The pine needles were tested on a cone calorimeter (ISO 5660-1:2015). The cone calorimeter test is a bench-scale fire test method to assess the contribution of the product tested to the rate of evolution of heat during its involvement in fire. The highly uniform irradiance over the entire specimen surface and the possibility of measuring quantities per unit area and unit mass of the material tested make the cone calorimeter an excellent instrument for determining material parameters and for other scientific purposes. The experiments were performed both for natural needles and milled needles. The specimens were preconditioned 5 days in 60 °C, so their moisture content at the test can be approximated to be quite low. The needles were milled to see how the actual material burns without the effect of the quite random ways how needles could be placed to the test holder. In other words, the test with milled needles gives information on the actual "bulk" material properties that can be used to make a model for the pyrolysis/burning of the real forest litter material containing lots of fallen needles. A cone calorimeter experiment of real needles does not give very much information on the properties of a needle, because the heat convection and radiation will dominate the heat flow in the sample as the needles form a quite porous sample. Thus, the heat conduction inside an individual needle is not very important for this kind of test.

In *Figure 48*, the results of the Norway-Sweden LL measurements done in cone calorimeter are displayed for both the natural needles and the milled needles. Shown is the heat release rate (HRR) measured per unit area. There were 5 tests done for the milled needles and 3 tests for the natural needles. The cone calorimeter tests were done under 50 kW/m^2 irradiance. The ignition time of the needle samples was 9 seconds, both for natural and milled needles. The thicknesses of the samples were 16 mm for both natural and milled needles. The weights of the samples were 8.4 g and 41.3 g in average corresponding to densities 52 and 258 kg/m^3 for natural and milled needles, respectively.

The Norway-Sweden LL data on the burning of pine needles were utilized in this work to construct a material model for FDS that will represent burning of forest ground formed mainly from fallen needles, like in a pine forest. It should be noted that the constructed model is preliminary, and it has not been tested or validated. There is too little experimental information on the needles studied. To do a better material model, one would need some micro-scale measurements on the pyrolysis chemistry of the needles, like TGA, DSC, and MCC experiments. For the present case, the TGA should be made for "fresh" samples as well as for the 5 days in 60 °C dried samples to see how much moisture has gone off during the drying phase. Also, for the estimation of good effective parameters for heat conduction and radiation absorption in the cone calorimeter samples, the cone calorimeter experiments should be conducted using several different

irradiance levels and, if possible, also under inert atmosphere and/or without the spark. A cone calorimeter measurement without the spark and/or in an inert atmosphere would allow a better modelling of the actual pyrolysis reactions and the estimation of thermal parameters as the irradiance at the sample surface is not affected by the heat coming from the flame after the ignition of the sample.

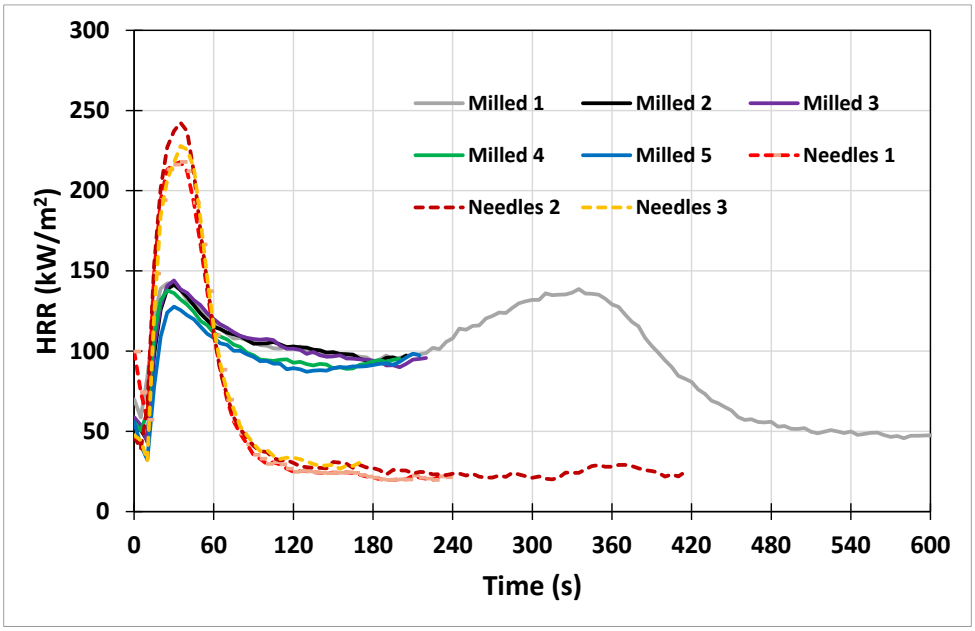

Figure 48. Heat release rate of natural pine needles and milled pine needles in cone calorimeter under 50 kW/m² irradiance measured by the Norway-Sweden LL (Holm Nygaard, 2024).

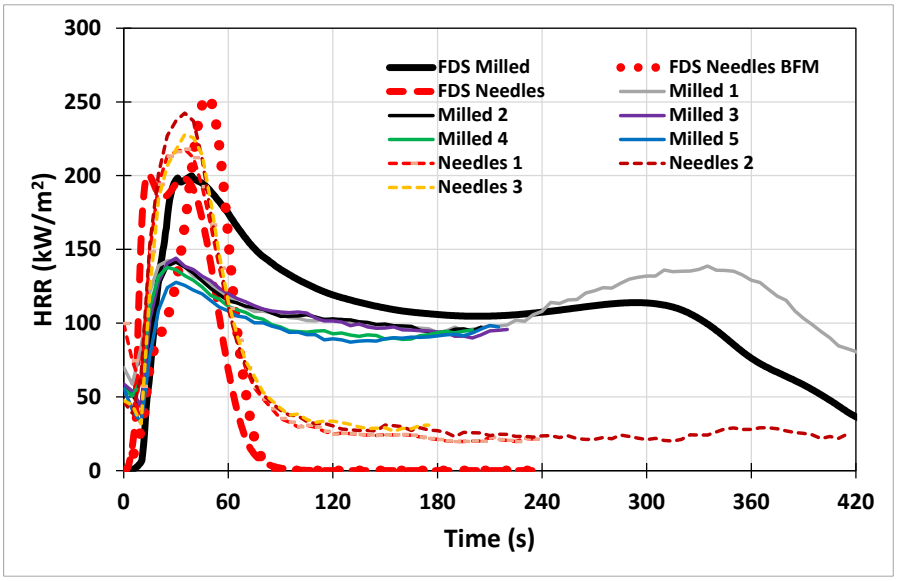

Figure 49. FDS results for the pine needles and milled pine needles compared to Norway-Sweden LL cone calorimeter experiments. Shown are the heat released rates in cone calorimeter under 50 kW/m² irradiance. The pine needles samples were modelled by two variations, one was the usual FDS surface model ("FDS Milled" and "FDS Needles"), the other the Boundary Fuel Model ("FDS Needles BFM").

As there was not enough experimental information to do a pyrolysis model of the pine needles from scratch, the already done material models found in the FDS Validation Guide (McGrattan et al. 2024b) were used. The "vegetation_model.txt" from the validation cases (same model used in both ones) "Crown_Fires" and "CSIRO_Grassland_Fires" (FDS Github repository revision FDS-6.9.1-752-g115fc2734) were used as a starting point for the material model of pine needles and milled pine needles. As there was not TGA or similar data available, the pyrolysis chemistry related parameters of the vegetation model were not changed, e.g., the activation energies, heats of reaction, etc. Thus, just the conductivities, densities, moisture content, and char production fraction were changed as the FDS cone calorimeter model was tried to optimize against the 50 kW/m^2 measurement data. The obtained FDS model outputs are compared to the measured HRR values in *Figure 49*. The FDS model for the cone calorimeter used 10 mm computational mesh and it also estimated the heat flux from the flame back to the surface like explained in the conference papers by Korhonen et al. (2021) and Korhonen et al. (2022).

The material models were not thoroughly optimized, because the experimental results available were very limited. The target was to create reasonable models to produce FDS input keywords for the next modelling step.

5.1.2 FDS models for (milled) pine needles

The first model describes the milled pine needles. As the milled pine needles form quite uniform and dense layer, just the normal FDS pyrolyzing surface model was used to model them. The milled pine needle layer was assumed to be 16,1 mm thick, and it was on top of the mineral wool in the cone calorimeter sample holder. The moisture content of the needles was assumed to be 1% as the samples were well dried. The starting point for all the pine needle (milled or not) FDS material models was the FDS Validation suite "vegetation_model.txt" file that is used in the validation cases Crown Fires and CSIRO_Grassland_Fires (FDS Github repository revision FDS-6.9.1-752-g115fc2734, McGrattan et al. 2024b). The vegetation model contains dry vegetation and moisture to start with, the moisture is evaporated away during the heating of the material, and dry vegetation undergoes a pyrolyzing reaction to form char and fuel gases. The char undergoes oxidation reaction to form ash and non-burning gases.

The reaction kinetics parameters, specific heats, heats of reaction, and heats of combustion were used as they were specified in the vegetation model of the FDS validation cases. The density of the unburned vegetation was taken from the experimental information given by Norway-Sweden LL and the densities of the reaction products char and ash were modified accordingly. The thermal conductivities, absorption coefficients for thermal radiation, and the pyrolysis reaction yield were used to optimize the material model compared to the Norway-Sweden LL measurements. These values were:

- Densities of dry vegetation, char, and ash were 258 kg/m^3, 150.6 kg/m^3, 33.634 kg/m^3, respectively.
- Absorption coefficient 11000 1/m was used both for dry vegetation and char.

- Thermal conductivity of dry vegetation was 0-1 W/m/K. Temperature dependent conductivity *k(T)* was used for char and ash, where *k* (20 °C) = 0.065 W/m/K, *k*(500 °C) = 0.2 W/m/K, and *k*(800 °C) = 0.4 W/m/K.
- The yield of char was 0.35 in the pyrolysis reaction.

The second model is for dried pine needles using a normal FDS surface definition (not wildfire specific) like above done for the milled needles. The pine needle layer was assumed to be 16.1 mm thick and if was on top of the mineral wool in the cone calorimeter sample holder. The moisture content of the needles was assumed to be 1% as the samples were well dried. The model for the dried pine needles was the same as above mentioned model for milled pine needles, but the following (optimized) parameters were used:

- Densities of dry vegetation, char, and ash were 52 kg/m^3, 30 kg/m^3, 6.7 kg/m^3, respectively.
- Absorption coefficient 7000 1/m was used for the dry vegetation.
- The temperature dependent thermal conductivity *k(T)* was used, where *k*(20 °C) = 0.065 W/m/K, *k*(500 °C) = 0.2 W/m/K, and *k*(800 °C) = 0.4 W/m/K for char, and *k*(20 °C) = 0.2 W/m/K, *k*(500 °C) = 0.4 W/m/K, and *k*(800 °C) = 0.8 W/m/K for ash.
- The yield of char was 0.35 in the pyrolysis reaction.

The third model is for dried pine needles, and it is using the Boundary Fuel Model of FDS that is used to describe wildland fire load, when the computational grid resolution is such that the fire load cannot be described accurately (each tree, branch, grass leaf, etc.). The vegetation above the ground is described as porous media. This model used 52 kg/m^3 as the mass per volume, as the density of pine needles in the cone calorimeter sample was measured to be this value. This model for the dried pine needles was the same as above-mentioned first model for dried pine needles, but the following (optimized) parameters were used:

- Densities of dry vegetation, char, and ash were 514 kg/m^3, 300 kg/m^3, 67 kg/m^3, respectively.
- Surface to volume (SAV) ratio was 201 1/m.
- Absorption coefficient 7,000 1/m was used for the dry vegetation.
- Thermal conductivity of dry vegetation was 0.5 W/m/K, and the temperature dependent conductivity *k(T)* was used, where *k*(20 °C) = 0.2 W/m/K, *k*(500 °C) = 0.4 W/m/K, and *k*(800 °C) = 0.8 W/m/K for dry vegetation and char, and *k*(20 °C) = 0.065 W/m/K, *k*(500 °C) = 0.2 W/m/K, and *k*(800 °C) = 0.4 W/m/K for ash.
- The yield of char was 0.35 in the pyrolysis reaction.

It should be noted that the material models for pine needles above are just tentative as the amount of experimental data was very limited. It could be argued that the generic vegetation models presented in FDS User Guide (McGrattan et al. 2023) and FDS

Validation Guide (McGrattan et al. 2024b) seem to be a quite good starting point for vegetation modelling of a wildfire scenario. It might be that the combustion properties and other vegetation material parameters are not the first ones to be changed, when realistic fuel load properties are needed in FDS simulations of wildfires. The other aspects of the fuel load, like its moisture content, SAV ratio, amount, height, drag properties and how detailed can its representation be in FDS simulation might affect much more on the results.

5.1.3 FDS simulation of pine needle ground fire

To test the above obtained material models for pine needles, a FDS simulation was made, where the CSIRO grassland fire case C064 setting was adopted for pine needles. This means that the fire load was changed from grass to pine needles. The BFM version of the pine needle material model was used as the pine needles are so small and they cannot be resolved in the simulation. The above-mentioned Norway-Sweden LL experimental results were obtained for relatively thin samples, but in the FDS simulation of a spreading fire on a ground containing pine needles as litter, it was assumed that there is 0.1 m thick layer of pine needles described as porous layer (boundary fuel model) on top of 0.1 m solid “dirt” ground material. The solid “dirt” material was similar to the CSIRO grassland fire model and other simulation parameters were identical, except the vegetation fire load definition and the ignition source. The ignition source used in the CSIRO grassland simulations did not ignite the pine needles. So, the ignitor HRR was increased (5,000 kW/m^2) and the duration of the maximum HRR at each point on the ignition line was increased to 30 s. These choices are somewhat arbitrary, but they were able to ignite the pine needles so that a forward spreading fire was forming, see *Figure 50*.

As the 0.1 m layer of pine needles was found to produce a forward spreading fire, thinner layers of pine needles were also simulated. Below in *Figure 52* and *Figure 52* resulting fires for 0.05 m and 0.02 m thick pine needle layers are shown, respectively. It is seen that thinner layers are not able to sustain a spreading fire in this scenario. It should be noted that the above model for the pine needles is quite crude, since there was not much experimental data that was used to construct the model. Thus, the results of the presented simulations are illustrating the existing capabilities to model forest fires when there is detailed information available on the fuel load.

As the 0.1 m layer of pine needles was found to produce a forward spreading fire, thinner layers of pine needles were also simulated. Below in *Figure 51* and *Figure 52* resulting fires for 0.05 m and 0.02 m thick pine needle layers are shown, respectively. It is seen that thinner layers are not able to sustain a spreading fire in this scenario. It should be noted that the above model for the pine needles is quite crude, since there was not much experimental data that was used to construct the model. Thus, the results of the presented simulations are illustrating the existing capabilities to model forest fires when there is detailed information available on the fuel load.

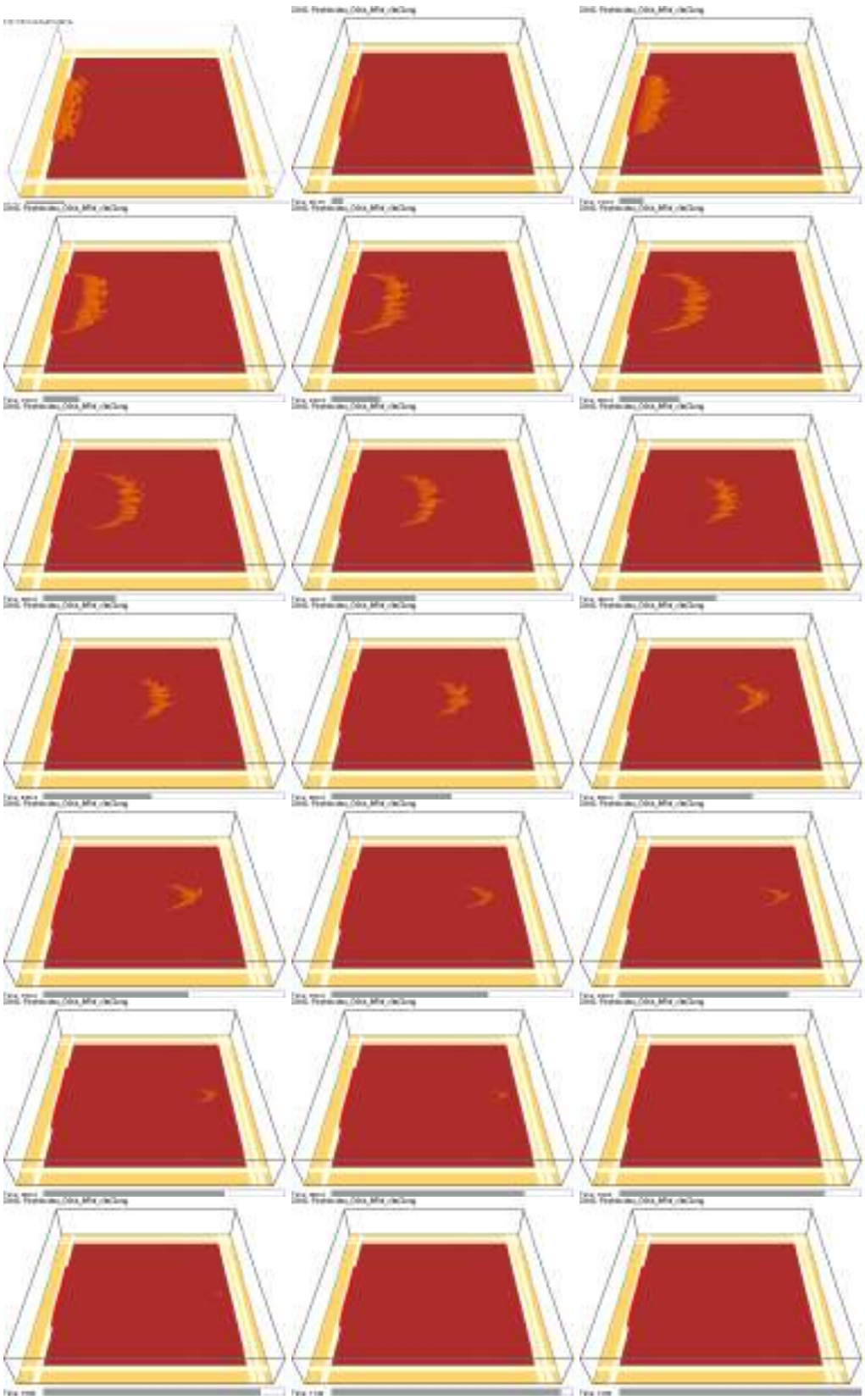

Figure 50. FDS simulation of a forest litter fire, where 0.1 m layer of pine needles forms the vegetation fire load and the BFM is used to describe the fire load. Shown are snapshots of the fire at 30 s, 60 s, 120 s, and at every 60 s up to 1200 s.

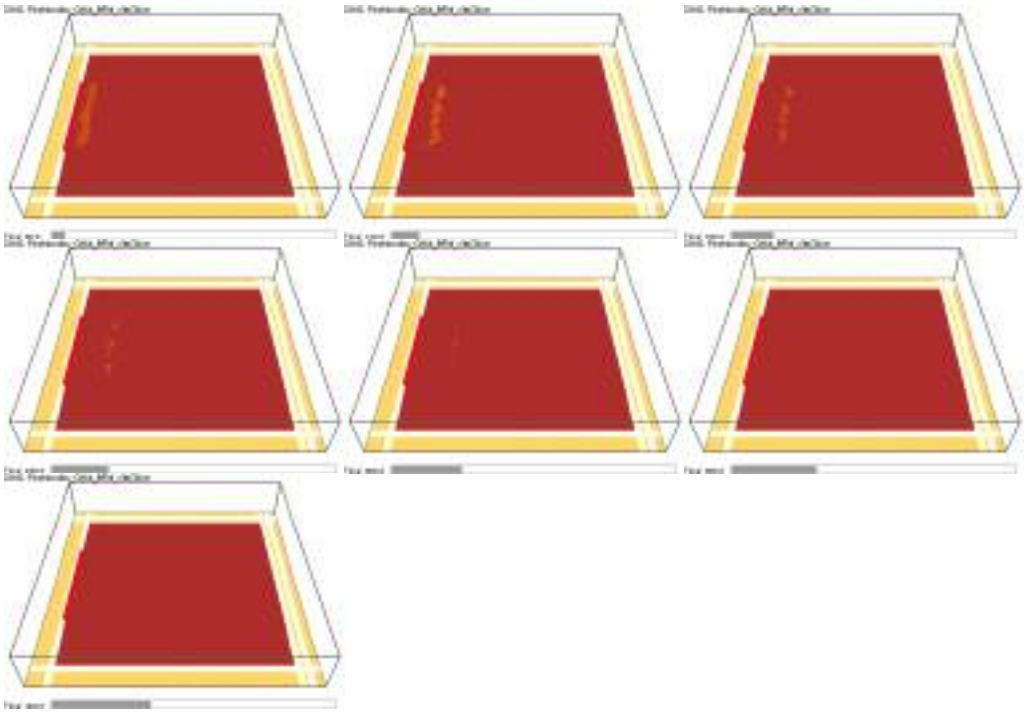

Figure 51. FDS simulation of a forest litter fire, where 0.05 m layer of pine needles forms the vegetation fire load and the BFM is used to describe the fire load. Shown are snapshots of the fire at 60 s, 120 s, and at every 60 s up to 420 s.

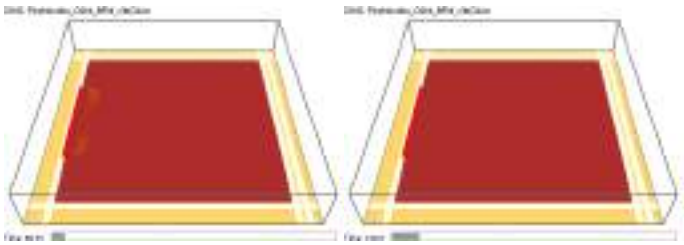

Figure 52. FDS simulation of a forest litter fire, where 0.02 m layer of pine needles forms the vegetation fire load and the BFM is used to describe the fire load. Shown are snapshots of the fire at 60 s and 120 s.

5.2 OpenFOAM simulations of forest fires

OpenFOAM is a general purpose CFD software which does not include specific models for the forest simulations. Therefore, trees or forest should be presented as a set of Lagrangian fuel particles. Description of the sets of Lagrangian clouds can describe individual tree or forest with different accuracy, which is always a matter of computational efforts. For the forest simulation every geometrical detail of the trees is not resolved, however, the forest is modelled in more details than uniform area, i.e. the empty spaces between the trees are taken into account and affect the CFD simulations.

Additional sub models should be introduced to include the effect of trees and correct modelling of the air flow in the computational domain.

5.2.1 Modelling approach and cases setups

OpenFOAM was applied to model the forest fire. Simplified model of the trees was applied. It was assumed that each tree consists of two parts: tree stem and small vegetation. Diameter of the tree stem was assumed to be 15 cm, which implies very small surface to volume ratio and therefore very slow burning. On the other hand, small vegetation was assumed to have large surface to volume ratio. Small vegetation includes needs and small branches. The model includes also ground vegetation (shrubs, grass, moss, etc). Vegetation parameters are presented in the *Table 10*.

Each vegetation type was modelled as a separate Lagrangian particle cloud. Domain was divided to sub areas based on the presence of prescribed Lagrangian clouds. Porosity properties, drag and turbulent forces parameters were prescribed based on the vegetation properties located in the corresponding area.

The trees were located in the computational domain so, that the stems positions were prescribed by the user and small tree vegetation was surrounding the stems. Position of the stem of simulated case A is shown in *Figure 53* together with the position of the small vegetation. Ground vegetation was placed uniformly along the whole computational area except of 20 metres from the sides of the domain.

Line ignition was applied with ignition speed 1 m/s. Ignition started in the middle of the area 20 metres from the side. Width of ignition line was 2 metres. Only ground vegetation was ignited, trees were not presented in the ignition line.

Wind velocity was assumed to follow log-model with the same parameters as for the FireFlux case, which model parameters are presented in *Table 6*. Wind was assumed to be fixed in time; wind direction was from the left to the right.

Three different tree layouts were considered, their positions are illustrated in *Figure 53*. Each layout included 63 trees. In the Case A, trees were set in the lines shifted with respect of each other. Distance from the tree centre in each line is 10 m, distance between lines 5 metres. For cases B and C, the position tree is in the straight lines with distances of 10 and 5 metres, respectively.

Figure 54 presents wind velocity before the fire was stated. Positioning of the trees affects the velocity distribution. Wide spaces between the trees channels the velocity in the case C, while the trees in every second line in the case A serve as obstacles and wind flows around the trees, which changes the wind directions.

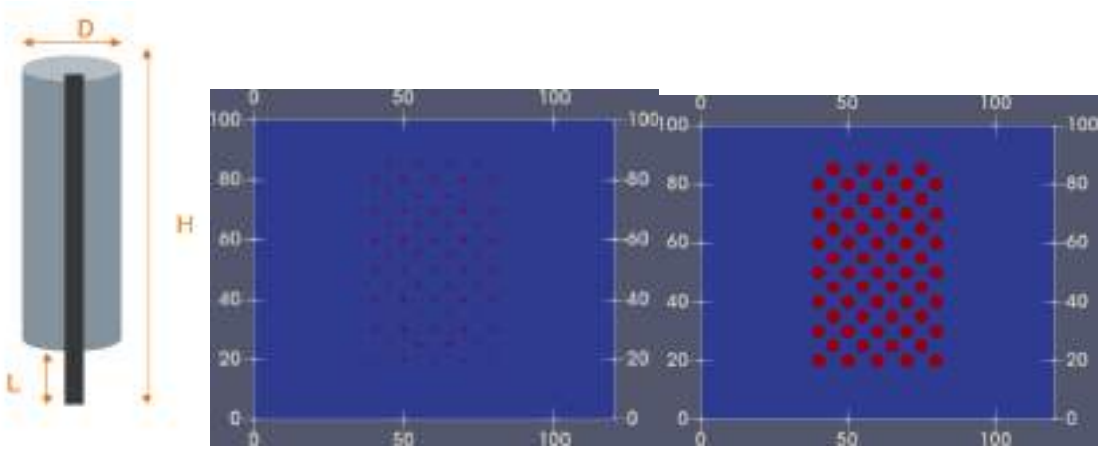

Figure 53. Case A. Schematic representation of the tree (left). Position of the stems of the trees (middle) and small vegetations (right).

Table 10. Vegetation parameters used in the OpenFOAM forest modelling.

Parameter	Ground vegetation	Tree stems	Trees small vegetation (needles etc)
Total mass	1,800 kg	11,690 kg	2,922 kg
Surface to volume ratio	6,000 1/m	40 1/m	6,000 1/m
Effective diameter	0.001 m	0.15 m	0.001 m
Height	0.6 m	15 m	15 m
L	--	--	1 m
D	--	0.15 m	2 m
Moisture	5.8%	15%	5.8%

5.2.2 Fire simulation results

Forest fire simulation results are presented from *Figure 55* to *Figure 57*.

Figure 55 illustrates the propagation of the fire front and the burned grass. Flames of the ground vegetation ignite the small vegetations of the trees. It also shows burning of the small vegetation of the trees. Presented flames are higher than the trees (15 m) and ranges from 20 to 25 metres from the ground.

Figure 56 demonstrates wind velocity in the cross section 3.5 m from the bottom and vertical cross section. Due to combustion of the vegetation in the high height from the ground, effect of the fire front is larger than in grass fire cases.

Figure 55 presents the amount of the burned small vegetation for each case. The amount of burned vegetation is larger in the bottom. Due to the large diameter stems of the tree do not burn in the process therefore heat of combustion is limited.

From the simulations it can be seen that not all the small vegetation of the trees is burned in the considered conditions. The amount of the burned vegetation is larger in the lower parts of the trees and smaller in the higher parts.

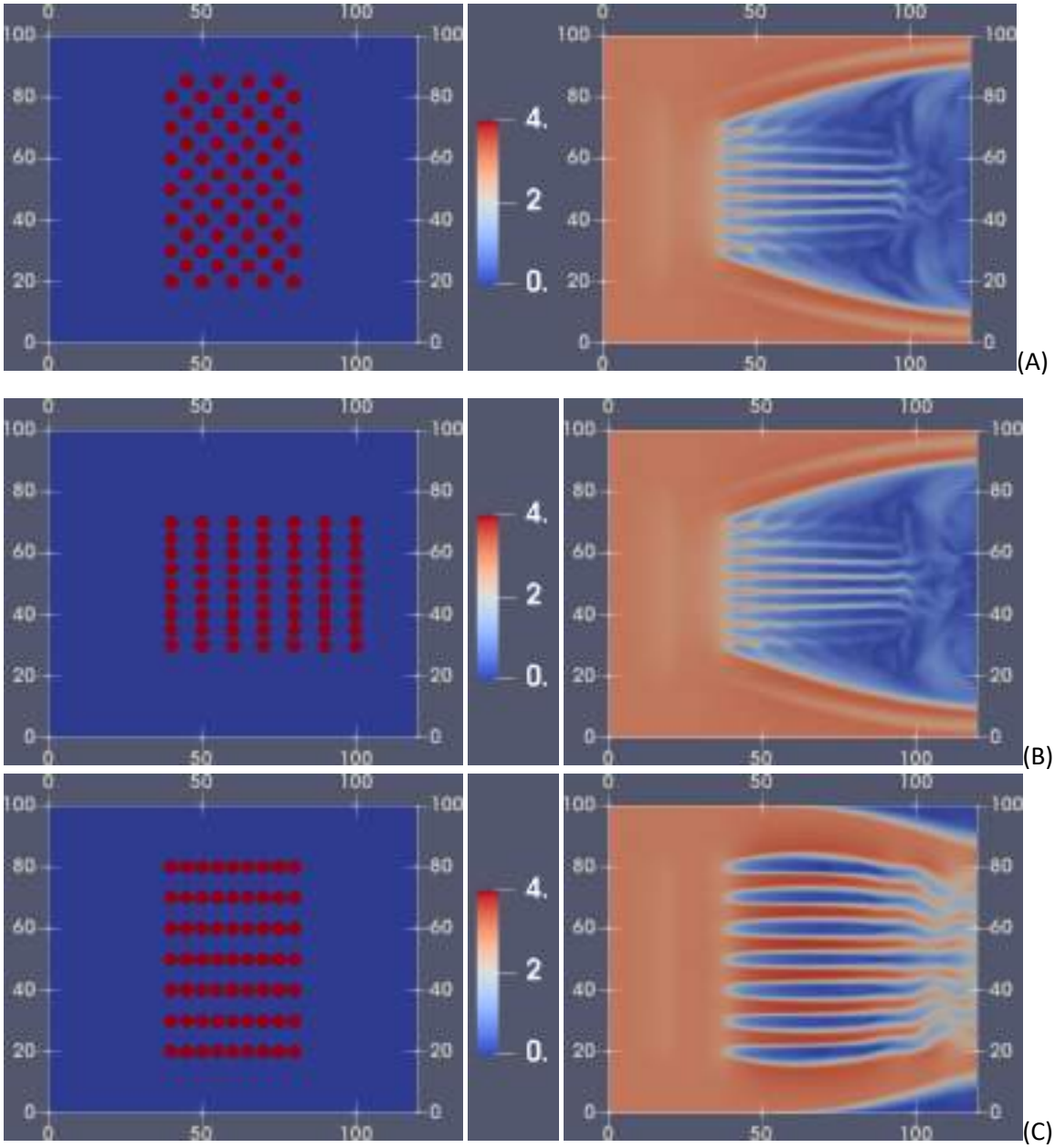

Figure 54. Position of the trees and wind velocity at level 3.5 m before the ignition. Cases A, B and C.

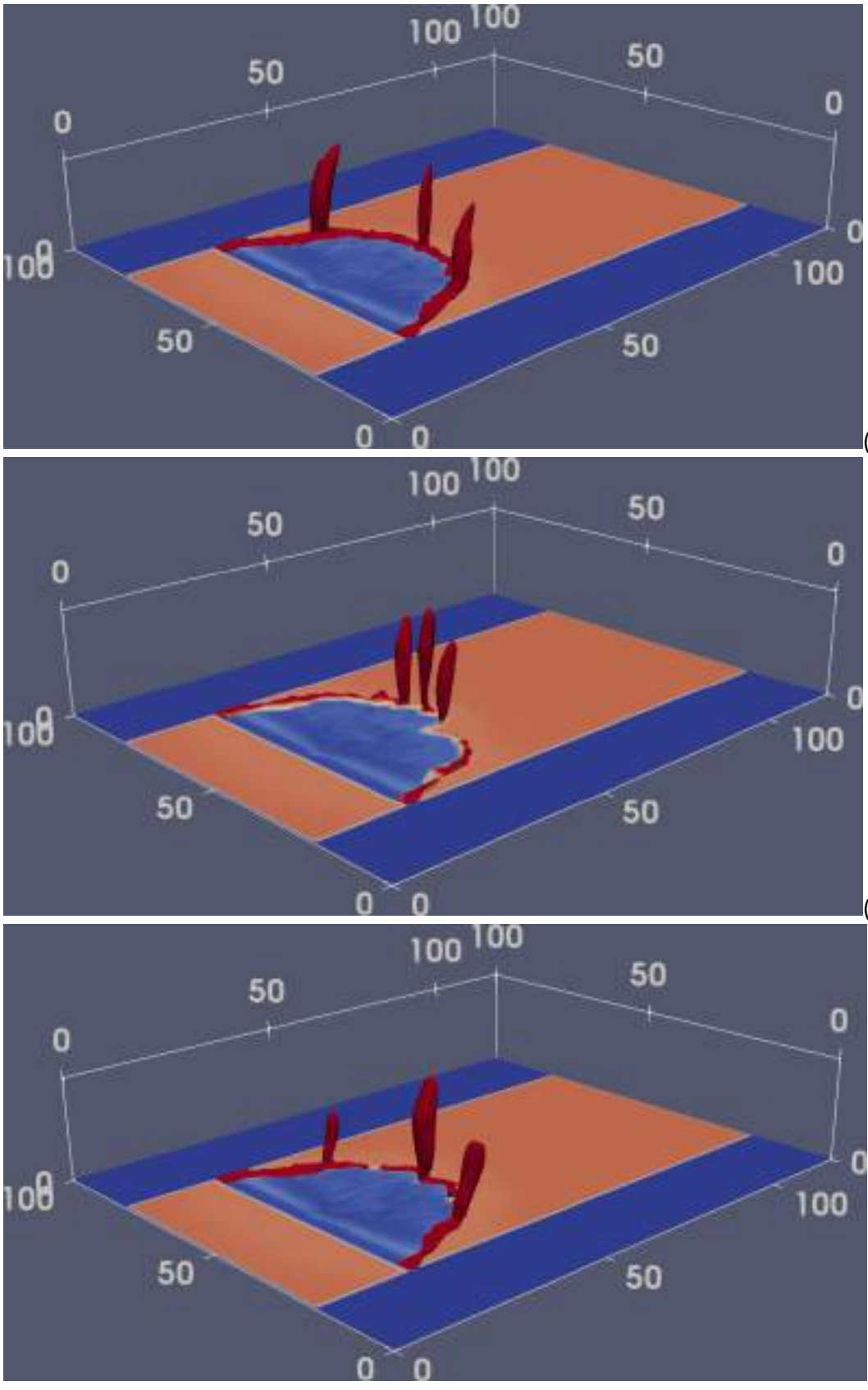

Figure 55. Burned gras and fire front propagation. 60 second after ignition. Case A, B and C.

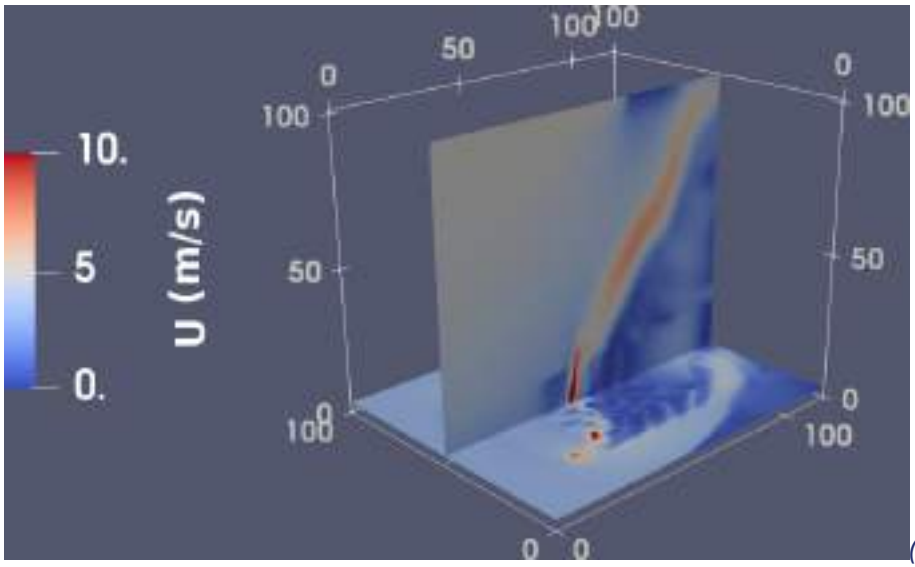

(A)

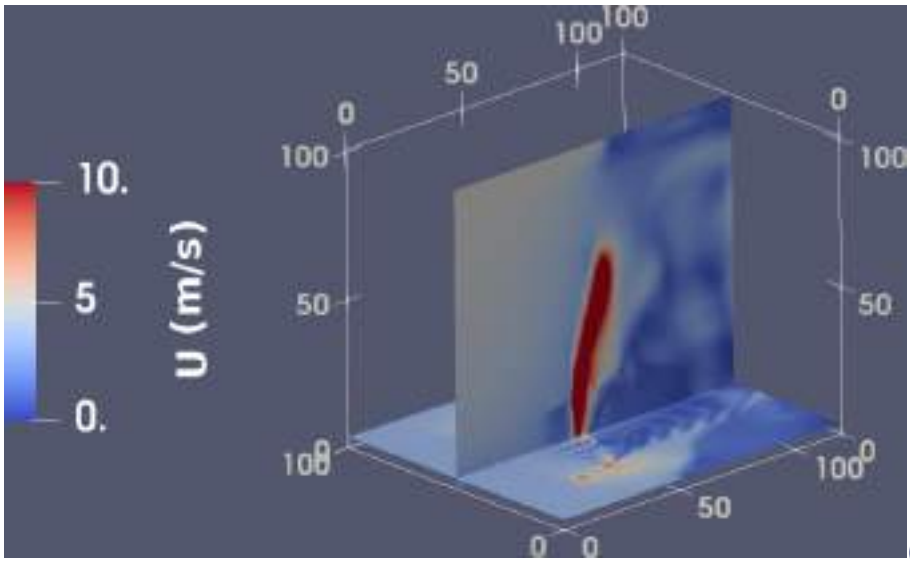

(B)

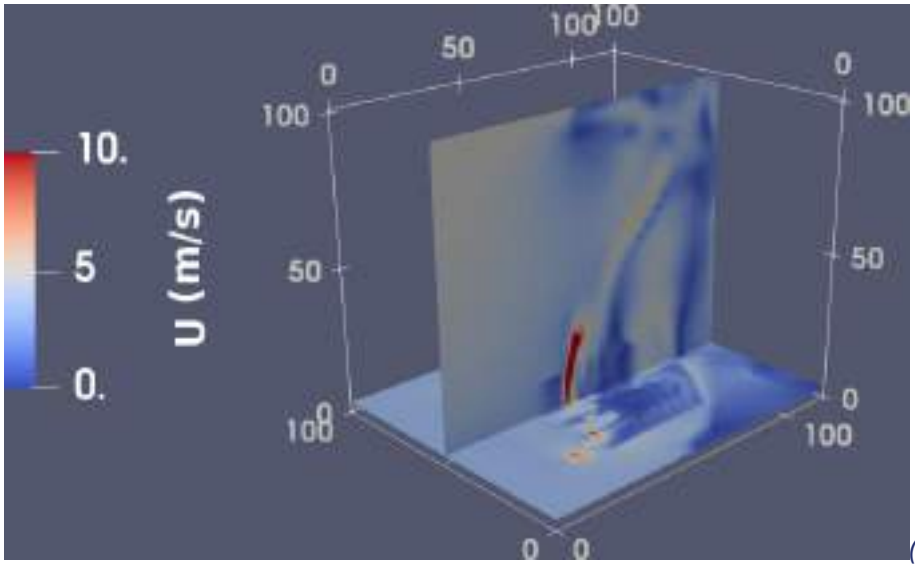

(C)

Figure 56. Velocity distribution 60 second after ignition. Cases A, B and C.

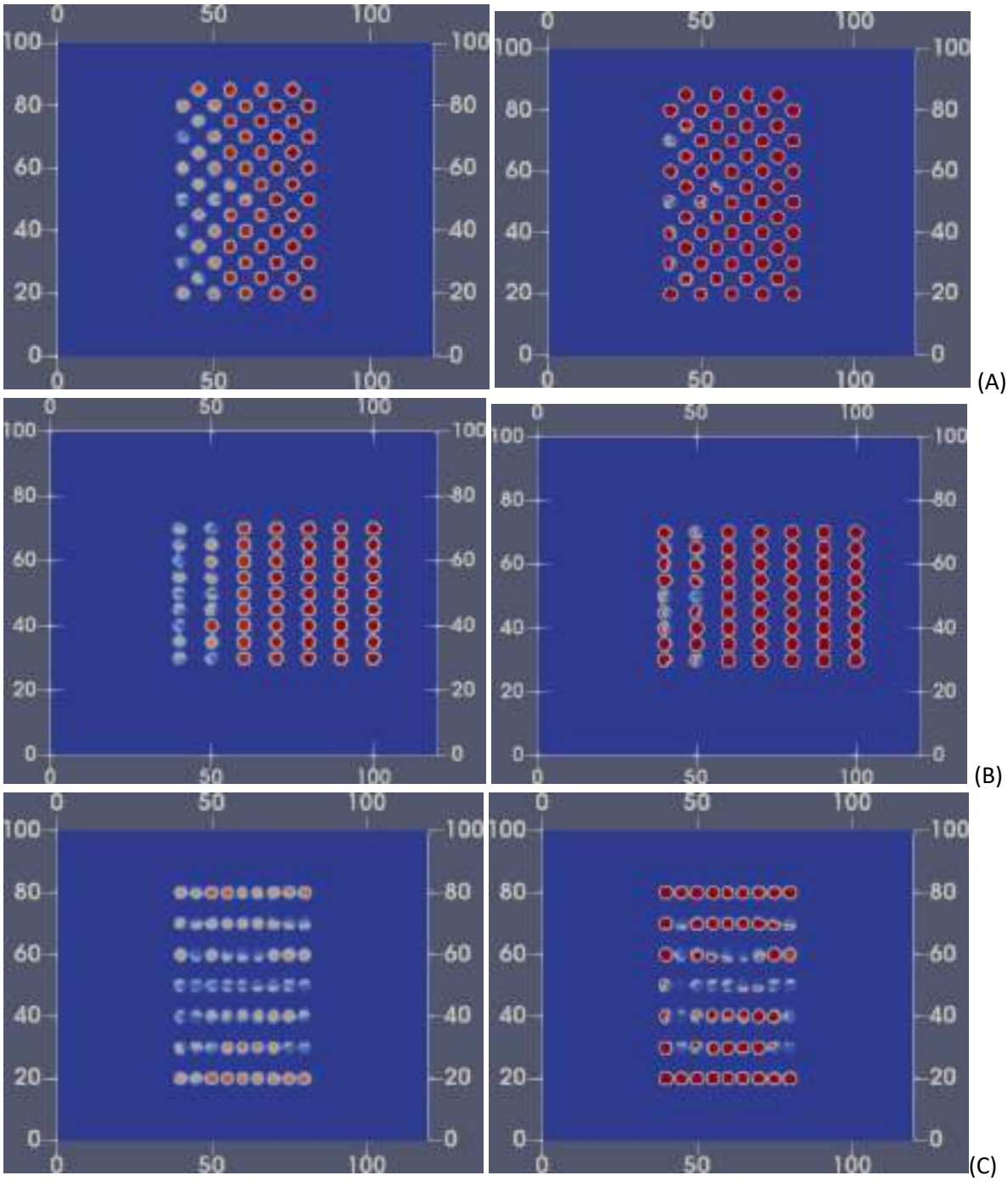

Figure 57. Burned trees' small vegetation. 2 min after grass ignition. Height 1.5 meter from the ground (left) and 6.5 meter from the ground (right). Cases A, B and C.

5.2.3 Analysis of OpenFOAM simulations

Simplified model of the trees was suggested for the OpenFOAM modelling of the forest fires. The model separated the tree stem and small easily burned vegetation with large surface to volume ratio (such as needles and small branches). In the simulated cases the trees were located withing 5−10 metres from each other. Thus, the separation of the vegetation type allows the wind flow between the trees. Simulations were done with

different layouts of the forest with same number and dimensions of the trees, but different tree positions in the area. The effect of the trees position was observed in the wind velocity distribution as well as the trees combustion. Due to their large size, the stems of the trees remained mainly unburned. The small vegetation was ignited by the high flames of the ground vegetation. After that the whole height of the trees was burning, the heights of the flames exceeded the tree height and reaches more than 20 metres. However, the combustion was not complete due to the insufficient heat release and the surrounding wind. Most of the combustion took place in the lower parts of the trees, while some parts of the top of the trees remains almost unburned. These were the first OpenFOAM simulation of the forest fire and they were not validated against the experimental data, which would be essential for the model improvement.

5.3 Predicting the onset of Extreme Wildfire

One of the most pressing concerns for wildfire risk managers is to determine whether a simple surface fire can transform into an extreme wildfire or not. The transition from a controllable surface fire to an uncontrollable extreme wildfire is marked by chaos and unpredictable fire spread. However, such transition can be noted by observing changes in some of the real time measurable behaviour parameters. Those parameters can be associated with Fire Category 4 (Normal fire), which is extremely difficult to control but not as impossible to manage as Fire Category 5 (Extreme Wildfire Event) (Tedim et al., 2018). The lower limit of real time measurable behaviour parameters such as rate of spread, fireline intensity, and flame length under Fire Category 4 can be taken as precursors for the onset of extreme wildfires, which can ultimately happen if unrestrained fire growth and transition continues to happen when the fire is already in Category 4 with sufficient fuel availability.

To facilitate the prediction of the onset of extreme wildfire events, a simple computational setting (CFD based simulation) for a forest has been made up to numerically study the values of such precursors. The values, which can act as precursors for the onset of extreme wildfires, are taken as 0.33 m/s for the rate of spread, 4000 kW/m for fireline intensity, and 3.5 m for flame length (start of category 4 fire). Understanding and utilizing these precursors for a given forest type can enable wildfire risk managers to deliberate on the potential of fire spread and anticipate extreme wildfire events (category 5 fire) effectively. Forest type in the computational setting can be changed to study different types of them with different environmental variables.

This work exemplifies how such precursors can be checked in a computational setting[1] with a made-up forest comprising Douglas Fir trees. Precursors are calculated against various input variables resulting in various charts and tables for decision making.

[1] All the simulations under this section have been carried out using FDS (version 6.8.0) with grid size 0.2 m unless stated otherwise.

5.3.1 Combustion of Douglas Fir trees

Due to the lack of experimental data, validated fire models for trees were searched. NIST (USA) has conducted a series of tree burn experiments in which they set different-sized Douglas Fir trees on fire. A few among them were 2 m high Douglas Fir trees, for which built fire models gave results close to the experimental results (Mell et al., 2009; see also this report chapter 4.2).

This study chose a Douglas Fir fire model with four types of vegetation (foliage, small roundwood, medium roundwood, and large roundwood) and a 14% moisture content for the forest setting. The experimental heat release rate of such a tree has been calculated by multiplying the heat of combustion (17,425 kJ/kg) with its mean profile of the mass loss rate. Burning a single Douglas Fir tree with static vegetation in the simulation produced a heat release rate profile that closely matched the experiment, see *Figure 58*. The simulation's slightly higher peak heat release rate partly compensates for the discrepancies.

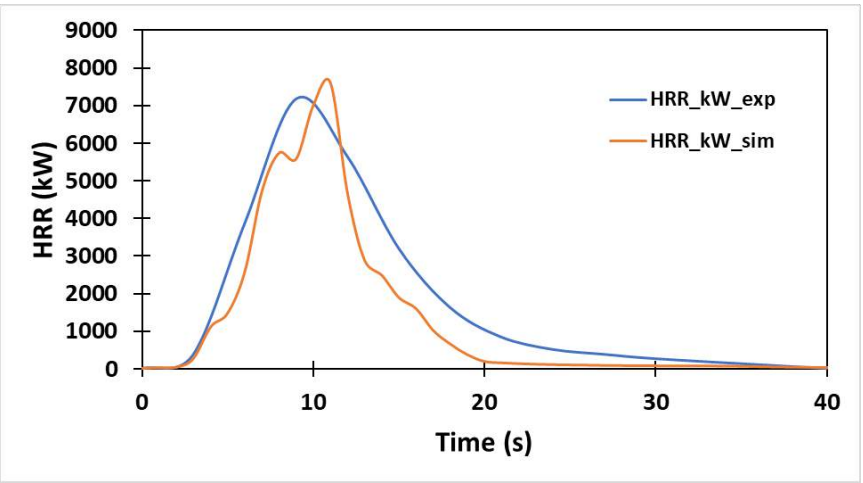

Figure 58. Heat release rate of 2 m Douglas Fir trees (Experiment vs Simulation)

5.3.2 Computational setting

The availability of computational resources for CFD-based simulations has always been a limiting factor. Consequently, the volume of the computational domain must be restricted. This limitation also applies in this case. Partly mimicking a wind tunnel geometrical features with wind along the longitudinal side, the made-up forest (*Figure 59*) with combustible Douglas Fir trees (brown & green) has a longitudinal length (x direction) around 100 m, a lateral width of 20 m (y direction), and a height of 12 m (z direction). Trees overlap each other by 0.5 m. Non-combustible Douglas Fir trees (blue & white) are also plotted along the longitudinal length to alter the wind reaching the combustible trees. Moreover, fire starts along the lateral length made about 7.5 m away from the start of the forest in -x direction. This fire acts as an approaching fire to the combustible Douglas Fir trees from the wind direction. The left out lateral length with trees (7.5 m from the edge) here also alters the wind reaching the trees getting ignited.

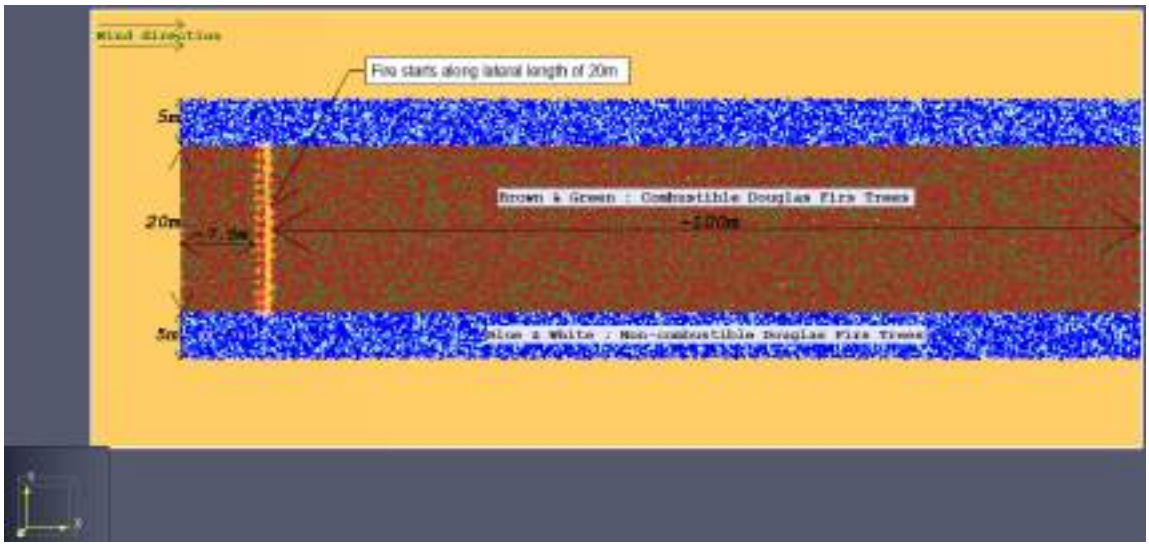

Figure 59. Forest layout in the simulation (top view): brown and green trees are combustible; blue and white trees are not combustible.

The wind profile is based on Monin-Obukhov Similarity theory. Wind speed is assigned for height 10 m from the ground. Atmospheric stability is considered neutral, and landscape classification includes forests. Details are provided in McGrattan et al., 2023.

The wind blows in the longitudinal direction, keeping the head of the fire propagating in the same direction (*Figure 60*). The lateral sides (+y & -y) have FDS based "PERIODIC FLOW ONLY" boundary condition. The top side (+z) and longitudinal end side (+x) are open in the computational domain. Ambient temperature and humidity are considered as 25°C and 50% respectively.

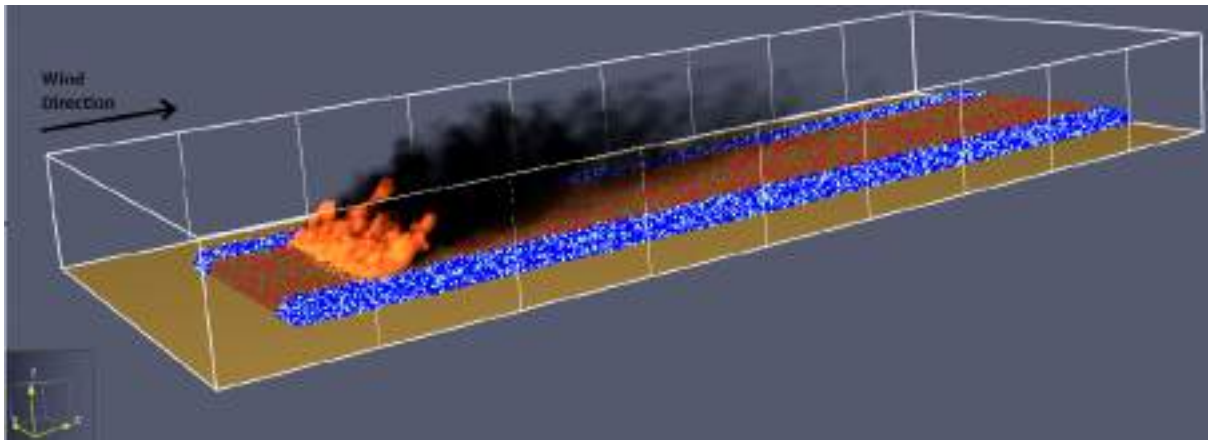

Figure 60. Forest layout in the simulation: forest on fire.

5.3.3 Approaching fire setting

In the simulations, trees along the lateral width are approached by the extrema of fire category 1, as shown in *Table 11* having fireline intensity taken as 500 kW/m.

Table 11. Different categories of fire (Tedim et al., 2018).

	Fire category	Fireline intensity range (kW/m)	Rate of spread (m/s)	Flame length (m)
Normal fires	1	<500	<0.08	<1.5
	2	500-2,000	<0.25	<2.5
	3	2,000-4,000	<0.33	2.5-3.5
	4	4,000-10,000	<0.83	3.5-10
Extreme Wildfire Events	5	10,000-30,000	<2.5	10-50

The heat release rate of the approaching fireline is determined using the following equation:

$$Heat\ release\ rate(approaching\ fire) = Approaching\ fireline\ intensity\ x\ 20m$$

where 20 m is fixed for all simulations as this is the lateral length of the approaching fireline. The resulting heat release rate of approaching fire is 10,000 kW. Using such heat release rate of the approaching fire, various simulations are run with different wind speeds. The purpose is to check whether fire reaches the predetermined values of precursors mentioned above while varying the wind speeds (at 10 m height) in the simulations, see *Table 12*.

Table 12. Wind speed in simulations.

Simulation name	Wind speed m/s
sim_2	2
sim_3	3
sim_4	4
sim_5	5
sim_6	6
sim_7	7
sim_8	8
sim_9	9
sim_10	10
sim_12*	12
sim_14*	14
sim_16*	16
Sim_18*	18

*sim_12 to sim_18 have stretched mesh in z direction well above tree height to avoid numerical instability due to high wind speed in simulations.

As a part of a sensitivity study, environmental humidity (50% vs 60%), temperature (25°C vs 30°C), and moisture content of the trees are also varied to understand their effect on the values of precursor with wind speed 16 m/s.

Estimations of precursors (Rate of spread)

The rate at which a fire spreads is determined by the speed at which the fire front moves forward. This was measured from the simulations at various distances with respect to time along the longitudinal length. When the heat release rate per unit volume exceeded 200 kW/m^3 at any point along the lateral length at any chosen distance, the fire was deemed to reach such longitudinal distance. This estimation used the values from slice files for heat release rate per unit volume kept horizontally approximately at the mid-height of Douglas Fir trees. Moreover, as the combustion of fireline (which ignited the trees) prevailed for 30 s from the start of the simulations, all the calculations of rate of spread were done after 30 s from the start of the simulation. This was done to exclude the initial effect of the fireline on the initial rate of spread.

Estimations of precursors (Fireline Intensity)

It is important to understand that fireline intensity denotes the power for 1 m of fire front. The key parameter to understand fireline intensity is the effective areal fuel density (fuel which will be definitely consumed in a fire). How the areal consumption of fuel proceeds forward dictates the fireline intensity. It is calculated using the following formula:

$$FLI = Heat\ of combustion\ x\ Fuel\ consumption\ per\ unit\ area\ x\ Rate\ of\ spread$$

The heat of combustion is taken as 17,425 kJ/kg (Mell et al., 2009). Fuel consumption per unit area has been taken as 0.95 kg/m^2 based on simulation files used for validation (Mell et al., 2009). It has been further noted in the full-scale simulations that fuel consumption per unit area have the efficiency of nearly one where burning has taken place.

The heat of combustion is multiplied by the fuel consumption per unit area, and the resulting quantity is area-based energy density (kJ/m^2). Moreover, the area-based energy density is multiplied by rate of spread of fire resulting in a quantity equivalent to power per unit length which is called fireline intensity. Thus, fireline intensity is a measure of the energy release rate along the advancing front of the wildfire per unit length.

Estimations of precursors (Flame length)

The flame length is also an important indicator of how severe a wildfire has become. Flame length is calculated using relationship between fireline intensity and flame length (Byram, 1959) as follows:

$$Flamelength = 0.0774\ x\ (fireline\ intensity)^{0.4608}$$

The relationship clearly shows that flame length is proportional to fireline intensity. The longer the flame, the more difficult it is to control. Moreover, strong winds tilt and elongate the flame, making the fire spread quickly.

5.3.4 Overall results

The wildfire parameters have been impacted by wind speeds (*Table 13*). Higher wind speeds have a greater impact on these parameters. Wind speeds between 2 and 8 m/s

did not cause any parameters to exceed the chosen precursors' values. However, at 9 m/s, two parameters (FLI and Flame length) started exceeding the chosen precursors' values. At 12 m/s, all three parameters (ROS, FLI, and Flame length) exceeded the precursor values (ROS 0.33 m/s, FLI 4000 kW/m, and Flame length 3.5 m).

Table 13. Douglas Fir forest fire parameters with different wind speeds (values in red have exceeded the chosen precursors' values)

Simulation name	Wind Speed, m/s	ROS, m/s	FLI, kW/m	Flame length, m
sim_2	2	0.07	1,082	1.9
sim_3	3	0.11	1,737	2.4
sim_4	4	0.13	2,153	2.6
sim_5	5	0.16	2,650	2.9
sim_6	6	0.19	3,159	3.2
sim_7	7	0.21	3,404	3.3
sim_8	8	0.23	3,773	3.4
sim_9	9	0.25	4,105	3.6
sim_10	10	0.28	4,630	3.8
sim_12	12	0.34	5,669	4.1
sim_14	14	0.44	7,213	4.6
sim_16	16	0.49	8,139	4.9
sim_18	18	0.51	8,424	5.0

The graph in *Figure 61* shows the rate of spread versus wind speed. The best-fitted growth line indicates an exponential growth curve. However, for wind speeds exceeding 16 m/s, the rate of spread deviates from the exponential growth curve, as evidenced by the rate of spread at 18 m/s wind speed. These points towards uncertainty about whether there is a maximum rate of spread at a critical wind speed, beyond which the rate of spread does not continue to follow the established trend (Beer, 1990). It is important here to note that the fire is already at category 4, and other factors such as downdrafts and spotting can change its course towards a category 5 wildfire at any time.

The graph in *Figure 62* shows the fireline intensity versus wind speed. The best-fitted growth line again indicates an exponential growth curve. However, again for wind speeds exceeding 16 m/s, the fireline intensity deviates from the exponential growth curve, as evidenced by the rate of spread at 18 m/s wind speed. These points towards uncertainty about whether there is a maximum fireline intensity at a critical wind speed, beyond which the fireline intensity does not continue to follow the established trend. It is reiterated here that the fire is already at category 4, and other factors such as downdrafts and spotting can change its course towards a category 5 wildfire at any time.

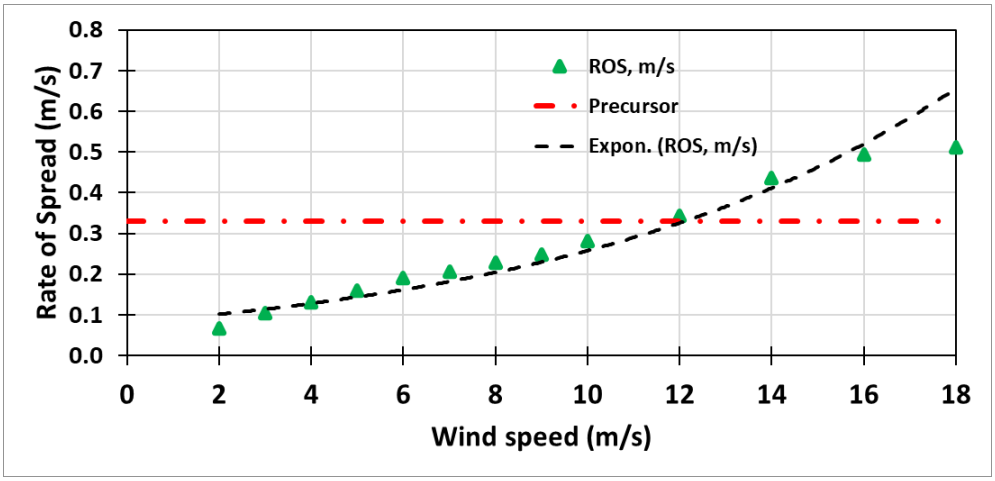

Figure 61. Rate of spread vs Wind speed (Douglas Fir Forest)

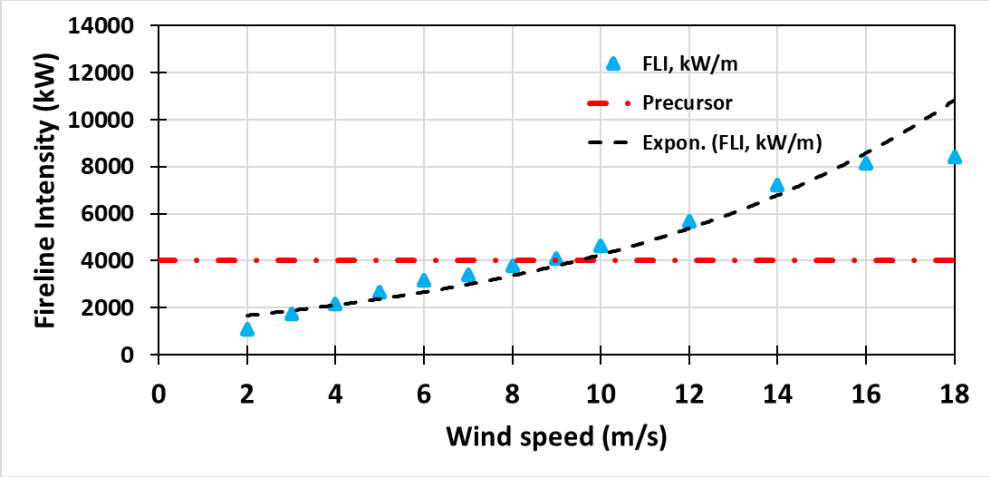

Figure 62. Fireline intensity vs Wind speed (Douglas Fir Forest)

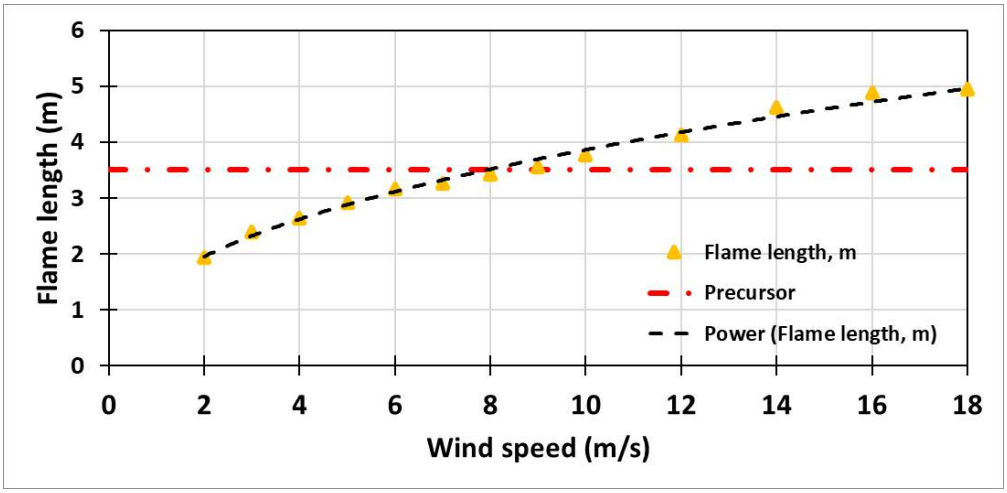

Figure 63. Flame length vs Wind speed (Douglas Fir Forest)

The graph in *Figure 63* shows the flame length versus wind speed. A logarithmic curve is shown by the growing line that best fits the data. At low wind speeds, increases in wind speed significantly raise flame length. However, at higher wind speeds, the increase in flame length tends to slow down, indicating diminishing returns as wind speeds continue to increase. For example, in the Rothaermel Fire Spread Model (Andrews, 2018) where wind speed is one of the key inputs, its effect on flame length is reflected in this model. At low to moderate wind speeds, the relationship between flame length and wind speed is steep, but as wind speed continues to rise, the incremental increases in flame length begin to flatten out. Although the effect of wind on flame length diminishes, the fire can still spread rapidly due to increased spotting and fire spread rates.

Effect of humidity (air)

The impact of humidity was examined at a wind speed of 16 m/s. When the humidity was raised from 50% to 60%, it resulted in a decrease in the rate of spread, leading to a reduction in fireline intensity and flame length. This indicates that added moisture in the environment slows down the drying of fuels. Conversely, the lower the humidity, the faster fuels can dry out, making them more susceptible to ignition.

Table 14. Effect of Humidity

Humidity	ROS, m/s	FLI, kW/m	Flame length, m
50%	0.49	8,139	4.9
60%	0.48	7,949	4.8

Effect of moisture content

The impact of vegetation's moisture content was examined at a wind speed of 16 m/s. When the moisture content was raised from 14% to 28%, it resulted in a decrease in the rate of spread, leading to a reduction in fireline intensity and flame length. It indicates that higher moisture content in the vegetation slows down the drying of fuels as it takes a high amount of energy to evaporate the water before combustion can occur. Moreover, when the moisture content was reduced from 14% to 0%, it resulted in a significant increase in the rate of spread, leading to a considerable rise in fireline intensity and flame length. This supports that the low moisture content allows fire to spread more quickly through the fuels, often jumping from one area to another with reduced resistance. With 0% moisture content, the fireline intensity has reached category 5 fire range, which lies in extreme wildfire events. It is worthwhile to note that the dry season can significantly alter the moisture content of vegetation, and hence, for conservative evaluation, vegetation fuels may also be evaluated with zero moisture content.

Table 15. Effect of moisture content.

Moisture content	ROS, m/s	FLI, kW/m	Flame length, m
Base_case (14%)	0.49*	8,139	4.9
Double (28%)	0.26	4,329	3.6
Zero (0%)	0.71	11,712#	5.8

*Red colour values exceed the precursor values; #Orange colour value belongs to EWE

Effect of ambient temperature

No conclusive results were obtained when the ambient temperature was increased. The effect of higher ambient temperature is believed to be apparent when such increased temperature is for a prolonged period, affecting at least the moisture content of the vegetation, making it drier and more susceptible to ignition. However, due to the limited time duration of the simulations of 10 minutes which had on average computational time of 4 days, such drying effects could not take place in simulations, leading to inconclusive results on the effect of ambient temperature on transition across different fire categories. As stated before, computational resources for CFD-based simulations have always been a limiting factor which has also restricted the long-time duration simulations where heating due to the ambient temperature can happen naturally.

Effect on combustibles near Wildland-Urban Interface[2]

Thermal exposure close to the wildland urban interface has been calculated with a wind speed of 16 m/s. It is again mentioned here that the forest setting has all three precursors in category 4 fire when the wind speed is 16 m/s. The exposure has been calculated at 5 m and 10 m from the interface at four different heights from the ground level: 0.4 m, 1 m, 2 m, 3 m, and 4 m. The exposure is evaluated through two physical parameters: adiabatic surface temperature (gas) and radiative heat flux (gas) which does not need any surface to be based upon. The adiabatic surface temperature (gas) shows an effective exposure temperature at a given point in the computational domain. It gives the gas phase thermal boundary condition, and the uncertainty associated with the solid phase heat conduction model does not affect the calculation. The radiative heat flux (gas) shows net radiative heat flux at a given point in the computational domain. Based on *Table 21.3* (Hurley, 2016), 350°C can be considered as a lower threshold for ignition for wood-based materials. On the other hand, based on *Table A.35* (Hurley, 2016), 10 kW/m^2 can be a lower threshold for critical heat flux for wood-based materials. Values for net radiative heat flux for wood are closely supported by the findings by Felicelli (2023), which have covered the flammability of decking sections found at the Wildland-Urban interface. Maximum readings are shown for the physical parameters in *Figure 64* and *Figure 65*.

To illustrate the tenability of humans and materials to radiant heat fluxes, the effects of some thermal radiation levels are reviewed below. Summer sunshine in the UK causes radiant heat flux of 0.67 kW/m^2 (Lawson, 1954). Examples of effects on skin exposure, collected by Drysdale (1999), are pain after 8 s at 6.4 kW/m^2 (Tan, 1967), pain after 3 s at 10.4 kW/m^2 (Lawson 1964), and blistering after 5 s at 16 kW/m^2 (Tan, 1967). Limits for firefighters' safe operation (wearing protective clothing for firefighting) are < 5 kW/m^2 for short term (< 7 min) and < 2.5 kW/m^2 for long term (> 7 min) (Järvinen 2014). As stated above, the critical heat fluxes for wood-based materials are steadily of the order of 10 kW/m^2. On the contrary, critical heat fluxes for other materials, such as synthetic ordinary polymers, show wide variation depending on the material, test method, and

[2] Length of the forest setting was made 80 m in 100 m long domain and devices for parameters were plotted at 5 m and 10 m from the end of 80 m marking the interface.

reference. For example, critical heat fluxes reported for polymethylmethacrylate (PMMA) vary in the range of 6–23 kW/m^2 (*Table A.35* in Hurley, 2016).

Based on *Figure 64*, the adiabatic surface temperature (gas) has only surpassed the threshold value at heights of 2 m, 3 m, and 4 m when located 5 m from the interface. *Figure 65* indicates that the radiative heat flux (gas) has exceeded the threshold value at all heights at the same distance from the interface. However, at 10 m from the interface, none of the parameters exceeded the threshold values. This suggests that 10 m distance is safe for combustible materials such as wood used for wood decking near these interfaces, assuming that heat transfer occurs only through conduction, convection, or radiation, and does not involve ignition through spotting or other unconventional phenomena.

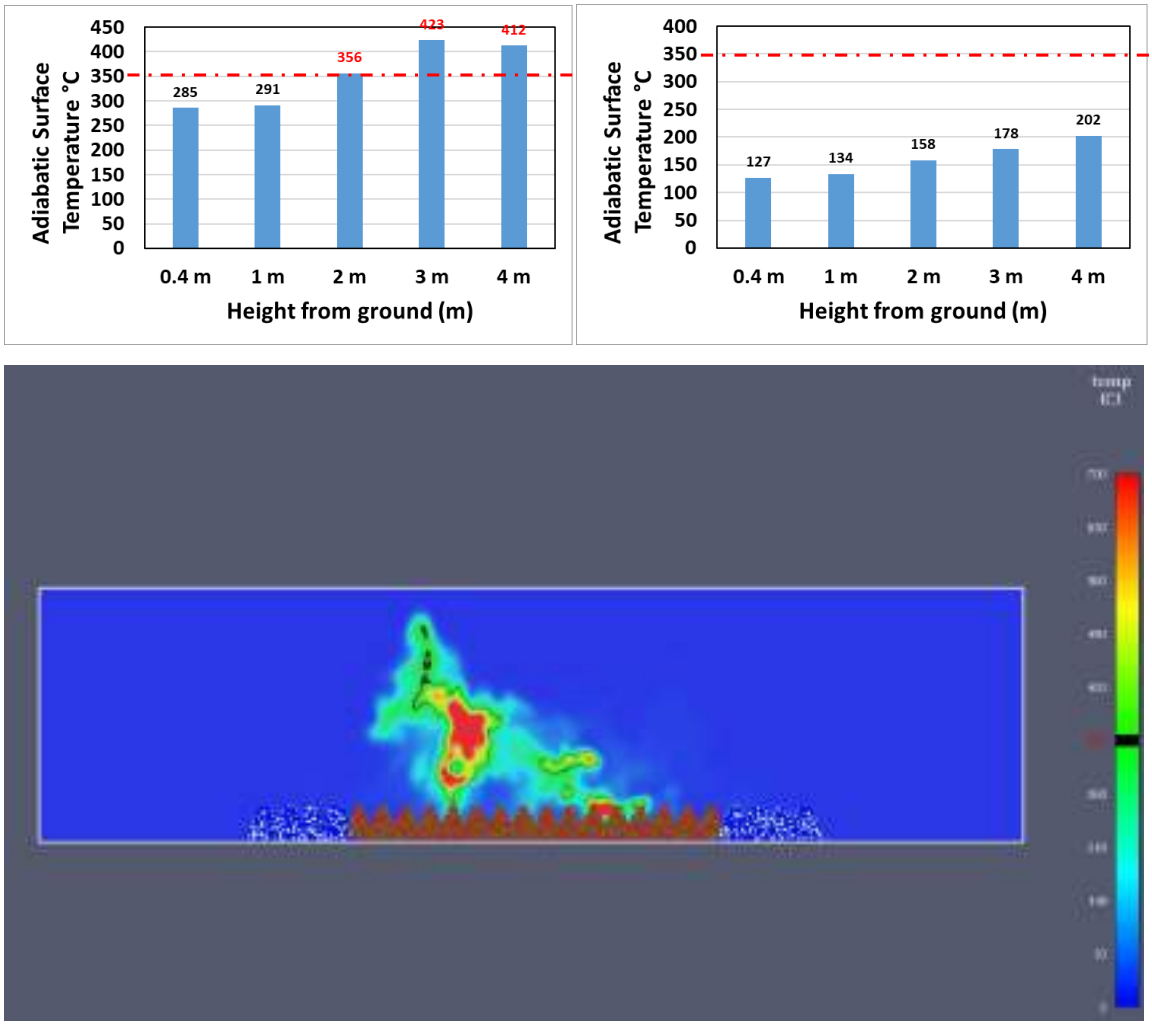

Figure 64. Maximum adiabatic surface temperature (gas) exposure at a distance of 5 m (left-top) and 10 m (right-top) from the interface. Vertical slice file at 5 m from the interface shows the temperature contour well above 350°C.

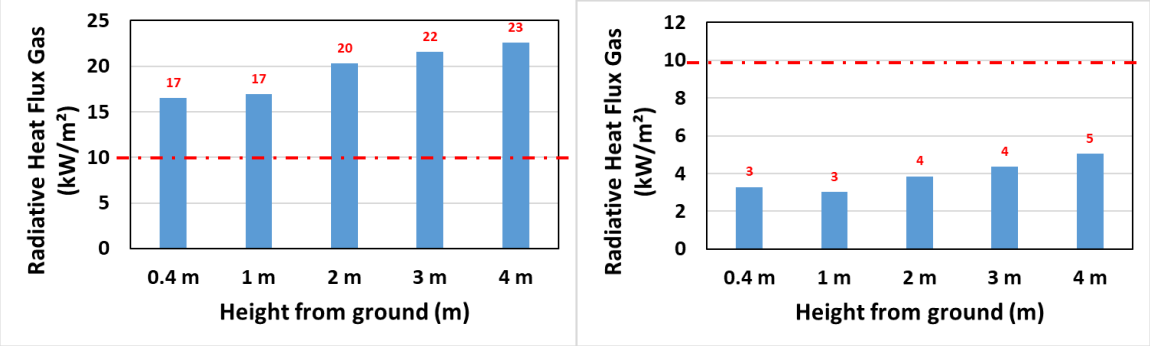

Figure 65. Maximum radiative heat flux (gas) exposure at 5 m (left) and 10 m (right) from the interface.

5.3.5 Analysis of the results

A simplified computational fluid dynamics-based forest setting has been presented for wildfire study. The setting and the applicable mathematical equation aid in studying the transition of wildfire from one state to target state, encompassing different fire categories. Precursors for extreme wildfire have been prudently chosen to indicate in advance the possibility of a wildfire turning into an extreme wildfire event. Precursors include real-time measurable parameters such as rate of spread, fireline intensity, and flame length. A fireline of low intensity has approached the forest setting, and its transition into a severe fire is studied by changing the dominant factor, which is wind speed. Various charts and tables have been produced covering the values of chosen precursors to understand the trend for decision making to deal with such fires.

For the chosen vegetation, the rate of spread and fireline intensity show, in general, an exponential growth trend with an increase in wind speed. Such an increase in the rate of spread when wind speed increases, consequently affecting fireline intensity, has already been observed (Scott et al., 2005). Moreover, the flame lengths show, in general, a logarithmic trend with an increase in wind speed where at low to moderate wind speeds, the relationship between flame length and wind speed is steep, but as wind speed continues to rise, the incremental increases in flame length begin to flatten out. Rothaermel Fire Spread Model (Andrews, 2018), where wind speed is one of the key inputs, has already shown such a trend. The setting has also been tested with different environmental humidities, vegetation moisture contents, and ambient temperatures. The results align with our expectations (except ambient temperature): higher humidity and vegetation moisture content led to less severe fires. Moreover, the forest setting has also been used for the estimation of thermal exposure on combustibles present near the wildland-urban interface.

Overall, the alignment of results with earlier findings and expected behaviour is encouraging as it reinforces our understanding of the complex dynamics of wildfires through computational fluid dynamics-based study. However, the experimental validation of such results is not readily feasible, given the sheer scale of the forest plot used in the simulation. Nonetheless, such simulations (with different trees and vegetation) are expected to provide indicative results that could be coupled with a

realistic understanding of wildfires and experiences in witnessing and facing them so that judicious firefighting decisions can be taken.

5.4 Sensitivity analysis

5.4.1 Sensitivity analysis with FDS

In FDS sensitivity analysis was conducted with forest fire, where trees were the accepted fir trees from validation for FDS in this report. Sensitivity analysis was done by selecting a base case and then varying parameters in that base case to see how results change.

Fireline Intensity is the indicator used for comparing different simulation results and it is calculated by the equation that was used also in chapter about Fireline Intensity in Encyclopedia of Wildfires and Wildland-Urban Interface (WUI) Fires. (Alexander, M. E., Cruz, M. G., 2019). The employed formulation is:

$I_B = H \times w \times r$

Where H is the fuel low heat of combustion (kJ/kg), w is the amount of fuel consumed in the active flaming front (kg/m^2) and r is the linear rate of fire spread (m/s). I_B is the Fireline Intensity.

In all simulations H is constant at 17,425 kJ/kg, w is calculated with device measuring fuel mass on the burn area and above it. All fuel, including the trees and grass are considered when calculating the mass. Mass loss is calculated by checking the initial total fuel mass and fuel mass after the fire has burnt out completely and then calculating the difference between those two values.

Rate of spread is calculated by arranging heat detecting devices in row in the direction of fire spread. Then it is checked when the devices reach threshold of 700 Celsius degrees and those timestamps are then used to calculate the speed of fire spread.

5.4.1.1 Simulation of base case 1

For base case 1, 2 m tall trees with 14% moisture content were used (Mell et al., 2009). For ground vegetation boundary fuel model was used and the parameters were chosen according to paper published by USDA (Scott, J. & Burgan, R., 2005) page 18 table. Fuel model code TU4 was chosen because it models dwarf canopy forest, and it is a very close description of what this sensitivity study is also about. Inert similar sized trees are placed around the burn area to simulate fire inside forest and not on an island. Base case was tested with both MO and WOW -wind methods. Ground vegetation and other parameters are on the list below.

- Ground vegetation (no live vegetation assumed, only dead fuel).
  - Moisture fraction: 6%.
  - Surface to volume ratio: 7,546 m^{-1}.
  - Mass per volume: 7.28 kg/m^3.
  - Fuel layer thickness: 0.1524.
- Ambient temperature: 20 °C (FDS default).
- Ambient humidity: 40% (FDS default).
- Fuel: Fir trees and ground vegetation as explained above.

- Fuel moisture: 14% for fir trees and 6% for ground vegetation.
- Wind speed: 3 m/s both in MO and WOW methods (reference point at 10 m height).
- Total mass per area: 2.22 kg/m^2 (space between each tree stem is 2 m and trees are placed in straight rows).
- Heat of combustion of the gaseous fuel: 17,425 kJ/kg.

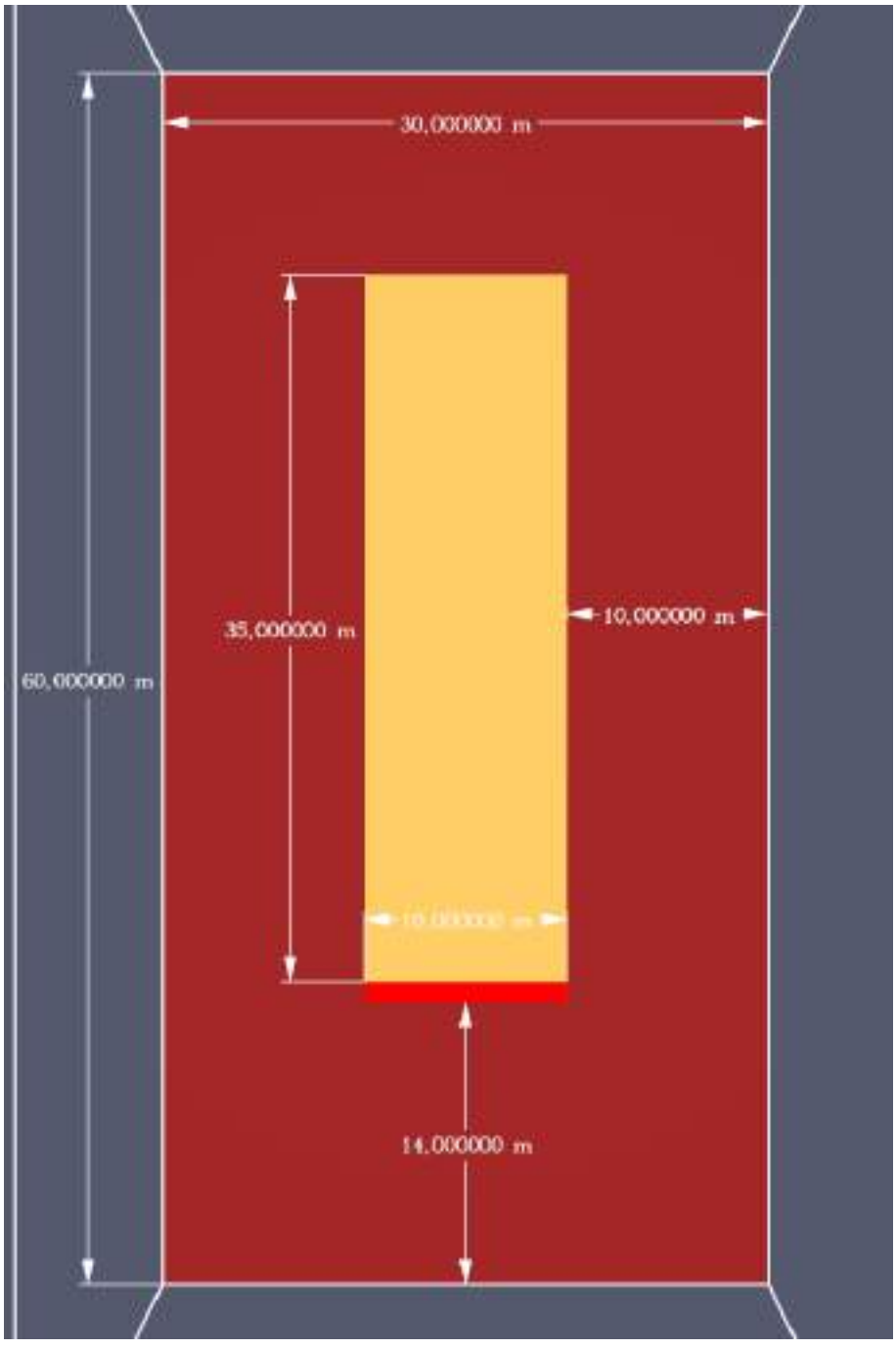

Figure 66. Domain dimensions. Wind direction is from down to up in the picture. Burn area with lighter brown in the middle and ignition line with red stripe.

Figure 67. Trees inserted to base case domain. Trees with yellow dots are inert and only act as wind shield.

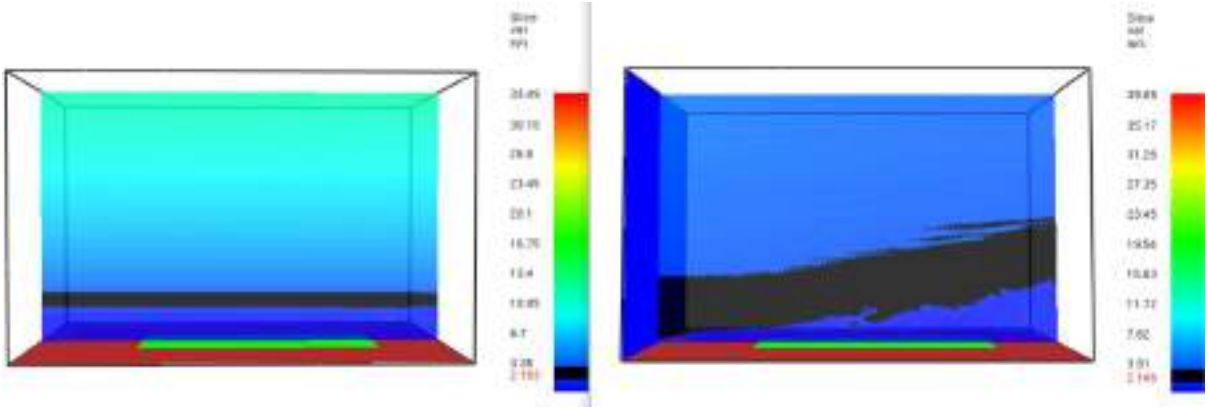

Figure 68. Wind profiles of 2.1 m/s wind speed highlighted with black. The right picture is for MO wind speed and left is for WOW wind speed. In the figure the wind speed profile is not constant and probably needs longer domain for the wind profile to develop. MO chosen for rest of the simulations so smaller domain can be used.

5.4.1.2 Simulation of 20% humidity and 25 °C ambient temperature (base case 2)

This simulation was chosen on basis of the guide published by CSIRO (Cruz et al., 2015). This is a guide to model Australian vegetation for fire spread modelling. In *Table 7.2* of the guide is listed what moisture should dead ground level fuel be (around 6%), as chosen for the base case, the humidity could be 20% and air temperature 25 °C. In the table, humidity and air temperature could vary for this level of fuel moisture but this was one of the options in the table.

For simulations that used base case 2 as template dead fuel content will be chosen according to the table in the CSIRO guide. Air temperature and humidity will also be according to the same table. Base case 1 does not differ in any other way from base case 2.

5.4.1.3 Simulation of base case 3

It was noticed that the ignition is so powerful that the fireline intensity is automatically always over 10,000 kW/m (extreme wildfire event). In base case 1 and 2 the ignitor for fire was a straight line with a total heat release rate of 10,000 kW and was on for 30 seconds. For base case 3 was investigated what kind of ignition would be proper heat release rate for to see to what fireline intensity the fire would rise naturally without big starter fire.

For this base case, 4 simulations were run. A more detailed description for each simulation is presented below.

Simulation 1:

- Ignition with 30 kW HRR (Heat Release Rate) rings placed under the first burnable trees on downwind.
- 5 ignitors used, with a total HRR of 150 kW.
- Ignitors were on for 10 s.
- Vegetation as in base case 2.

Ignitor's HRR is based on the ignitors used in the Fir tree experiment (Mell et al., 2009).

Simulation 2:

- Ignition with 130 kW HRR (Heat Release Rate) rings placed under the first burnable trees on downwind.
- 4 ignitors used, with a total HRR of 480 kW.
- Ignitors were on for 30 s.
- Vegetation as in base case 2, except that trees are 5 m tall and placed similarly as in the case "Simulation of 5 m tall trees".

Simulation 3:

- Ignition with 120 kW HRR (Heat Release Rate) line placed in the beginning of the burn area on downwind.
- Ignitors were on for 10 s.
- Vegetation as in base case 2.

Ignitor's HRR was integrated from the rings in Simulation 1. The distance between each ignitor particle is the same on this line as on each ignitor ring, but just laid on straight line.

Simulation 4:

- Ignition with 343.4 kW HRR (Heat Release Rate) line placed in the beginning of the burn area on downwind.
- Ignitors were on for 30 s.
- Vegetation as in base case 2, except trees are 5m tall and placed similarly as in the case "Simulation of 5 m tall trees".

Ignitor's HRR was integrated from the rings in Simulation 2. The distance between each ignitor particle is the same on this line as on each ignitor ring, but just laid on straight line.

For 2-metres-tall trees, the Fireline Intensity does not vary much between the base cases. Simulations done with base case 1 as a template are as valid as simulations done with base cases 2 and 3. Between base case 1 and 2, the difference was 20 units of percent in ambient humidity and 5 degrees in ambient temperature. Difference between base case 2 and 1 to base case 3 was 9,850 kW – 9,870 kW HRR for the ignitor. The fire develops quickly even with smaller ignition because of large surface-to-volume ratio.

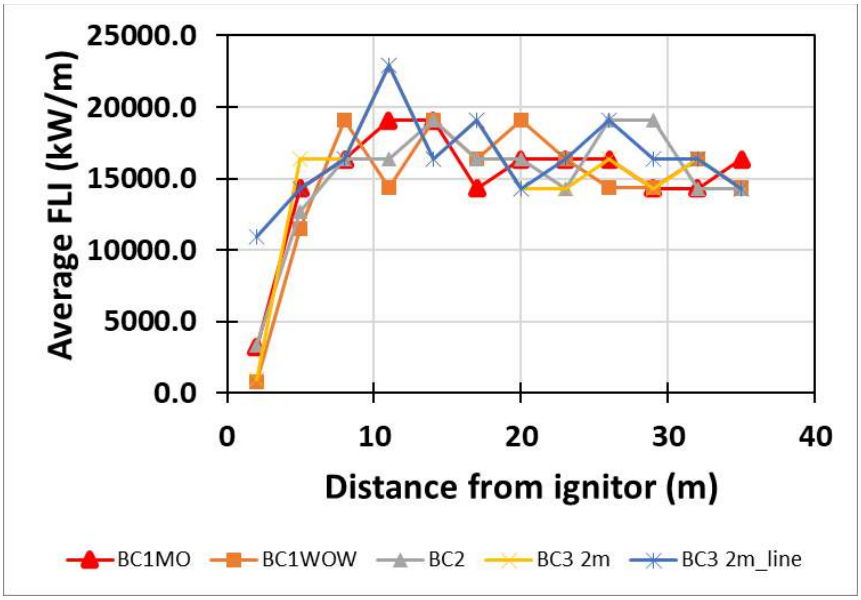

Figure 69. Fireline Intensity for 2-metres tall trees. BC1MO stands for base case 1 done with MO wind method and BC1WOW for same but with WOW wind method. BC2 is the base case 2 (also with MO wind method). BC3 2m is the same as base case 3 simulation 1 and BC3 2m_line is the same as base case 3 simulation 3.

Table 16. Average Fireline Intensities

	BC1MO	BC1WOW	BC2	BC3 2m	BC3 2m_line
FLI (kW/m)*	15021.06	14670.97	15135.21	15153.49	16389.07

*Standard deviation for the average Fireline Intensities is 583.92 kW/m, mean value is 15,273.96 kW/m. Coefficient of Variation (583.92/15,273.96) kW/m = 0.038

Most notable differences can be seen in base case 3 with line ignition compared to others. After the ignition, in that case FLI is in the beginning much larger than in other cases. This also affects the average value where all the Fireline Intensities are mostly over 15,000 kW/m, but the average stays at around 15,000 kW/m in other cases than BC3 2m_line.

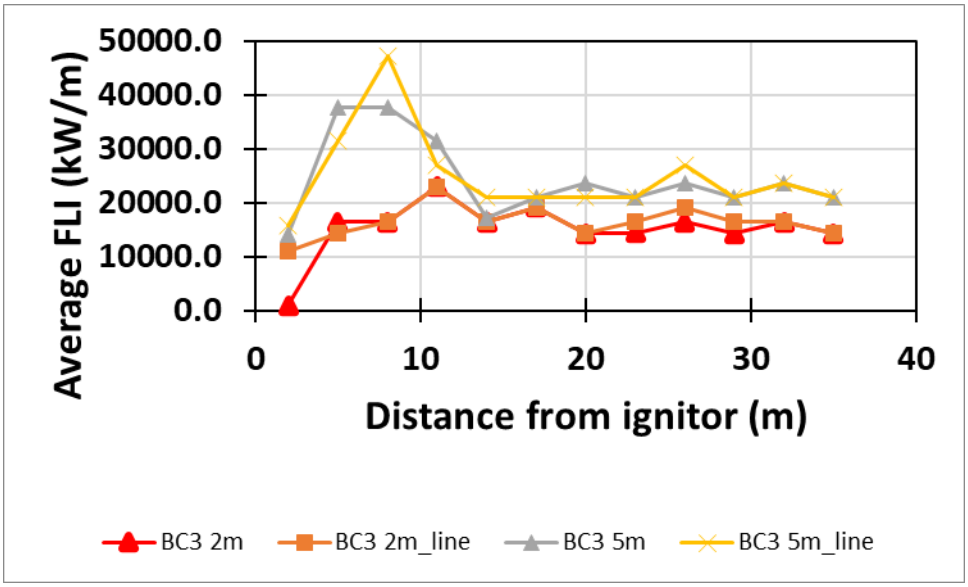

Figure 70. Comparison between simulations 1, 2, 3 and 4 (BC3 2m, BC3 2m_line, BC3 5m and BC3 5m_line, respectively). Sensitivity studies about tree heights were not done more thoroughly and, in these cases, also the tree trunks were separated by 2 m with 2-metres tall trees and 3 m with 5-metres tall trees, so the results are not completely comparable.

5.4.1.4 Simulations with varying wind speeds

Base cases 1 and 3 were used as templates for wind speed effect testing. Figures in this chapter show the development of Fireline Intensities. The reference point for each wind speed is established at 10 m height.

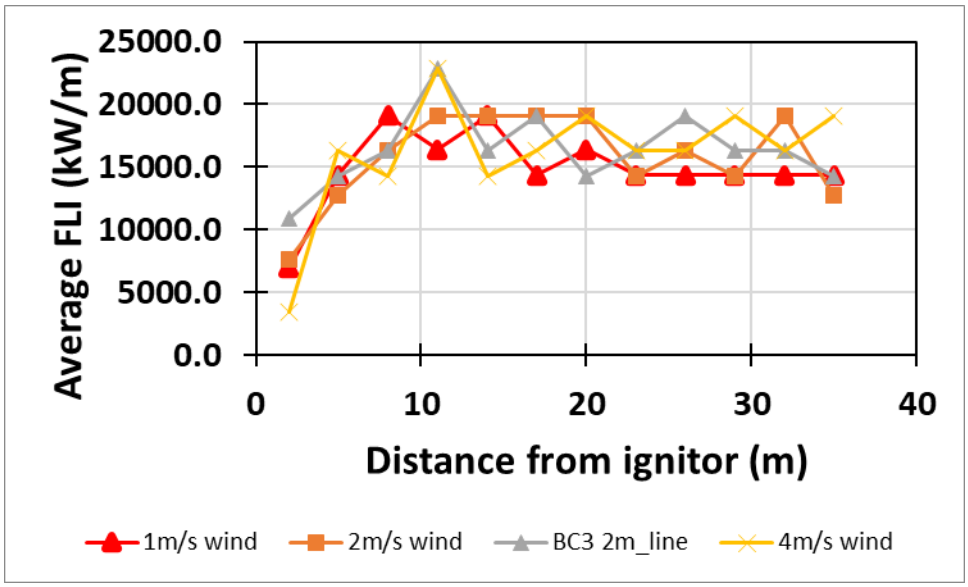

Figure 71. Fireline Intensities for 1 to 4 m/s wind speeds. 4 m/s wind speed uses base case 1 as template, but as established at base case simulations, the simulations done on all base case templates are comparable to each other. BC3 2m_line has 3 m/s wind speed.

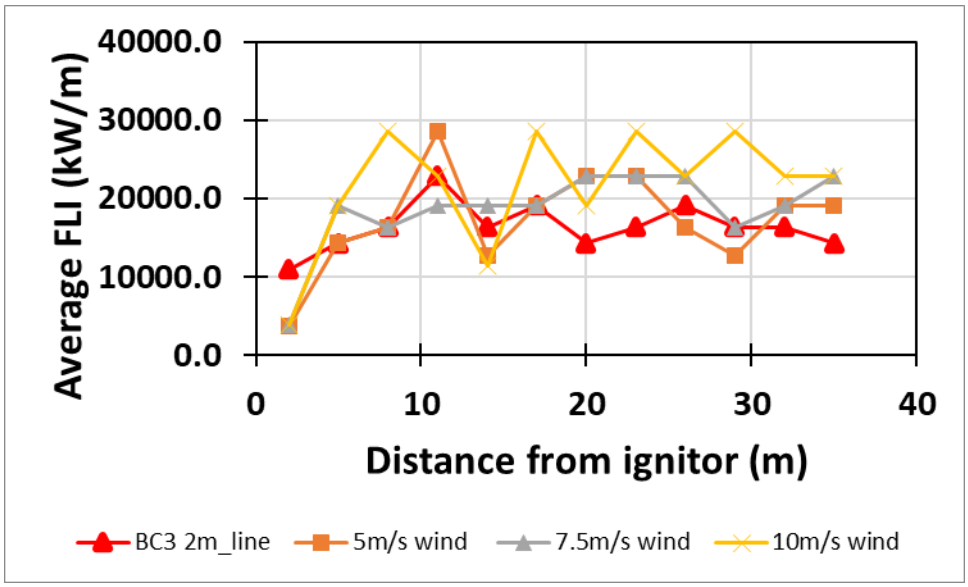

Figure 72. Fireline Intensities for 5 to 10 m/s wind speeds and base case 3 (with 3 m/s wind speed) visible for comparison.

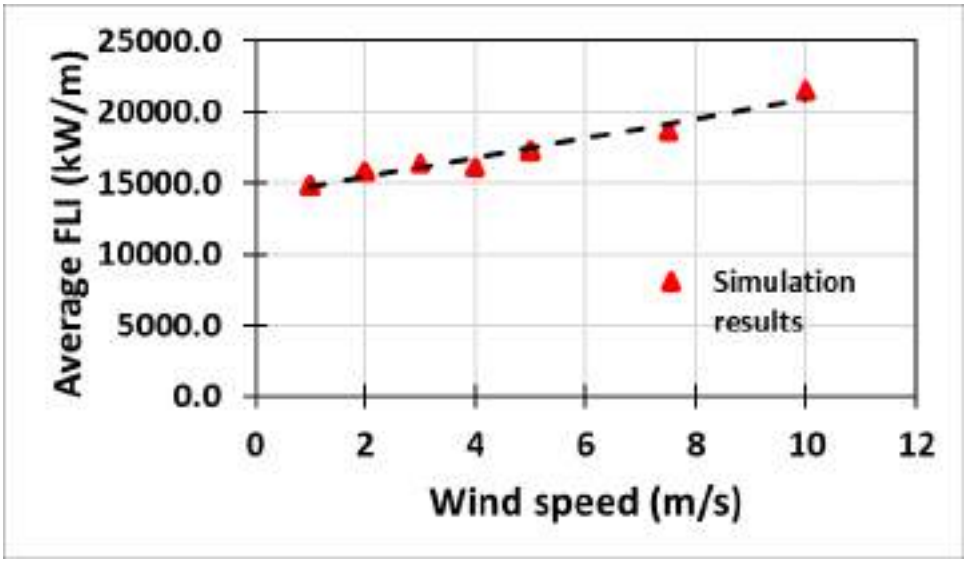

Figure 73. Average FLI compared to wind speed. For every unit of wind speed change (m/s) the FLI changes 673.8 kW/m.

5.4.1.5 Simulation of varying ambient humidities

Base case 3 used as a template, except for one case with 9% ground vegetation moisture content, 40% ambient humidity and 20 °C temperature (40% humidity, see *Figure 74*).

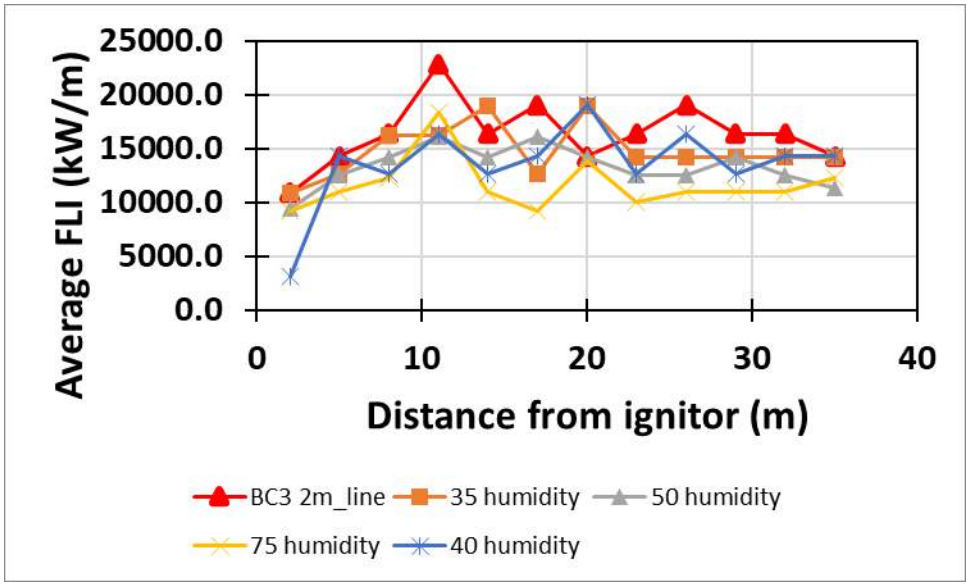

Figure 74. Fireline Intensity measured at different distances from the ignitor. Base case 3 (BC3 2m_line) for comparison and test with 40% humidity also added with 20 °C temperature. Rest of the variations have 25 °C temperature, including the base case 3.

In addition to ambient humidity, the ground vegetation was modified in accordance with the guide published by CSIRO (Cruz et al., 2015).

The parameters that were varied in the simulations (including the base case 3) were the following:

Base case 3:

- Humidity: 20%
- (Temperature: 25 °C)
- Ground vegetation moisture fraction: 6%.

Humidity 35:

- Humidity: 35%
- (Temperature: 25 °C)
- Ground vegetation moisture fraction: 8%.

Humidity 50:

- Humidity: 50%
- (Temperature: 25 °C)
- Ground vegetation moisture fraction: 10%.

Humidity 75:

- Humidity: 75%
- (Temperature: 25 °C)
- Ground vegetation moisture fraction: 13%.

Humidity 40:

- Humidity: 40%
- Temperature: 20 °C
- Ground vegetation moisture fraction: 9%.

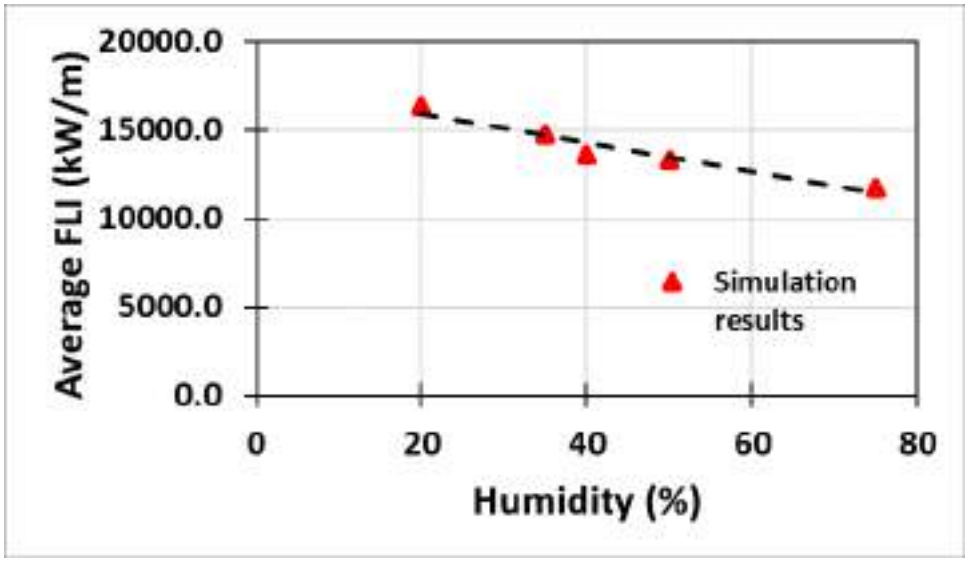

Figure 75. Average FLI compared to ambient humidity. For every percent of humidity change the FLI changes -82.6 kW/m.

5.4.1.6 Simulations of varying ground vegetation

Base case 3 was used as a template for these simulations. Mass of ground vegetation was only modified; trees were the same as in base case 3.

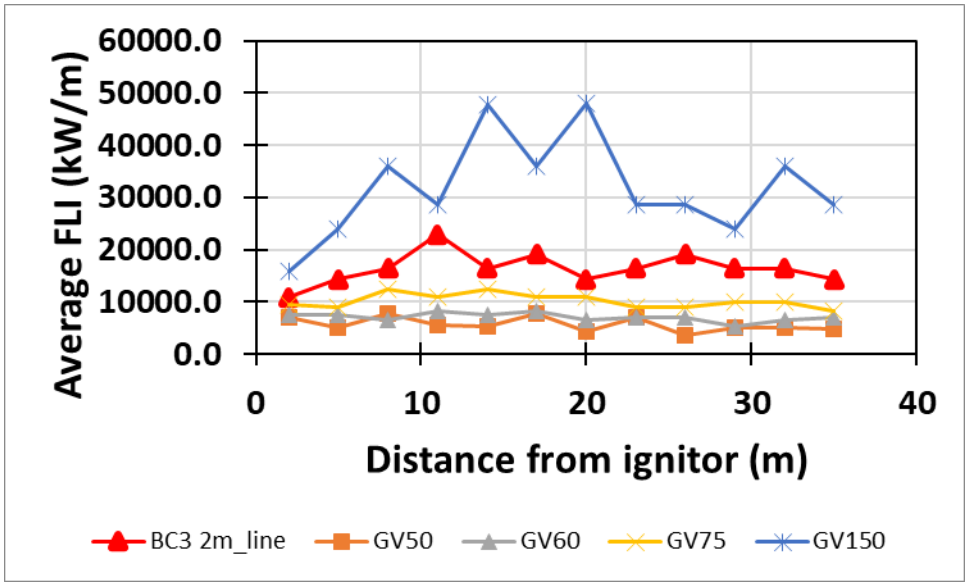

Figure 76. Fireline Intensity measured at different distances from the ignitor. Base case 3 (BC3 2m_line) for comparison. GV50, GV60 and GV75 stand for ground vegetation 50, 60 or 75 percent compared to the base case 3. GV150 has 150 % mass on ground compared to base case 3.

Ground vegetation amounts per area:

- GV50:
  - 1.67 kg/m^2
- GV60:
  - 1.78 kg/m^2
- GV75:
  - 1.95 kg/m^2
- GV150:
  - 2.78 kg/m^2

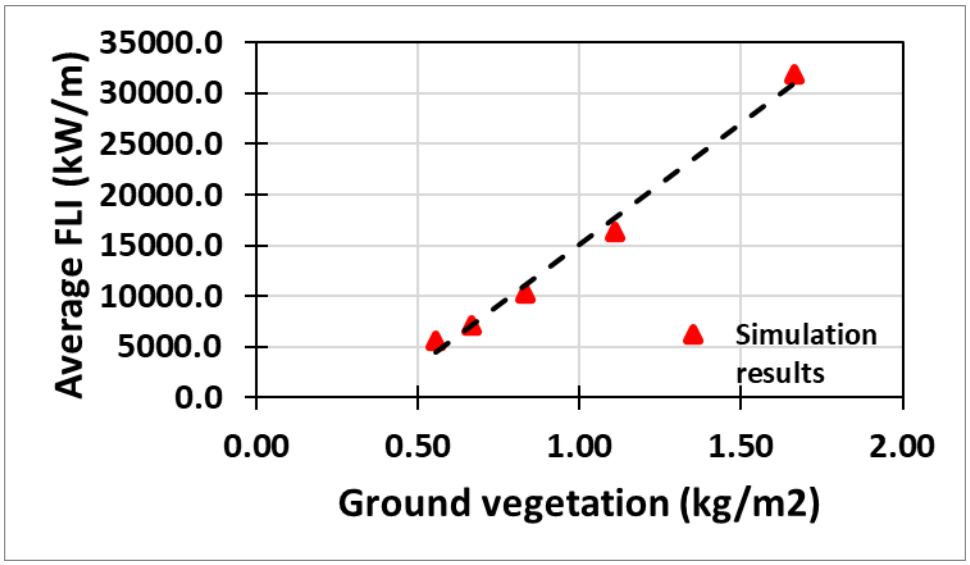

Figure 77. Average FLI compared to ground vegetation fuel density. The fire dies out before reaching the end of burn area when the ground vegetation density is lower than 0.5 kg/m^2. For every unit of ground vegetation fuel density change (kg/m^2) the FLI changes 23,968.7 kW/m.

From *Figure 78*, the amount of ground level vegetation highly affects the Fireline Intensity. With low enough amount of ground level vegetation (less than 0.5 kg/m^2), the fire dies out as mentioned in the caption of figure above. Only when the ground vegetation reaches about 0.8 kg/m^2 fuel density the fires start to be extreme. Adding more and more fuel will increase the Fireline Intensity linearly.

5.4.1.7 Simulations of different ignitions

Base case 2 was used as a template for different ignition simulations. Ignition power was modified according to *Figure 79* for different simulations. Ignition time for all simulations was similarly to base case 2, (i.e. 10 seconds).

The trendline shows little change to Fireline with a large ignition power change. From *Figures 79* to *80*, a high ignition mainly affects how quickly the fire starts, but the Fireline Intensity still stabilizes to the same level as in cases with lower ignition power. Already at 5-metre distance from the ignition, the Fireline Intensity, in all cases, is at a similar level.

For further studies it can be safe to assume that the ignition does not affect the result of the fire if the fuel in the forest ignites properly, and the fire starts supporting itself.

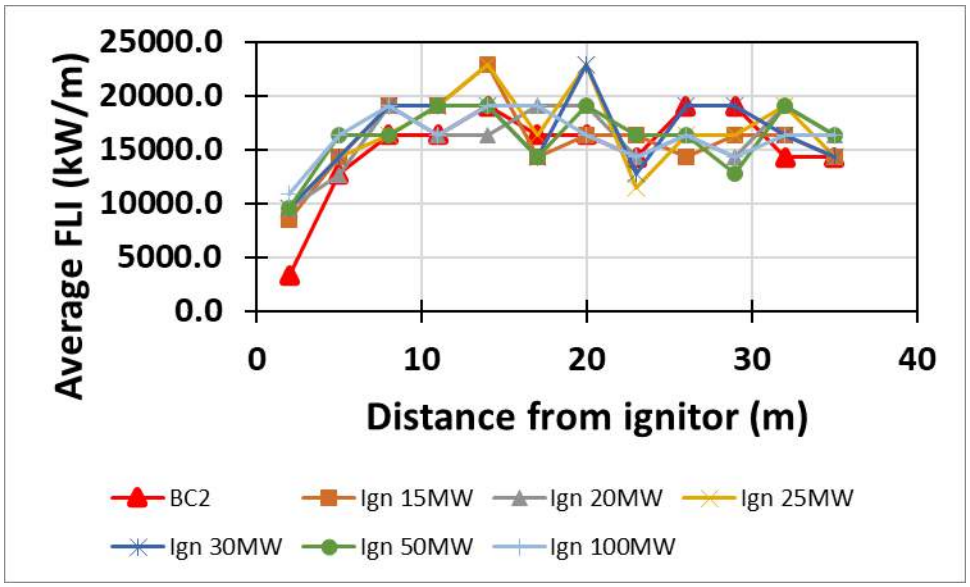

Figure 78. Fireline Intensity measured at different distances from the ignitor. Base case 2 (BC2) for comparison. Base case has 10 MW ignition and other ignitions are marked on graph.

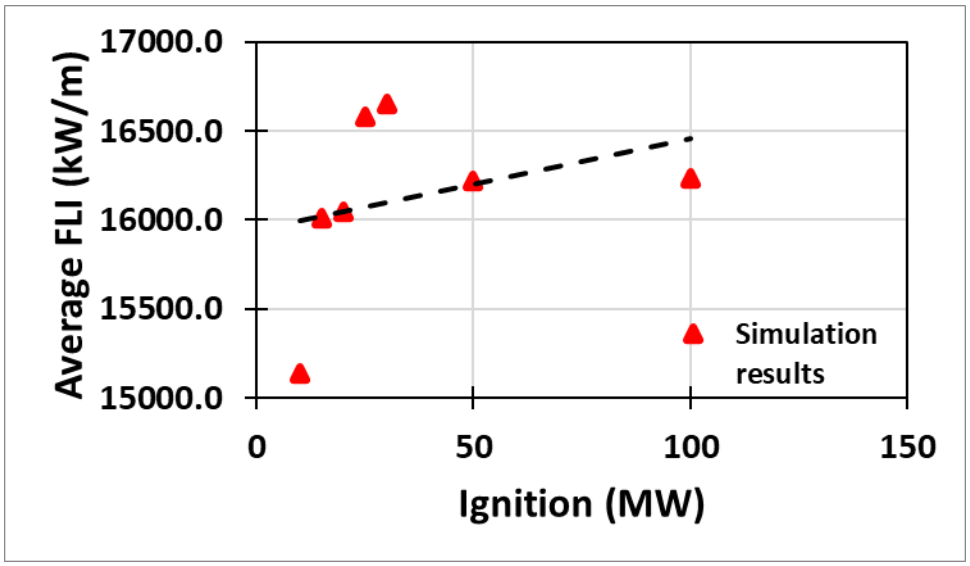

Figure 79. Average FLI compared to the ignitor's power. For every unit of ignition power change (MW) the FLI changes 5.1 kW/m.

5.4.1.8 Simulations of varying ambient temperatures

Base case 3 was used as a template for the varying ambient temperature simulations. The guide by CSIRO (Cruz et al., 2015) was employed to determine the ground level vegetation's moisture percent. According to the CSIRO guide, ground level vegetation moisture percent is 7 for all temperatures below base case 3 (see *Figure 81*) at temperatures -15 °C, 5 °C and 15 °C). All other temperatures have the vegetation moisture content at ground level vegetation as 6, similarly to the base case 3.

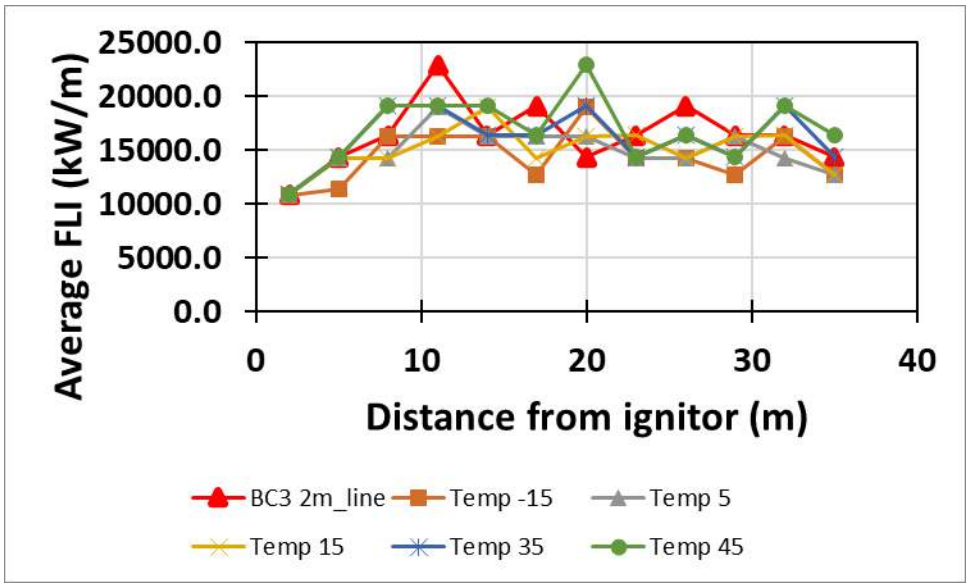

Figure 80. Fireline Intensity measured at different distances from the ignitor. Base case 3 (BC3 2m_line) for comparison. Base case has 25 ºC ambient temperature and other ambient temperatures are marked on graph.

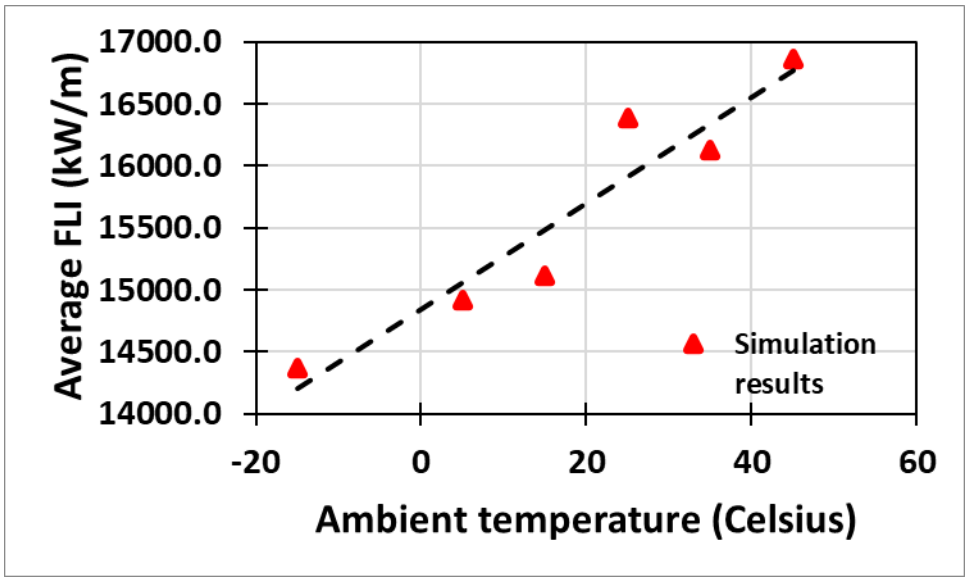

Figure 81. Average FLI compared to ambient temperature. For every unit of ambient temperature change (ºC) the FLI changes 42.6 kW/m.

5.4.1.9 Simulations of varying initial vegetation temperatures

Base case 3 was used as a template for varying initial vegetation temperatures. Initial temperatures of the fir trees and ground vegetation was varied. During these simulations, ambient parameters stayed the same as in base case 3 and only the initial temperature of particles, that are used for modelling the tree, and initial temperature of the ground fuel were modified.

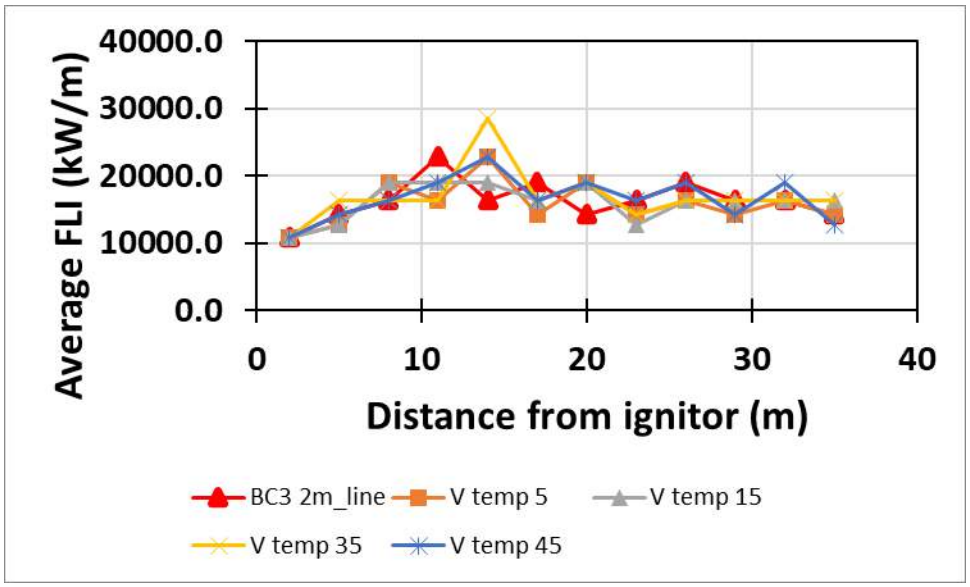

Figure 82. Fireline Intensity measured at different distances from the ignitor. Base case 3 (BC3 2m_line) for comparison. Base case has 25 ºC initial vegetation temperature and other ambient temperatures are marked on graph.

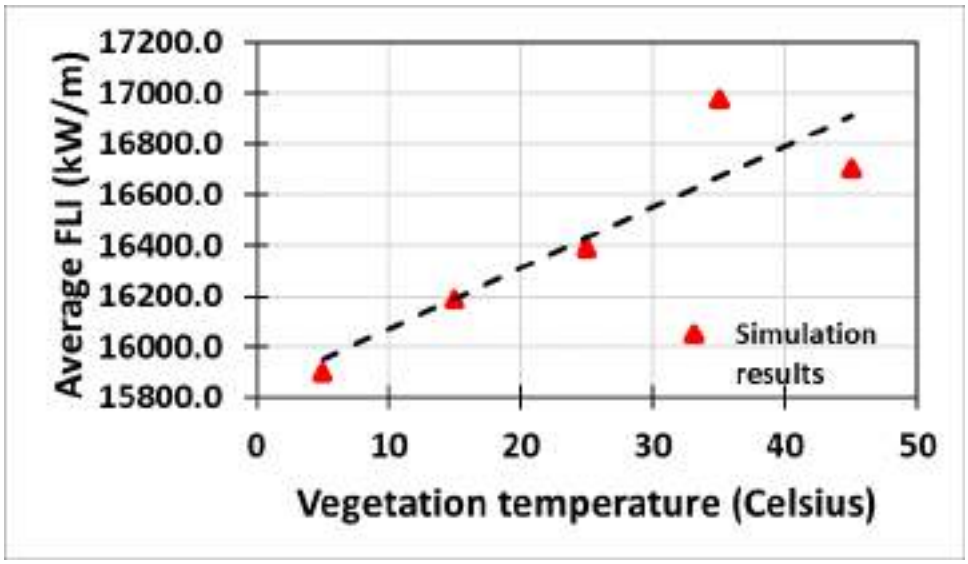

Figure 83. Average FLI compared to the initial temperature of vegetation. For every unit of vegetation temperature change (ºC) the FLI changes 24.0 kW/m.

5.4.1.10 Simulations of varying ground vegetation moisture

Base case 3 was used as a template. Moisture content of the ground level vegetation was modified according to *Figure 85*. The trees had the same moisture content as in base case 3 in all simulations, so only the ground level vegetation was modified.

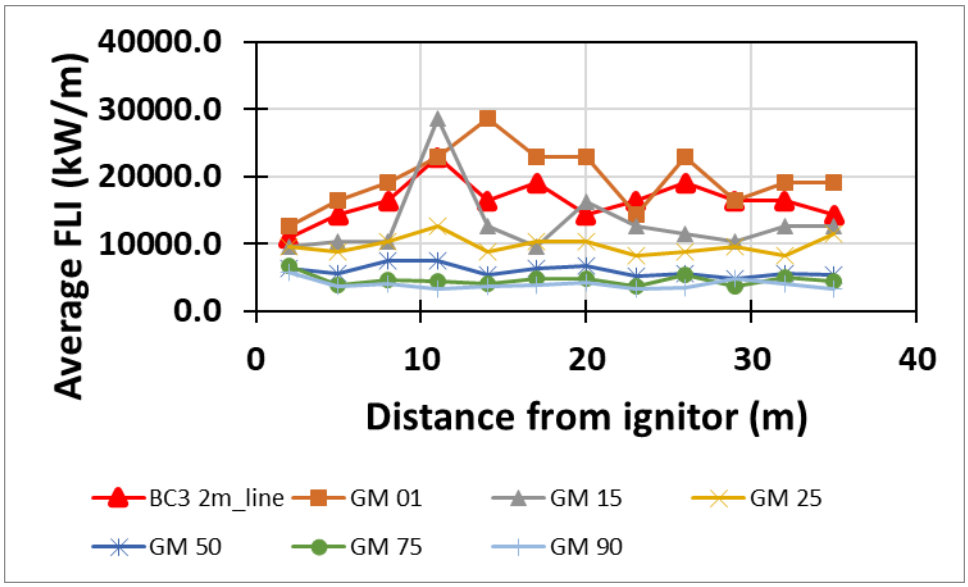

Figure 84. Graph for Fireline intensity development over time. Base case 3 (BC3 2m_line) for comparison with 6% moisture content on ground vegetation. Base case 3 has 6% of ground vegetation moisture and GM 01, GM 15, GM 50, GM 75 and GM 90-have 1%, 15%, 50%, 75% and 90% ground moisture content, respectively.

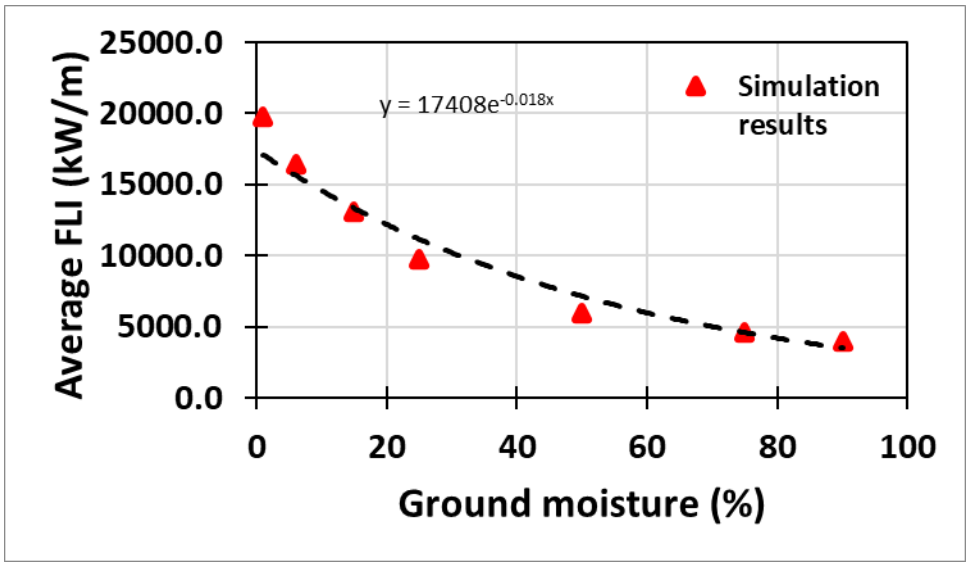

Figure 85. Average FLI compared to ground vegetation moisture percentage. FLI decreases exponentially with higher moisture content.

From *Figure 86*, with enough vegetation moist at ground level the fire, which is supported mostly by the ground level vegetation, will be under the limit of extreme wildfire event (10,000 kW/m), even when the dry amount of the same forest could develop into an extreme wildfire.

5.4.1.11 Comparison between different sensitivity study simulations

All sensitivity studies, except ground moisture percent altering sensitivity study, have a seemingly linear change in Fireline Intensity compared to the altered parameter. Ground

moisture percent affects the Fireline Intensity exponentially; with the dry ground being the source of the highest Fireline Intensity and wet ground the source of the lowest.

Table 17. Slopes of the fitted trendlines for each sensitivity study according to the varied parameter. For ground moisture percentage, exponential curve fits better to the data, but for the comparison slope of the fitted line in ground, moisture percent is presented in this table.

Varied parameter	Slope (FLI/varied parameter)
Wind speed (m/s)	673.8
Ambient humidity (%)	-82.6
Ignition power (MW)	5.1
Vegetation temperature (°C)	24.0
Ground vegetation (kg/m^2)	23,968.7
Ambient temperature (°C)	42.6
Ground moisture (%)	-163.1

From *Table 17*, parameters such as ambient humidity percent and ground moisture content are negatively affecting to the development of Fireline Intensity. Ground vegetation moisture content, since it is the primary fire sustaining fuel, is more critical for the development of Fireline Intensity than ambient humidity.

Parameters that affect positively, but not significantly to the Fireline Intensity, are ignition power, vegetation temperature and ambient temperature. Ignition is not as relevant to the Fireline Intensity because the fire anyway starts supporting itself after 10 seconds of ignition time. Ambient or vegetation temperatures do not affect the outcome either that much, because the temperature is changing between -15 °C to 45 °C in the ambient and between 5 °C to 45 °C in vegetation temperature. If the temperature was closer to the ignition point of the fuel, then the Fireline Intensity would probably be more affected, but 45 °C is already a quite high temperature for the climate where fir trees grow.

Wind speed and ground vegetation mass affected the most to the Fireline Intensity. Wind speed has a big effect to the Fireline Intensity since it heavily depends on the rate of spread and larger wind speeds push the fire to spread faster. Ground vegetation mass is the most important of the tested parameters that affect the Fireline Intensity. Adding only one kg of fuel per m^2 increases the Fireline Intensity by almost 24 MW/m, at least with the amounts of fuel used in sensitivity studies.

5.4.2 Sensitivity analysis with OpenFOAM

Sensitivity analysis in OpenFOAM was done based on the fireflux experiment. The base case is described in section 4.1.2.2. Model parameters are presented in *Table 5*.

Sensitivity analysis was done by varying one model parameter at a time and observing the effect to the fire front propagation. To make model sensitivity analysis clearer and avoid unnecessary complications, the boundary conditions were simplified to a constant wind velocity. Rate of spread and corresponding fire line intensity of the simulations were selected as primary compared quantities. Rate of spread calculation is described above

in the section 3.3.4. The temperature-based rate of spread evaluation method was selected. Fireline intensity was computed with the following formula:

$FLI = H \times w \times ROS$

Where *H* is the fuel heat of combustion (kJ/kg), *w* is the amount of consumed fuel (kg/m^2), and ROS is the linear rate of fire spread (m/s). In the simulation of the grass fires, it can be assumed, that the whole mass of the grass is burned immediately, therefore, the overall mass of grass can be used.

The effects of the following model parameters were investigated:

- Wind speed, i.e. inlet velocity. Only constant inlet velocity was considered.
- Mass of the grass. The grass properties, such as moisture, composition and heat of combustion were assumed to be constant.
- Moisture content of the grass. It was assumed that the weight of the dry mass of the grass is constant and increase of the moisture comes from e.g. rain or air humidity.
- Inclination of the ground. Propagation of the fire downhill or uphill was investigated.

The result of the sensitivity studies is presented in the following sections. The parameter ranges and the value used in the base case are combined in *Table 18* together with a short conclusion.

Table 18. Parameters used in the sensitivity study and the effect on the rate of spread and fire line intensity.

Parameter	Base case	Range in sensitivity analysis	Effect of increasing the parameter
Inlet velocity	4 m/s	3 m/s – 6 m/s	ROS increases, FLI increases
Mass of the grass (change in % to the mass of the base case; kg/m^2)	0 %; 1.08 kg/m^2	-50% -- +50% 0.54 kg/m^2 – 1.62 kg/m^2	ROS does not change, FLI increases
Grass moisture	5%	5% – 30%	ROS decreases, FLI decreases
Ground inclination	0° (flat prairie)	-30° – + 30°	ROS increases FLI increases

5.4.2.1 Sensitivity study: Effect of wind velocity.

For the sake of simplicity, the base case for the sensitivity study was selected to be a case with the constant wind from one side of the domain. Wind speed was constant with respect of the time and with respect of the height. Wind velocity in the base case was equal to 4 m/s. Effect of the wind velocity was investigated. Simulations with 3, 3.25, 3.5, 3.75, 4.5, 5, 5.5, and 6 m/s were performed. Each of the simulation results were analysed

and ROS and FLI were evaluated. In the simulations of 3 m/s the fire did not propagate through the whole domain and died out, therefore, ROS could not be evaluated. Simulated results are presented in *Figure 86*, *Figure 87* and *Table 19*.

Fire front propagation as a function of time is presented *Figure 86*. Some random behaviour can be observed due to the turbulence nature of the fluid dynamic calculation. However, the trend of the rate of spread behaviour is well pronounced. Increasing the simulated wind speed resulted in increased fire propagation, as expected, and therefore the fire line intensity increased.

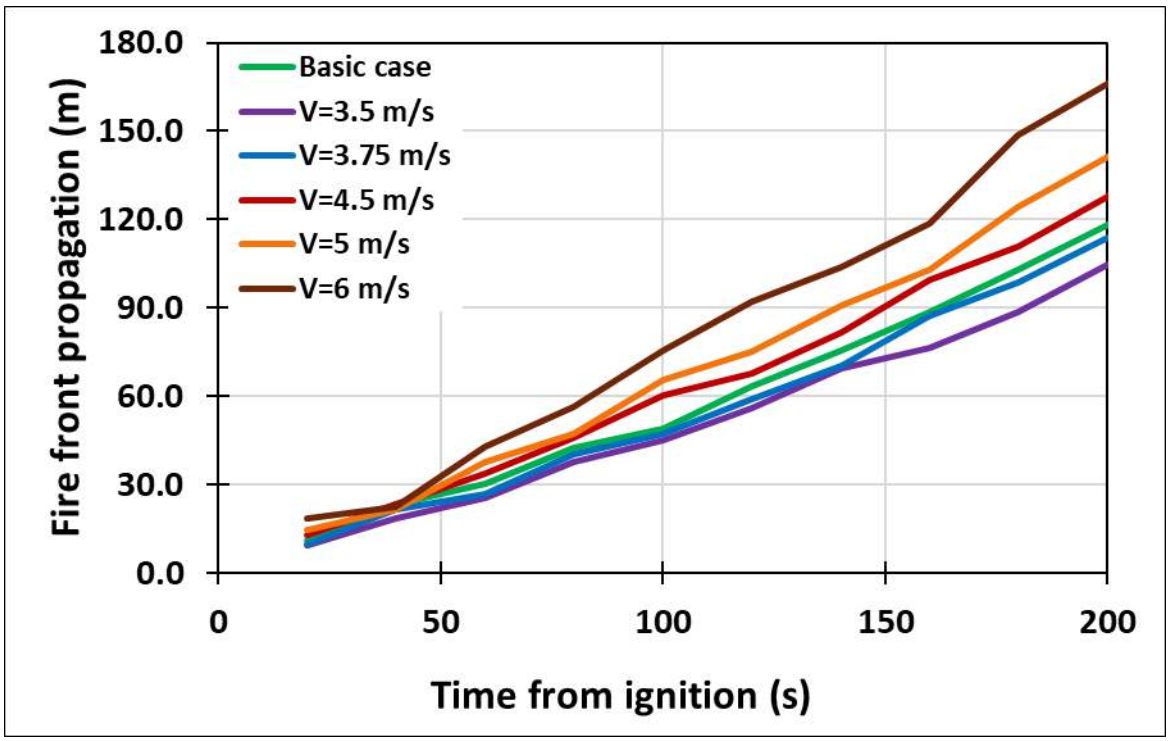

Figure 86. OpenFOAM simulation results of fire front propagation. Sensitivity study of inlet velocity.

Table 19. OpenFOAM simulation results. Sensitivity study of inlet velocity.

Velocity, m/s	3	3.25	3.5	3.75	4	4.5	5	5.5	6
ROS, m/s	-	0.47	0.49	0.53	0.56	0.61	0.68	0.75	0.78
FLI, kW/m	-	8,916	9,313	10,129	10,591	11,589	12,877	14,309	14,879

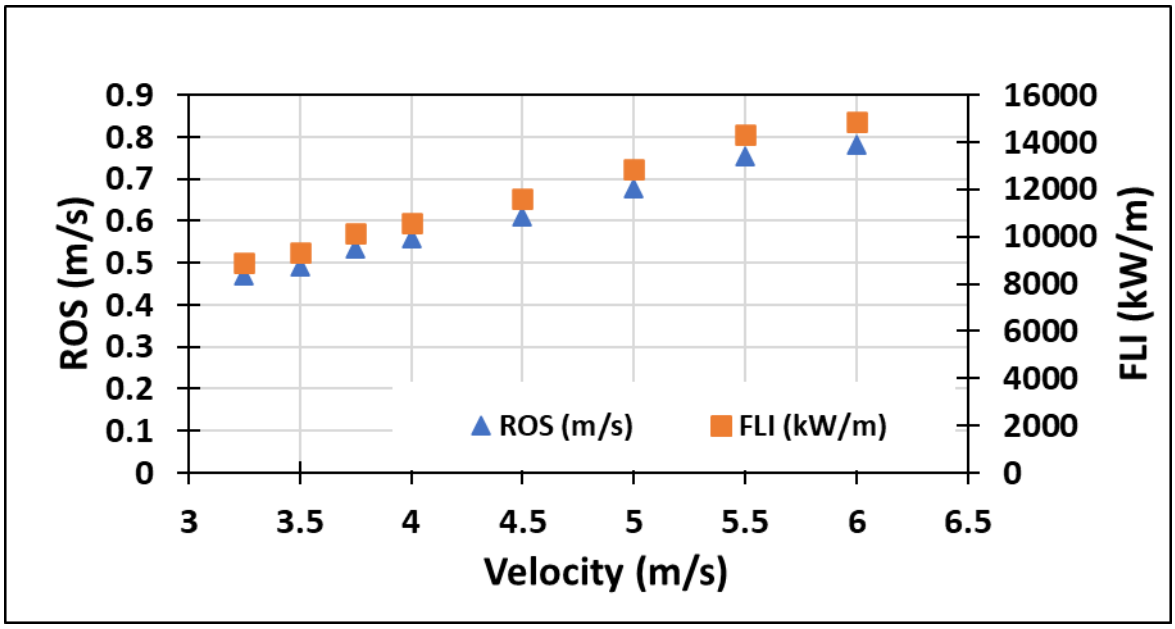

Figure 87. OpenFOAM simulation results of rate of spread and fireline intensity. Sensitivity study of inlet velocity.

5.4.2.2 Sensitivity study: Effect of grass mass.

In the base case, the amount of the grass was taken from the data presented in *Table 18*. Data samples reported from the different part of the prairie were weighted and the average value of 1.08 kg/m^2 was used. In the simulations, grass was assumed to be distributed uniformly around the domain. As described in the case setup, the areas around the measuring towers were cut, this were included in the simulations. For the sensitivity study the mass was decreased in 50%, 20%, 10% and increased in 10%, 20% and 50%. Corresponding average fuel masses are 0.54, 0.864, 0.972, 1.188, 1.296 and 1.62 kg/m^2. Each of the simulation results were analysed and ROS and FLI were evaluated. Simulated results are presented in *Figure 88*, *Figure 89* and *Table 20*. Properties of the grass were the same as well as in the base case. *Figure 88* shows the fire front propagation. Some randomness of the results can be observed at some time moment. Nevertheless, the overall behaviour of the fire front propagation is very similar for all the cases. This reflects the close agreement of the rate of spread values for each case. Little variation can be explained by the randomness and the method of analysis of the rate of spread. Independence of the rate of spread of the fuel mass are also confirmed in the literature. The dependence of the fireline intensity on the fuel mass is presented in *Figure 89* and *Table 20*. A clear trend of the FLI increase directly follows the almost constant ROS.

Table 20. OpenFOAM simulation results. Sensitivity study of grass mass.

Mass change, %	-50	-20	-10	0	10	20	50
ROS, m/s	0.59	0.56	0.55	0.56	0.56	0.56	0.59
FLI, kW/m	5,560	8,532	9,492	10,591	11,713	13,136	16,941

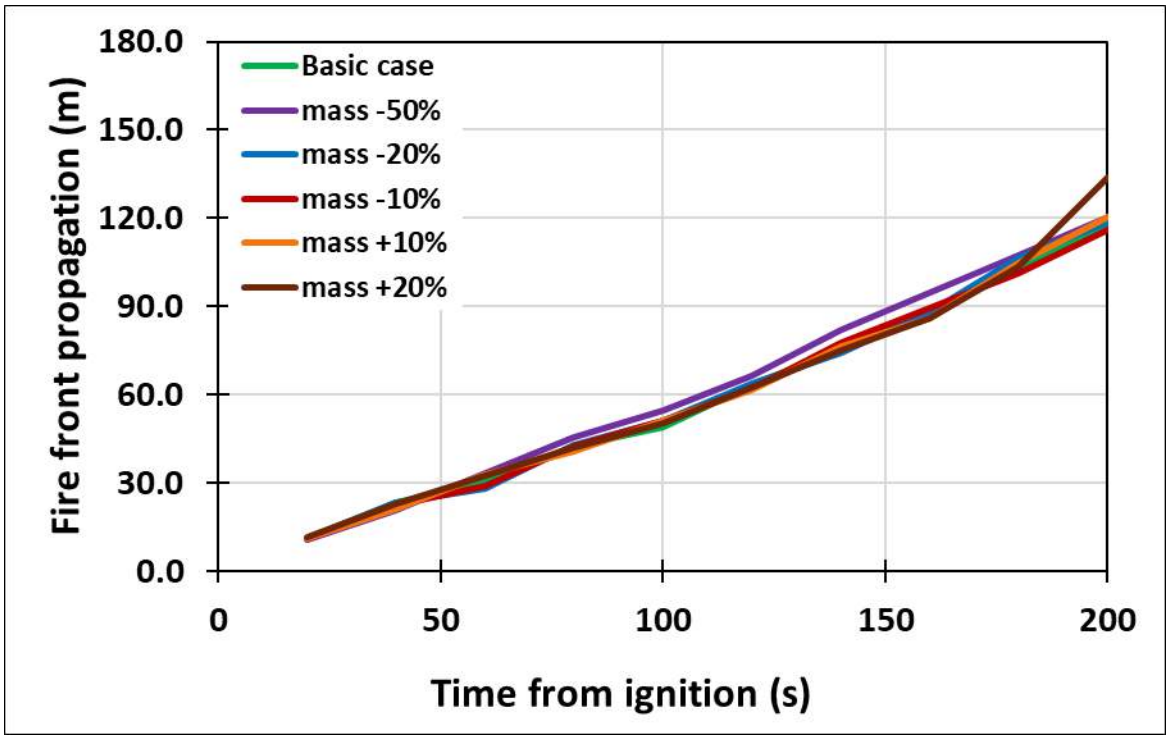

Figure 88. OpenFOAM simulation results of fire front propagation. Sensitivity study of grass mass.

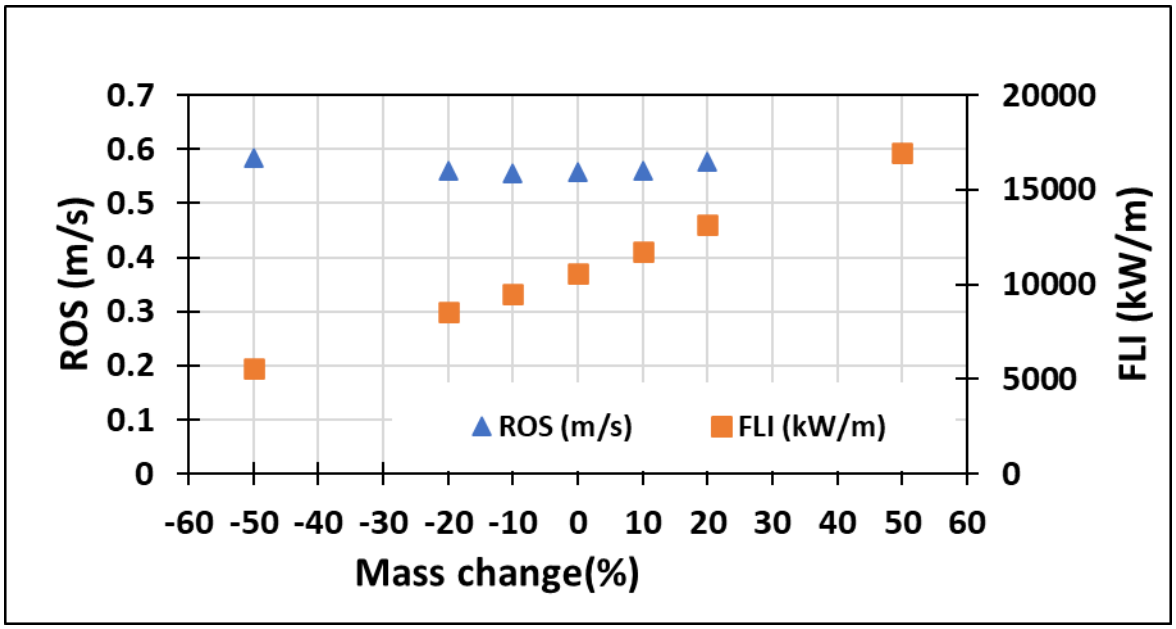

Figure 89. OpenFOAM simulation results of rate of spread and fireline intensity. Sensitivity study of grass mass.

5.4.2.3 Sensitivity study: Effect of fuel moisture content.

Grass moisture of the base case was 5%. This corresponds to the 1.08 kg/s of the grass. During the sensitivity studies, the moisture of the grass was increased so, that the weight of the dry mass remains the same. I.e. it describes the situation with the increase moisture due to the air humidity or the rain. Therefore, overall mass of the grass in the simulation increased, but mass of the dry fuel was kept constant. Moreover, these changes affect the values of corresponding heat of combustion (kJ/kg), so heat of combustion was decreased along with increasing of the moisture.

Simulation results are presented in *Figure 90*, *Figure 91* and *Table 21*. It can be observed that the rate of spread decreases while moisture increases. Despite the increase of the total grass mass, the fireline intensity decreases together with the rate of spread. This follows naturally from the fact that dry fuel mass was kept constant in the considered simulation, therefore, heat of combustion decreases.

Table 21. OpenFOAM simulation results. Sensitivity study of moisture content.

Moisture, %	5	10	15	20	30
ROS, m/s	0.56	0.52	0.52	0.50	0.45
FLI, kW/m	10,716	9,918	9,808	9,523	8,582

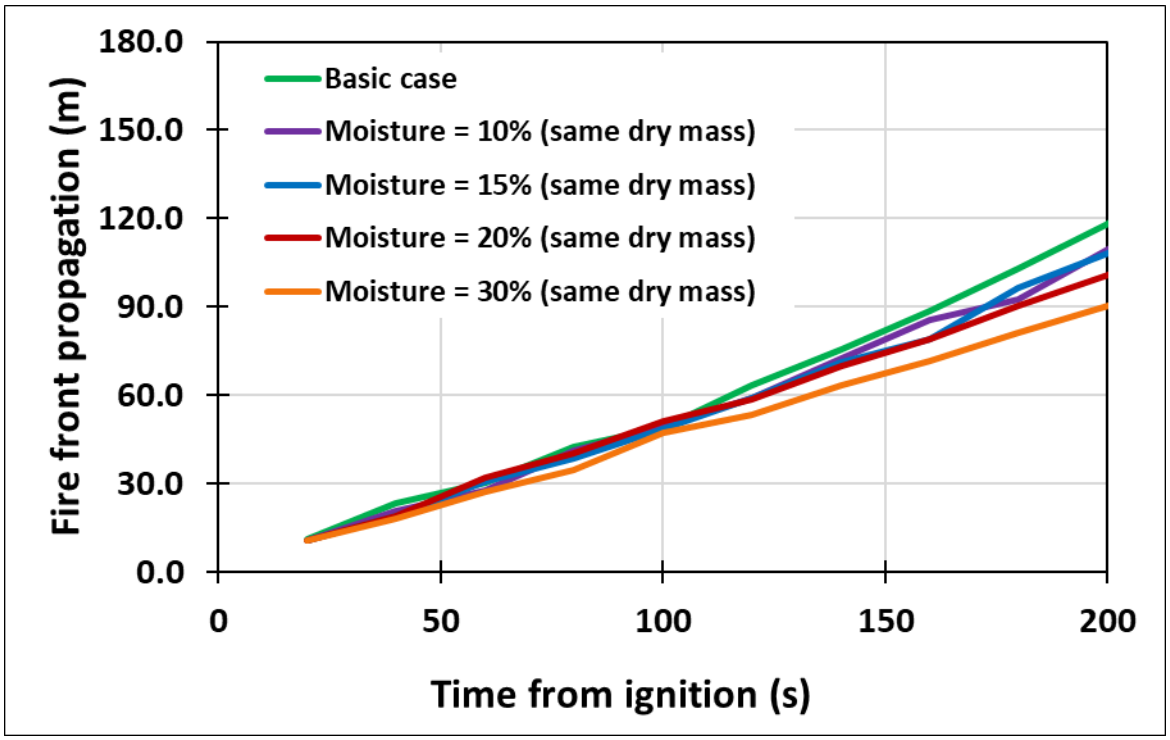

Figure 90. OpenFOAM simulation results of fire front propagation. Sensitivity study of moisture content.

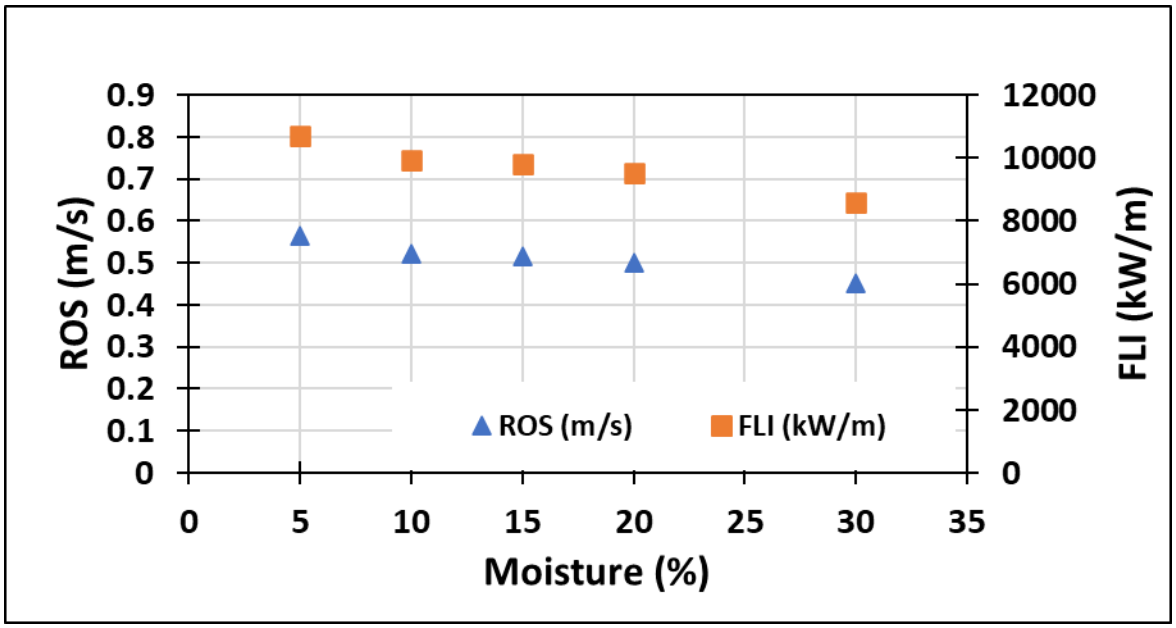

Figure 91. OpenFOAM simulation results of rate of spread and fire line intensity. Sensitivity study of moisture content.

5.4.2.4 Sensitivity study: Effect of ground slope

In the base case we assumed that the ground is flat, i.e. wind is coming directly form one direction and orthogonally to the area. In the following study we test how the spreading of the fire is affected by the ground inclination, namely how the grass fire is spreading in the presence of the hills or lowness of the ground level. Thus, we assume inclination of the ground -30°, -15°, -5°, 10°, 15° and 30°, i.e., we consider the fire propagation in the downhill direction and uphill direction with different inclinations. From the computational point of view, these simulations were done by changing the direction of inlet velocity to the prescribed angle. Simulation results are presented in *Figure 92*, *Figure 93* and *Table 22*. Some simulation with the negative inclination produced the fire dying out, whereas positive ground inclination promoted uphill fire propagation and increases dramatically the rate of spread. The corresponding fireline intensity of the simulated case with 15° and 30° inclination reaches the value of 10,000 kW/m and can be considered as an extreme fire event.

Although it should be noticed that the prairies with such a high grass are not growing in the hills with such a large slope and this study does not have practical application, the robustness of the numerical model in these conditions were confirmed and a clear trend was observed.

Table 22. OpenFOAM simulation results. Sensitivity study of ground slope.

Ground slope, degrees	-30°	-15°	-5°	0°	10°	15°	30°
ROS, m/s	--	--	0.46	0.56	0.71	0.82	1.10
FLI, kW/m	--	--	8,747	10,591	13,558	15,575	20,912

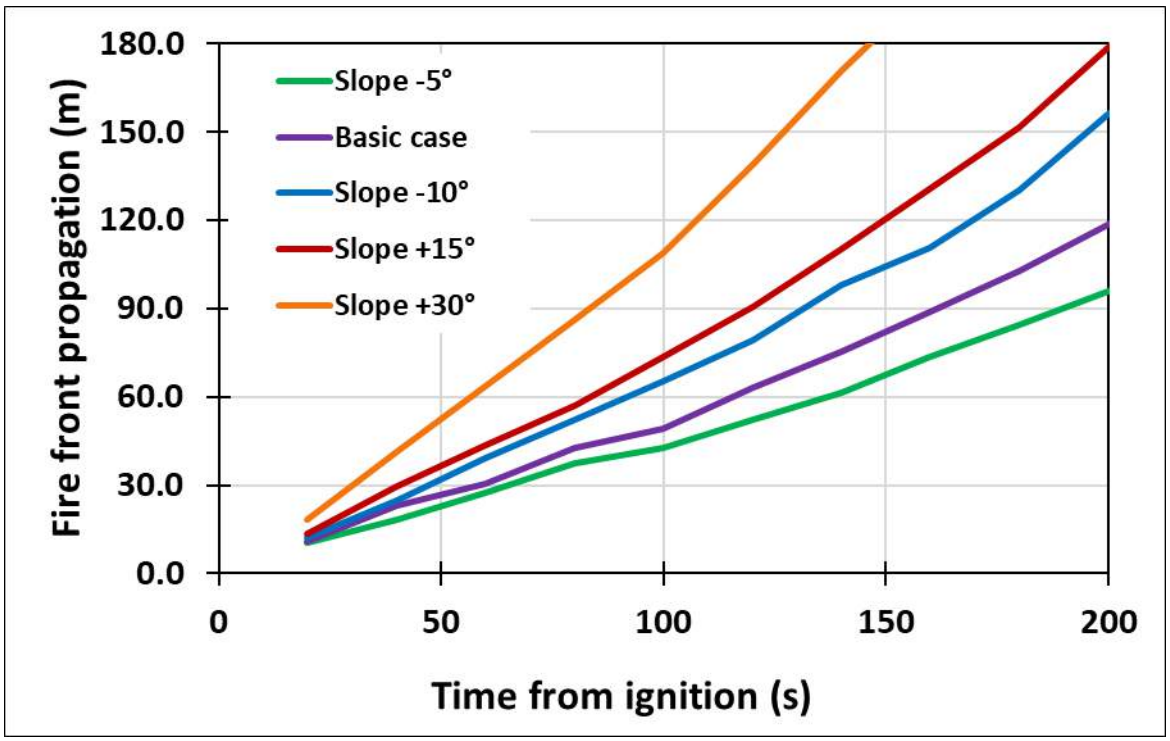

Figure 92. OpenFOAM simulation results of fire front propagation. Sensitivity study of ground slope.

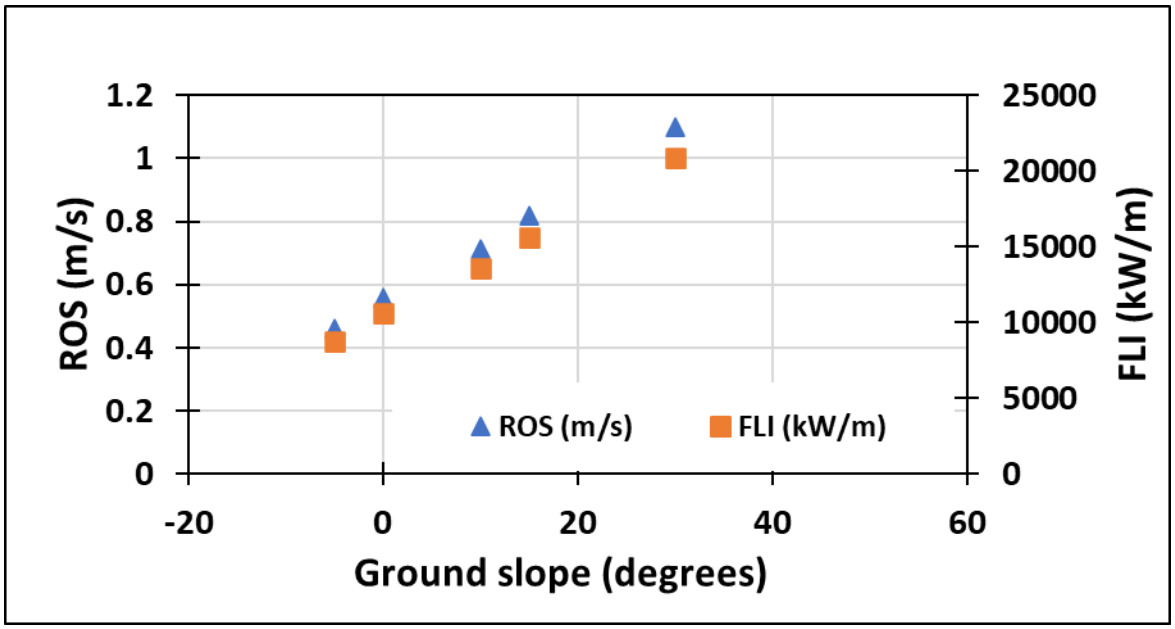

Figure 93. OpenFOAM simulation results of rate of spread and fire line intensity. Sensitivity study of ground slope.

6.SUMMARY AND CONCLUSIONS

In this chapter, we summarize the issues presented in the report, and finally we comment on the development that our work has produced in the simulation of wildfires and the prediction of EWE.

6.1 From empirical to physical models

The simulation of wildfires has long been mainly limited to empirical models that are based on fire tests performed in the laboratory. While this approach works well for relatively homogeneous environments, it does not work as well for more heterogeneous environments. A more physical modelling approach is also needed to better explore the parameters governing behaviour related to vegetation, topography, wind, etc. and their relative importance.

The physical model of a wildfire is written as a set of differential equations that describe the behaviour and interactions of the key processes and the change of each dependent variable in relation to another variable, usually in time and spatial dimension. Usually, the equations are non-linear and linked, creating a complex network of variables, coefficients, and parameters necessary to describe the behaviour of a given phenomenon and its evolution over time. Solutions are obtained using numerical calculation methods that provide approximate solutions to a set of equations. Physical model validation, testing, and evaluation are perhaps the most critical steps in the model development process. Comparing model results with observations is the basis of validation, which measures the model's ability to accurately represent reality.

In the proposed approach, we used two different computational fluid dynamics (CFD) software, namely Fire Dynamics Simulator (FDS) and OpenFOAM. We first tested the suitability of the selected CFD models for the simulation of wildfires by simulating well-known fire experiments described in the scientific literature. The validation cases included both grass fires and tree fires. Once an understanding of the applicability and calculation accuracy of the models was obtained in the validation cases, some applications were made and the simulations were extended by interpolating and extrapolating; with the aim of sensitivity analysis to determine fire behaviour under different conditions, including situations where extreme fire behaviour is typically observed.

6.2 New knowledge

By the sensitivity analysis of a prairie grass fire case with OpenFOAM, it could be demonstrated how the rate of spread increased significantly by an increasing wind speed, as it was expected. When the mass of the grass was varied, a clear indication could be seen in the fireline intensity, rate of spread instead was almost the same for all masses. When the fuel moisture content was varied, it could be observed how the rate of spread decreases while moisture increases. Despite the increase of the total grass mass, the fireline intensity decreases together with the rate of spread. Finally, it was tested how the spreading of the fire is affected by the ground inclination. Simulations with negative inclination produced the fire dying out, but positive ground inclination (i.e. uphill fire

propagation) increases dramatically the rate of spread. The corresponding fireline intensity of the simulated grass fire case with 15° and 30° inclination reaches the value of 10,000 kW/m and can be considered as an extreme fire event. Similarly, sensitivity analysis was made with FDS for the validated tree fire (burning Douglas Fir) and its further development: burning forest of Douglas Fir trees.

6.3 New scenarios of application

The modelling capabilities of FDS were applied to the combustion of pine needles, for which Norway-Sweden LL had provided us with measurement data related to the boreal pine forest. The pine needles samples were modelled by two variations, one was the usual FDS surface model ("FDS Milled" and "FDS Needles"), the other the Boundary Fuel Model ("FDS Needles BFM"). These material models are just tentative, as the amount of experimental data was very limited and the missing data was completed using generic vegetation models presented in FDS User Guide and FDS Validation Guide, which seemed to be quite good starting point for vegetation modelling of a wildfire scenario.

To test the material models for pine needles, a FDS simulation was conducted, where one of the validation cases (CSIRO grassland fire case C064) setting was adopted for pine needles, i.e. the fire load was changed from grass to pine needles. The BFM version of the pine needle material model was used, as the pine needles are so small, and they cannot be resolved in the simulation. The ignition source used in the CSIRO grassland simulations did not ignite the pine needles, but when ignitor HRR was increased (5,000 kW/m^2) and the duration of the maximum HRR at each point on the ignition line was increased to 30 s, the pine needles were ignited, and a forward spreading fire was forming.

Next, a simplified computational fluid dynamics-based forest setting was presented to study the transition of wildfire from one state to target state, encompassing different fire categories from normal to extreme fire. Precursors for extreme wildfire were prudently chosen to indicate in advance the possibility of a wildfire turning into an extreme wildfire event. Precursors include real-time measurable parameters such as rate of spread, fireline intensity, and flame length. A fireline of low intensity approached the forest setting, and its transition into a severe fire was studied by changing the dominant factor, which is wind speed. Various charts and tables were produced covering the values of chosen precursors to understand the trend for decision making to deal with such fires.

For the chosen vegetation, the rate of spread and fireline intensity show, in general, an exponential growth trend with an increase in wind speed. Moreover, the flame lengths show, in general, a logarithmic trend with an increase in wind speed where wind speeds range from low to moderate, the relationship between flame length and wind speed is steep, but as wind speed continues to rise, the incremental increases in flame length begin to flatten out. The behaviours observed in the simulations are in line with what has been observed and reported in real fires. The setting was also tested with different environmental humidities, vegetation moisture contents, and ambient temperatures. The results align with our expectations (except ambient temperature): higher humidity and vegetation moisture content led to less severe fires. Moreover, the forest setting has also been used for the estimation of thermal exposure on combustibles present near the wildland-urban interface.

Overall, the alignment of results with earlier findings and expected behaviour is encouraging as it reinforces our understanding of the complex dynamics of wildfires through computational fluid dynamics-based study. However, the experimental validation of such results is not readily feasible, given the sheer scale of the forest plot used in the simulation. Nonetheless, such simulations (with different trees and vegetation also) are expected to provide indicative results that could be coupled with a realistic understanding of wildfires and experiences in witnessing and facing them so that judicious firefighting decisions can be taken.

6.4 Innovation and technology readiness progress

Technology Readiness Levels (TRL) are a type of measurement system used to assess the maturity level of a particular technology. TRL 1 is the lowest meaning “basic principles observed and reported”; TRL 9 is the highest meaning “actual system proven through successful mission operations”. CFD modelling and simulation have long ago been verified and found to be good and practical methods; and the tools we use, FDS and OpenFOAM, have been extensively validated and in practical use in many applications. FDS, which has been developed especially for fire safety applications, is widely used in verifying fire safety in the infrastructure and construction industry. On the other hand, wildland and forest fires of natural sites are so challenging as modelling objects that, for them, CFD methods on a practical level are just the next generation in their infancy. Using the method requires a lot of competence and data, which is still very little available. The cost of the calculation (i.e., calculation capacity and time required), still limits the use of the method in practical applications.

The developments presented in this report, to apply CFD modelling to wildland fire problems, represents TRL levels between 2 and 5. The simulations of the grass fire test on the prairie are placed at TRL level 5 ("validation in relevant environment"), and the simulations of the Douglas fir fire test at TRL level 4 ("validation in laboratory environment"). These validation simulations were possible because suitable data was available. Our other applications aim to extend validation in general and especially to forest fires for which no suitable validation data could be found, and the development work can therefore be placed at TRL level 3, "analytical and experimental critical function and/or characteristic proof-of-concept". In addition, we developed a method for the prediction of EWE risk, which represents TRL level 2 "technology concept and /or application formulated".

REFERENCES

Accary, G. & Morvan, D. (2024). How can CFD contribute to the understanding of wildfire behaviour? Computers & Fluids, Volume 279, 30 July 2024.

Albini, F. A. (1976). Estimating Wildfire Behavior and Effects. Research Paper INT-30, Intermountain Forest and Range Experiment Station, USDA Forest Service, Ogden, Utah, USA.

Alexander, M. E., Cruz, M. G. (2013). Are the applications of wildland fire behaviour models getting ahead of their evaluation again? Environmental Modelling & Software, Volume 41, March 2013, Pages 65−71.

Alexander, M. E., Cruz, M. G. (2019). Encyclopedia of Wildfires and Wildland-Urban Interface (WUI) Fires. Fireline Intensity.

Anderson, H.E. & Rothermel, R.C. (1965). Influence of moisture and wind upon the characteristics of free-burning fires", Symp. Int. Combust. 10 (1965), no. 1, p. 1009−1019.

Andrews P.L. (2018), The Rothermel surface fire spread model and associated developments: A comprehensive explanation, Rocky Mountain Research Station, General Technical Report, RMRS-GTR-371

Baines, P. (1990). Physical mechanisms for the propagation of surface fires. Math. Comput. Modelling Vol. 13, No. 12, pp. 83−94, 1990.

Balbi, J.H., Morandini, F., Silvani, X., Filippi, J.B. & Rinieri, F. (2009). A physical model for wildland fires. Combust. Flame 156 (2009), no. 12, p. 2217−2230.

Balbi, J.H., Chatelon, F.J., Morvan, D., Rossi, J.L., Marcelli, T. & Morandini, F. (2020). A convective–radiative propagation model for wildland fires. Int. J. Wildland Fires 29 (2020), no. 8, p. 723−738.

Beer, T. (1990), The interaction of wind and fire. Bushfire Research Program, CSIRO Private Bag 1, PO Mordialloc Vic. 3195 Australia

Borg, A., Husted, B. P. & Njå, O. (2014), The concept of validation of numerical models for consequence analysis, Reliability Engineering & System Safety, Volume 125, May 2019, Pages 36−45.

Byram, J.K. (1959). Field test of a rate-of-fire spread model in slash fuels. USDA For. Serv. Res. Pap. INT-116, 24 p. Intermt. For. And Range Exp. Stn., Ogden, Utah.

Castellnou, M. (2019). Forest fires and climate change interaction and problem in global & European context. Keynote lecture in Forest & Photonics 2019 held in 7th−8th of October 2019 in Koli National Park, Finland. https://www.youtube.com/watch?v=Y7sHbjmEj4U

Castellnou, M., Nebot, E., Estivill, L., Miralles, M., Rosell, M., Valor, T. & Casals, P. (2022a). D1.1 Transfer of lessons learned on extreme wildfire events to key stakeholders. FIRE-RES: Innovative technologies & socio-ecological-economic solutions for fire resilient territories in Europe. https://fire-res.eu/wp-content/uploads/2023/02/D1.1.pdf

Castellnou, M., Bachfischer, M., Miralles, M., Ruiz, B., Stoof, C. R., & Vilà-Guerau de Arellano, J. (2022b). Pyroconvection classification based on atmospheric vertical

profiling correlation with extreme fire spread observations. Journal of Geophysical Research: Atmospheres, 127, e2022JD036920. https://doi.org/10.1029/2022JD036920

CFD Direct (2024), OpenFOAM Documentation https://cfd.direct/openfoam/documentation/

Clark, T.L., Jenkins, M.A., Cohen, J.L. & Packham, D.R. (1996). A coupled atmosphere-fire model: convective feedback on fire-line dynamics", J. Appl. Meteorol. Clim. 35 (1996), no. 6, p. 875−901.

Clements, G.B., Zhong, S., Bian, X., Heilman, W.E. & Byun, D.W. (2008). First observations of turbulence generated by grass fires. Journal of Geophysical Research113 (2008), D22102. https://doi.org/ 10.1029/2008JD010014

Clements, G.B., Zhong, S., Goodrick, S., Li, J., Potter, B.E., Bian, X., Heilman, W.E., Charney, J.J., Perna, R., Jang, M., Lee, D., Patel, M., Street, S. & Aumann, G. (2007). Observing the Dynamics of Wildland Grass Fires. American Meteorological Society, BAMS Sep. 2007, p. 1369–1382.

Comissão Técnica Independente, (2017). Análise E Apuramento de Factos Relativos Aos Incêndios Que Ocorreram Em Pedrogão Grande, Castanheira de Pera, Ansião, Alvaiázere, Figueiró Dos Vinhos, Arganil, Góis, Penela, Pampilhosa Da Serra, Oleiros E Sertã, Entre 17 E 24 de Junho de 2017; Assembleia da República: Lisbon, Portugal, 2017.

Cox, G., (1998). Turbulent closure and the modelling of fire by using computational fluid dynamics. Philosophical Transactions of the Royal Society A Mathematical, Physical and Engineering Sciences, Volume 356, Issue 1748, Pages 2835–2854.

Cruz, M., Gould, J., Alexander, M., Sullivan, A., McCaw, W., Matthews, S., (2015). A guide to rate of fire spread models for Australian vegetation. CSIRO Land and Water.

Drysdale, D. (1999). An Introduction to Fire Dynamics. Second Edition. Chichester, UK: John Wiley & Sons Ltd. 451 p.

Egorov, Y., & Menter F.R. (2008). Development and Application of SST-SAS Model in the DESIDER Project. Advances in Hybrid RANS-LES Modelling, Notes on Num. Fluid Mech. And Multidisciplinary Design, Volume 97, 261-270.

Felicelli V.T., Pietri K. M., Santoni P.A., Morandini F., Pieri A., Barboni T., (2023), Flammability study of decking sections found at the Wildland–Urban interface at different scales, Fire Safety Journal 139 (2023) 103838

Finney, M.A. (2004). FARSITE: fire area simulator, model development and evaluation. Research Paper RMRS-RP-4 Revised. Ogden, UT: US Department of Agriculture, Forest Service, Rocky Mountain Research Station.

Filippi, J.B., Bosseur, F., Pialat, X., Santoni, P.A., Strada, S. & Mari, C. (2011). Simulation of coupled fire/atmosphere interaction with the MesoNH-ForeFire models. J. Combust. 2011 (2011), article no. 540390.

Finney, M.A., Cohen, J.D., Forthofer, J.M., McAllister, S.S., Gollner, M.J., Gorham, D.J., Saito, K., Akafuah, N.K., Adam, B.A. & English, J.D. (2015). Role of buoyant flame dynamics in wildfire spread. Proc. Natl. Acad. Sci. USA 112 (2015), no. 32, p. 9833−9838.

Forney, G.P. (2007). User's Guide for Smokeview Version 5 - A Tool for Visualizing Fire Dynamics Simulation Data, NIST Special Publication 1017-1.

Frandsen, W.H. (1971). Fire spread through porous fuels from the conservation energy. Combust. Flame 16 (1971), p. 9−16.

Hanson, P.H., Bradley, M.M., Bossert, J.E., Linn, R.R & Younker, L.W. (2000). The potential and promise of physics-based wildfire simulation. Env. Sci. Policy 3 (2000), p. 161−172.

Holm Nygaard, P. 2024. Private communication (email 13th Feb 2024), Norwegian Institute of Bioeconomy Research, Ås, Norway.

Hurley, M. J. (2016), SFPE Handbook of Fire Protection Engineering, 5th Edition, Society of Fire Protection Engineers 2016.

ISO 5660-1:2015. Reaction-to-fire tests – Heat release, smoke production and mass loss rate – Part 1: Heat release rate (cone calorimeter method) and smoke production rate (dynamic measurement). Third edition 2015-03-15. Geneva: International Organization for Standardization, 2015. 55 p.

Järvinen, M. (2014). The limits of rescue services in the case of fire in road tunnels. Helsinki City Rescue Department.

Karlsson, B. & Quintiere J. G. (1999). Enclosure Fire Dynamics, Fire plumes and flame heights, 1st Ed., CRC Press, 1999, pp. 47-80.

Korhonen, T., Hakkarainen, T., Tissari, A., Korkealaakso, A., Kling, T., & Verma, N. (2021). Kartiokalorimetrikokeen mallitus FDS-ohjelmalla. Pelastustieto: Palontorjuntatekniikka-erikoisnumero, pp. 72-76. https://www.spek.fi/wp-content/uploads/2021/11/Palotutkimuksen_paivat_2021.pdf

Korhonen, T. Korkealaakso, A., Verma, N., Kling, T., Hakkarainen, T. & Viitanen, A., (2022). Fast cone calorimeter model for optimization of pyrolysis parameters. Book of Abstracts, Nordic Fire & Safety Days, June 21-22, 2022, Lund, Sweden. RISE Research Institutes of Sweden, Borås, Sweden, pp. 30-31.

Lawson, D. I. (1954). Fire and the atomic bomb. Fire Research Bulletin No. 1. London, UK: HMSO.

Mandel, J., Beezley, J.D. & Kochanski, A.K. (2011). Coupled atmosphere-wildland fire modeling with WRF-Fire version 3.3. Geosci. Model Dev. 4 (2011), p. 591–610.

Magnussen, B. F. (2005, June). The Eddy Dissipation Concept - A Bridge Between Science and Technology. In ECCOMAS thematic conference on computational combustion (pp. 21-24).

Matala, A. (2013). Methods and applications of pyrolysis modelling for polymeric materials, VTT Science 44, 2013.

McGrattan, K. (2017), Progress in Modeling Wildland Fires using Computational Fluid Dynamics, 10th U.S. National Combustion Meeting Organized by the Eastern States Section of the Combustion Institute, April 23–26, 2017, College Park, Maryland.

McGrattan, K., Hostikka, S., Floyd, J., McDermott, R., Vanella, M., Mueller, E. (2023). Fire Dynamics Simulator User's Guide. U.S. Department of Commerce: National Institute of Standards and Technology (2023). https://github.com/firemodels/fds/tree/master/Manuals/FDS_User_Guide

McGrattan, K., Hostikka, S., Floyd, J., McDermott, R., Vanella, M. & Mueller, E. (2024a). Fire Dynamics Simulator, Technical Reference Guide, Volume 1: Mathematical Model, NIST Special Publication 1018-1, Sixth Edition.

McGrattan, K., Hostikka, S., Floyd, J., McDermott, R., Vanella, M. & Mueller, E. (2024b). Fire Dynamics Simulator, Technical Reference Guide, Volume 3: Validation, NIST Special Publication 1018-3, Sixth Edition.

McNamee, M., Meacham, B., van Hees, P., Bisby, L., Chow, W.K., Coppalle, A., Dobashi, R., Dlugogorski, B., Fahy, R., Fleischmann, C., Floyd, J., Galea, E.R., Gollner, M., Hakkarainen, T., Hamins, A., Hu, L., Johnson, P., Karlsson, B., Merci, B., Ohmiya, Y., Rein, G., Trouvé, A., Wang, Y. & Weckman, B. (2019). IAFSS agenda 2030 for a fire safe world. Fire Safety Journal 110 (2019) 102889. https://doi.org/10.1016/j.firesaf.2019.102889

Mell, W., Maranghides, A., McDermott, R., L. Manzello, S. (2009). Numerical simulation and experiments of burning douglas fir trees, Combustion and Flame, Volume 156, Issue 10, October 2009, Pages 2023-2041.

Morvan, D., Accary, G., Meradji, S. and Frangieh, N. (2022). Fifty years of progress in wildland fire modelling: from empirical to fully physical CFD models, Published online as part of special issue: More than a half century of Computational Fluid Dynamics, Guest editor: Mohammed El Ganaoui (Professeur des Universités, Spécialiste: Mécanique des Fluides et Transferts de Chaleur et de Masse, Université de Lorraine). https://doi.org/10.5802/crmeca.133

Mueller, E.V., Skowronski, N.S., Clark, K.L., Gallagher, M.R., Mell, W.E., Simeoni, A & Hadden, R.M. (2021). Detailed physical modeling of wildland fire dynamics at field

scale - An experimentally informed evaluation, Fire Safety Journal, Volume 120, 2021.

NRC, 2016. Verification and Validation of Selected Fire Models for Nuclear Power Plant Applications: Supplement 1, NUREG-1824 Supplement 1 and EPRI 3002002182. U.S. Nuclear Regulatory Commission, Office of Nuclear Regulatory Research (RES) and Electric Power Research Institute (EPRI), 2016.

Liu, N., Lei, J., Gao, W., Chen, H. & Xie, X. (2021). Combustion dynamics of large-scale wildfires. Proceedings of the Combustion Institute 38 (2021) 157–198.

Rego, F.C., Rigolot, E., Alexandrian, D. & Fernandes, P. (2007). EU project FIRE PARADOX: Moving towards integrated Fire Management. The 5th International Wildland Fire Conference, Sun City, South Africa, 9–13 May 2011.

Rothermel, R. C. (1972). A mathematical model for predicting fire spread in wildland fuels. Tech. Report Research paper INT-115, USDA Forest Service, Ogden, Utah, USA.

Scott, J. & Burgan, R. (2005). Standard Fire Behavior Fuel Models: A Comprehensive Set for Use with Rothermel's Surface Fire Spread Model, USDA Forest Service.

Shafizadeh, F. (1982). Introduction to pyrolysis of biomass. Journal of Analytical and Applied Pyrolysis, Volume 3, Issue 4, April 1982, Pages 283-305.

Sullivan, A. L. (2017a). Inside the inferno: fundamental processes of wildland fire behaviour. Part 1: Combustion chemistry and energy release. Fire Science and Management, Volume 3, pages 132–149.

Sullivan AL (2017b) Inside the inferno: fundamental processes of wildland fire behaviour. Part 2: Heat transfer and interactions. Fire Science and Management, Volume 3, pages 150–171.

Tan, S. H. (1967). Flare system design simplified. Hydrocarbon Processing, 46, pp. 172–176.

Tedim, F., Leone, V., Amraoui, M., Bouillon, C., Coughlan, M.R., Delogu, G.M., Fernandes, P.M., Ferreira, C., McCaffrey, S., McGee, T.K., Parente, J., Paton, D., Pereira, M.G., Ribeiro, L.M., Viegas, D.X. & Xanthopoulos, D. (2018). Concept Paper: Defining Extreme Wildfire Events: Difficulties, Challenges, and Impacts. Fire 2018, 1, 9; doi:10.3390/fire1010009.

Torero J. (2016). SFPE Handbook of Fire Protection Engineering, Flaming Ignition of Solid Fuels, 5th Ed., Springer, 2016, pp. 633-681.

van den Bosch, C.J.H. & Weterings, R.A.P.M. (Eds.) (2005). Methods for the calculation of physical effects – 'Yellow Book,' CPR 14E. 3rd ed., 2nd revised print. The Hague: Committee for the Prevention of Disasters, 2005.

Viegas, D. X., Viegas, T. S. P. & Ferreira, D. (1992). Moisture content of fine forest fuels and fire occurrence in central Portugal. International Journal of Wildland Fire, Volume 2, Issue 2, Pages 69–86,1992.

Viegas, D. X. & Pita, L. P. (2004). Fire spread in canyons. International Journal of Wildland Fire, Volume 13, Issue 3, Pages 253–274, 2004.

Viegas, D.X., Figueiredo A.M., Ribeiro, L.M., Raposo, J., Viegas, M.T., Oliveira, R., Alves, D., Pinto, C., Jorge, H., Rodrigues, A. (2017). O Complexo de Incêndios de Pedrogão Grande E Concelhos Limítrofes, Iniciado a 17 de Junho de 2017. Universidade de Coimbra: Coimbra, Portugal, 2017.

Weber, R. O. (1991). Modelling fire spread through fuel beds. Progress in Energy and Combustion Science, Volume 17, Issue 1, 1991, Pages 67–82.

Węgrzyński, W., Lipecki, T. & Krajewski, G. Wind and Fire Coupled Modelling—Part II: Good Practice Guidelines. *Fire Technol* 54, 1443–1485 (2018).

Williams, F. A. (1982). Urban and wildland fire phenomenology. Progress in Energy and Combustion Science, Volume 8, Issue 4, 1982, Pages 317-354.

Williams, F. A. (1985). Combustion Theory: The Fundamental Theory of Chemically Reacting Flow Systems. Addison-Wesley, Reading

FIRE-RES